BOSTON UNIVERSITY

GRADUATE SCHOOL OF ARTS AND SCIENCES

Dissertation

THE ROLE OF WIND WAVES ON SALT MARSH MORPHODYNAMICS

by

ANTHONY MICHAEL PRIESTAS

A.A., St. Petersburg College, 2002
B.S., Florida State University, 2005
M.S., Florida State University, 2005

Submitted in partial fulfillment of the

requirements for the degree of

Doctor of Philosophy

2013

BOSTON UNIVERSITY

© 2013 by
Anthony Michael Priestas
All rights reserved

Approved by

First Reader _____

Sergio Fagherazzi, Ph.D.
Associate Professor of Earth and Environment

Second Reader _____

Robinson W. Fulweiler, Ph.D.
Assistant Professor of Earth and Environment

Third Reader _____

Guido D. Salvucci, Ph.D.
Professor of Earth and Environment

Dedication

This work is fondly dedicated to those who have encouraged me to finish what I started.

Your encouragement does not go unnoticed, and I am grateful for it.

Acknowledgements

Over the past eight years I have had the great privilege of working with my coach and mentor, Dr. Sergio Fagherazzi, as both a masters student and doctoral candidate. My gratitude for your support and encouragement, in difficult times and through my own self-doubt, cannot be overstated. Thank you for putting things into perspective and keeping me on track. It has been a tremendous journey.

Thank you to my committee members for providing valuable feedback and helping to shape and clarify my ideas. I extend my appreciation to the entire Earth Sciences faculty for providing a supportive environment for a graduate student, and I am humbled by the level of ability and productivity you have as a department.

This work would not have been possible were it not for my courageous, fellow graduate students willing get stuck in the muck to help me collect data - thank you, Christine Harrington, Carol Wilson, and Giulio Mariotti for your camaraderie and all your efforts in the field. Giulio Mariotti contributed significantly to the third chapter of the manuscript through modeling efforts. Thanks to David Boyd and Chris Buck for captaining and assisting in additional field work, as well as Art Swarzschild, Donna Fauber, and staff at the Anheuser-Busch Coastal Research Center, Virginia for their assistance and use of their wonderful facilities. I would also like to thank W. Guthrie Perry and the staff of the Rockefeller Wildlife Refuge, Louisiana for their hospitality and field support.

My wife, Janelle, has been a vital confidante and cornerstone for me to lean on during this process and helped to keep my sprits elevated. Thank you for believing in me. I love you.

Of course, none of this could have been possible without my mother, whose advice keeps me grounded and whose encouragement keeps me goal-oriented. Her unwavering drive, grit, and intellect are traits I will always continue to emulate. She is the epitome of a heroine.

This research was supported by the Office of Naval Research award #472 N00014-10-1-0269 and N00014-07-1-0664, the Department of Energy NICCR program 473 award #TUL-538-06/07, and by the VCR-LTER program award #GA10618-127104. Additional support was made possible through Teaching Fellowships from Boston University. Thank you.

THE ROLE OF WIND WAVES ON SALT MARSH MORPHODYNAMICS

(Order No.)

ANTHONY MICHAEL PRIESTAS

Boston University Graduate School of Arts and Sciences, 2013

Major Professor: Sergio Fagherazzi, Associate Professor of Earth and Environment

ABSTRACT

The stability and survival of salt marshes is typically linked to the competing influences of sea-level rise, subsidence, and sediment accumulation and erosion. However, consideration must also be made for wind waves that regulate the erosion of salt marsh shorelines and resuspend sediments in bordering tidal flats thus providing material for marsh accretion. This thesis examines the mechanisms in which wind waves affect marsh morphology, the mechanisms of salt marsh boundary erosion, in addition to linking the processes responsible for sediment mobilization between tidal flats and adjacent salt marshes.

Sediment concentration within an open-coast marsh creek along the Louisiana chenier plain is shown to be related to the local wave climate and channel velocity. Calculations of sediment fluxes during ebb and flood tides indicates that while large

volumes of sediment are mobilized into the marsh when wind waves are present, only a small portion is stored during each tidal cycle.

In the coastal lagoon setting of Hog Island Bay, Virginia, marsh shoreline erosion rates were estimated from direct surveys and through analysis of aerial photographs. Erosion rates averaged 1.3 m/yr, similar to the 50-year historical average determined from previous work at the same location. Based on a calibrated numerical model for wind waves, the average erosion rate was linked to the energy of the waves attacking the marsh boundary. Additionally, results suggest that the effect of large waves forming during storms on erosion rates is negligible. Variations in erosion rates were linked to shoreline sinuosity (a proxy used to describe the result of wave concentration through erosive gullies), sediment characteristics, faunal activity, and marsh elevation.

The culmination of the work leads to the hypothesis that waves have two opposite effects on salt marshes. On one hand they erode marsh boundaries thus reducing marsh area; on the other hand they mobilize large volumes of sediments in nearby tidal flats which may facilitate marsh accretion thus contrasting sea-level rise. In conclusion, wind waves destabilize marshes along the horizontal direction despite their potential vertical stability.

TABLE OF CONTENTS

DEDICATION iv
ACKNOWLEDGEMENTS v
ABSTRACT vii
LIST OF TABLES xii
LIST OF FIGURES xiii
PREFACE xvi

CHAPTER I. Sediments and water fluxes in a muddy coastline – Interplay between waves and tidal hydrodynamics 1
1.1 Introduction 1
1.2 Study site 3
1.3 Methods 5
1.4 Results 7
1.4.1 Correlation between wind, waves and storm surges 9
1.4.2 Controls on sediment concentration in tidal channels 12
1.4.3 Sediment and water fluxes 17
1.4.4 Storm surge of December 22 21
1.4.5 Low tides of January 1 and 2 25
1.5 Conclusions 30
1.6 References 31
CHAPTER II. Morphology and hydrodynamics of wave-cut gullies 35
2.1 Introduction 35
2.2 Study site 39
2.3 Methods 42
2.3.1 Short-term erosion measurements 42
2.3.2 Topographic surveying 42

2.3.3 Wave data collection and analysis 43
2.4 Results 45
2.4.1 Short-term gully erosion rates 45
2.4.2 Gully morphometric analysis 50
2.4.3 Gully morphology changes 55
2.4.4 Wave analysis 56
2.5 Discussion 62
2.5.1 Wave-gully hydrodynamics 62
2.5.2 Morphodynamic evolution of wave-gullies 65
2.5.3 The role of shell fragments 70
2.5.4 Implication for the erosion of marsh boundaries 71
2.6 Conclusions 74
2.7 References 75
CHAPTER III. Coupled wave energy and erosion dynamics along a salt marsh boundary, Hog Island Bay, Virginia 80
3.1 Introduction 80
3.2 Empirical formulations for wave erosion of marsh boundaries 85
3.3 Study area 87
3.4 Methods 90
3.4.1 Surveys of marsh shoreline erosion 90
3.4.2 Estimating marsh erosion rates from aerial photography 93
3.5 Modeling wind waves and determination of wave power 95
3.5.1 Wave hindcasting 95
3.5.2 Time series and model validation 97
3.5.3 Proxy for salt marsh boundary erosion 99
3.6 Results 102
3.6.1 Boundary retreat estimates 102
3.6.2 Retreat as a function of shoreline sinuosity 103
3.6.3 Retreat as a function of wave power 105

3.6.4 Retreat as a function of wave erosion thresholds, wave height, and water level108
3.7 Discussion 109
3.7.1 Erosion rate variability 109
3.7.2 Future marsh survival and sediment fate 115
3.7.3 Sea-level rise and implications for marsh stability 117
3.8 Conclusions 118
3.9 References 120

BIBLIOGRAPHY 125
CURRICULUM VITAE 136

LIST OF TABLES

Table 2.1: Summary of wave and swash characteristics measured inside a wave-cut gully.....59

Table 3.1: Summary of marsh edge erosion rates measured in Hog Island Bay, Virginia.....103

Table 3.2: Summary values of erosion rates with sinuosity index 104

Table 3.3: Summary of correlation coefficients between erosion rates and various wave variable thresholds.....109

LIST OF FIGURES

Figure 1.1: Location of the Little Constance Bayou in the Rockefeller National Wildlife Refuge, Louisiana, USA. 4

Figure 1.2: Channel cross-sections at the mouth and at the ADCP location, Little Constance Bayou 5

Figure 1.3: Calibration of the Nortek ADCP backscattering intensity with sediment concentration data collected in the field. 7

Figure 1.4: Measurement of hydrodynamic and sedimentological parameters at the tidal channel from December 18 to December 24, 2007; (A) wind speed; (B) wind direction; (C) measured and predicted tidal elevations at the NOAA station in Calcasieu Pass, LA; (D) significant wave height; (E) wave period at the channel mouth; (F) water depth; (G) tidal velocity; (H) sediment concentration in the tidal channel. 8

Figure 1.5: Wind, waves, and storm surges distribution from December 17, 2007, to January 14, 2008 11

Figure 1.6: Correlations between sediment concentration in the channel, tidal elevation, flow velocity, and wave height 13

Figure 1.7: Relationship between sediment concentration and (A) significant wave height during flood and (B) tidal channel velocity during ebb. 15

Figure 1.8: Correlation coefficient ρ between sediment concentration and various water levels 16

Figure 1.9: Time series of (A) wave height at the channel mouth, (B) tidal elevation in the channel, (C) channel discharge, (D) sediment load in the channel for the entire study period, (E) cumulative water volume and (F) cumulative sediment mass that entered the marsh 20

Figure 1.10: Detail of the December 22, 2007, storm surge: (A) tidal elevation in the channel compared to the predicted and measured tidal elevations at Calcasieu Pass; (B) significant wave height in the bay; (C) channel velocity; (D) sediment concentration in the channel. 25

Figure 1.11: Detail of the January 1 and January 2, 2007, meteorological low tides: (A) tidal elevation in the channel compared to the predicted

and measured tidal elevations at Calcasieu Pass; (B) channel velocity; (C) sediment concentration in the channel. 27

Figure 1.12: Sediment fluxes under different meteorological conditions: (A) during large storms; (B) moderate storms with waves; (C) extreme low tides. 29

Figure 2.1: Study site at the mouth of the Little Constance Bayou along the Louisiana chenier plain 41

Figure 2.2: Morphology of ten wave gullies and related erosion rates. 47

Figure 2.3: Lateral, headward, and vertical erosion in gully 3 48

Figure 2.4: Size of mud balls measured near different gully heads 49

Figure 2.5: Spacing, width and length of the wave gullies 51

Figure 2.6: Elevation of the marsh platform and gully bottom between vegetated and non-vegetated conditions 53

Figure 2.7: Slope at the gullies' apex 54

Figure 2.8: Gully incision as a function of gully slope 55

Figure 2.9: Digital elevation model of a wave-cut gully 56

Figure 2.10: (A) Significant wave height measured in the bay in front of the wave gullies from 12/17/07 to 02/19/08; (B) wind speed and (C) wind direction measured at Calcasieu Pass. (D) Distribution of wind intensity and direction 57

Figure 2.11: (A) Time series of pressure-corrected water elevation at the gully head (B) Wind speed and (C) wind direction measured at Calcasieu Pass 60

Figure 2.12: Changes in swash velocities as a function of significant wave height and period 62

Figure 2.13: Snapshots of a wave propagating in wave gully 64

Figure 2.14: Evolution of the chenier plain shoreline at the study site from 1998 to 2007 66

Figure 2.15: Schematic evolution of wave gullies.....69

Figure 3.1: Location map of the study area located in Hog Island Bay, Virginia 88

Figure 3.2: Changes in marsh shoreline positions for the three study sites 92

Figure 3.3: (A) Digital elevation model of Hog Island Bay bathymetry. (B) The distribution of wind speed (m/s) and directions used to force the model. 96

Figure 3.4: Model simulations of significant wave height and wave period validated against measured data for the three study sites. 99

Figure 3.5: Sample time series reconstruction of modeled wave height, wave thrust, and wave power using measured and predicted water levels for two study sites.....101

Figure 3.6: Marsh edge erosion as a function of shoreline sinuosity.....103

Figure 3.7: Cumulative erosion (measured by erosion pins) plotted as a function of cumulative wave energy.....105

Figure 3.8: Cumulative erosion (determined from shoreline surveys) plotted as a function of cumulative wave energy 106

Figure 3.9: Marsh boundary erosion rate derived from GIS shoreline analysis as a function of average wave power 107

Figure 3.10: Degradation of marsh scarps in Hog Island Bay, Virginia, and Plum Island Sound, Massachusetts. 111

Figure 3.11: Upshur Neck marsh shoreline boundary mapped through time with two representative transects.....114

Figure 3.12: Example of a marsh block before (A) and after (B) disintegration.....115

PREFACE

Salt marshes are ecologically significant environments despite their low aggregate land cover. One of the most productive ecosystems in the world, salt marshes facilitate complex trophic webs and filter pollutants and excess nutrients from land-use activities. Additionally, salt marshes are economically significant in that they help to buffer shorelines against storm surges, contribute habitat to support fisheries, and provide recreational opportunities. Historically, the greatest loss of salt marsh area was due to development. Since being protected from additional land use, the primary threats to marsh loss are arguably from submergence in the face of sea-level rise, and erosion at the salt marsh boundary. In either scenario, the processes that control the exchange of sediments between the marsh and intertidal environment influence the morphodynamics of the system.

The stability and survival of salt marshes is typically addressed in terms of the competing influences of sea-level rise and subsidence to sediment accumulation on the marsh platform. However, consideration must also be made for wind waves that regulate the erosion of salt marsh shorelines and resuspend sediments in bordering tidal flats thus providing material for marsh accretion. Therefore, this thesis examines the mechanisms in which wind waves affect marsh morphology, the mechanisms of salt marsh boundary erosion, in addition to linking the processes responsible for sediment mobilization between tidal flats and adjacent salt marshes.

Chapter 1 quantifies sediment fluxes within a salt marsh tidal channel along Louisiana's chenier plain and relates those fluxes to channel velocity and the local wave climate for different meteorological conditions and tidal stages.

Chapter 2 examines the geomorphic features of wave-cut gullies, a process of wave concentration in erosive gullies that incise the marsh edge and enhance erosion. This is the first known study to investigate the hydrodynamics and geomorphic response within a wave gully.

Chapter 3 links the average shoreline erosion rates in a coastal lagoon to the average wave energy impacting the marsh boundary while identifying marsh attributes that explains the inter-site and intra-site variability. In addition, the work addresses the role of storm conditions to normal meteorological conditions in regulating marsh boundary erosion rates.

CHAPTER 1: SEDIMENTS AND WATER FLUXES IN A MUDDY COASTLINE - INTERPLAY BETWEEN WAVES AND TIDAL CHANNEL HYDRODYNAMICS

1.1 Introduction

Muddy coastlines lack barrier islands and sandy beaches that typically separate the ocean from terrestrial and intertidal landforms. As a result, salt marshes and chenier plains are the main morphological features, directly exchanging water and sediments with the ocean through a series of tidal channels. The morphology of chenier plains strongly depends on the supply of fine sediments from the shelf and on the resuspension of sediments by wind waves. In particular, the flux of sediments in and out of tidal channels plays a critical role in coastal evolution. In fact, channels provide sediments to the marsh surface, and thus determine whether the entire coastal area is able to keep pace with sea level rise (Kirwan and Murray, 2007; D'Alpaos et al., 2007; Marani et al., 2007). Similarly, in a marsh under erosion sediments are convoyed to the ocean from the interior of the marsh through tidal channels.

In intertidal environments, it is common to assume a deposition rate that varies as a function of water depth (French, 1993; Morris et al., 2002). This is particularly true for salt marshes, in which the inundation period, and therefore the time available for suspended sediments to settle, decreases with elevation when the marsh becomes emergent. Recent studies in the Netherlands have also shown that sediment concentration in the water column is controlled by tidal inundation, and increases

linearly with inundation height at high tide (Temmerman et al., 2003). Other studies showed that, in some cases, sediment concentrations initially spike during high flood-dominated tidal currents then decrease to low concentrations with rising tide (Green and Coco, 2007). Empirical relationships between tidal elevation and sediment concentration have been used to model the long-term evolution of the entire marsh system (Kirwan and Murray, 2007). Other studies have used a constant concentration of sediments in the marsh channels to study accretion of the marsh platform and the related feedbacks with marsh vegetation (D'Alpaos et al., 2007) and the evolution of the channel cross section in time (D'Alpaos, et al., 2006). However, all these studies do not directly address the link between sediment fluxes and the processes responsible for the resuspension and transport of sediments in the nearshore area. Recent research carried out by French et al. (2008) found that suspended sediment concentration varies intermittently as a function of meteorological surges and wind stress forcing, which generates waves and sediment resuspension.

A more process based approach is also deemed necessary for the charachterization of the sediment export from the marsh interior to the ocean, since different mechanism regulate the sediment concentration in tidal channels during ebb. For example, Mwamba and Torres (2002) emphasize the critical role of rainfall and, in particular, the detachment of sediment particles produced by raindrop impact on the erosion of the marsh platform and the related sediment flux to the ocean. More recently, Green and Coco (2007) also note the role rainfall has on increasing sediment loads and corresponding sediment exchange between mudflats and tidal channels. Goni and

Gardner (2003) indicate that seepage flow from marsh banks during low tide can export significant volumes of both dissolved organic and sediment particles to the ocean.

The effect of wind waves on sediment substrate has been the focus of recent research projects in the nearshore area (Traykovski et al., 2007; Kineke et al., 2006; Sheremet et al., 2005; Jaramillo et al., 2009). All these studies indicate that waves are the chief mechanism for sediment resuspension in muddy environments. Wind waves have also been recognized as critical morphological agents for the evolution of tidal flats and intertidal landscapes in general (Fagherazzi, et al., 2006, 2007; Defina et al., 2007).

In this chapter, we seek to link the processes responsible for sediment mobilization in tidal flats to the supply of sediments to adjacent salt marshes. In particular, through high resolution field measurements, we will determine the effects of tides and waves on the sediment fluxes in a tidal channel along a muddy coastline.

1.2 Study Site

We focus our study on Little Constance Bayou, a tidal channel in the Grand Chenier Plain, Louisiana, USA (Fig. 1). The tidal channel is located within the Rockefeller National Wildlife Refuge, in one of the fastest eroding coastlines in the United States, with an average erosion rate higher than 10 m/yr between 1884 and 1994 (Byrnes, et al., 1995). The chenier plains in Louisiana are a system of shelly, elongated ridges perched on muddy sediments (Russel and Howe, 1935). Shell fragments are episodically deposited by waves at the coastline (white areas in Fig. 1, right panel), but the entire system is mud-dominated. Erosion of muddy sediment is cause by wind waves

propagating from offshore (Elgar and Raubenheimer, 2008) and lead to a uniform retreat of the coastline (subsequent chapters discuss the scale dependency of erosion rates along the coastline).

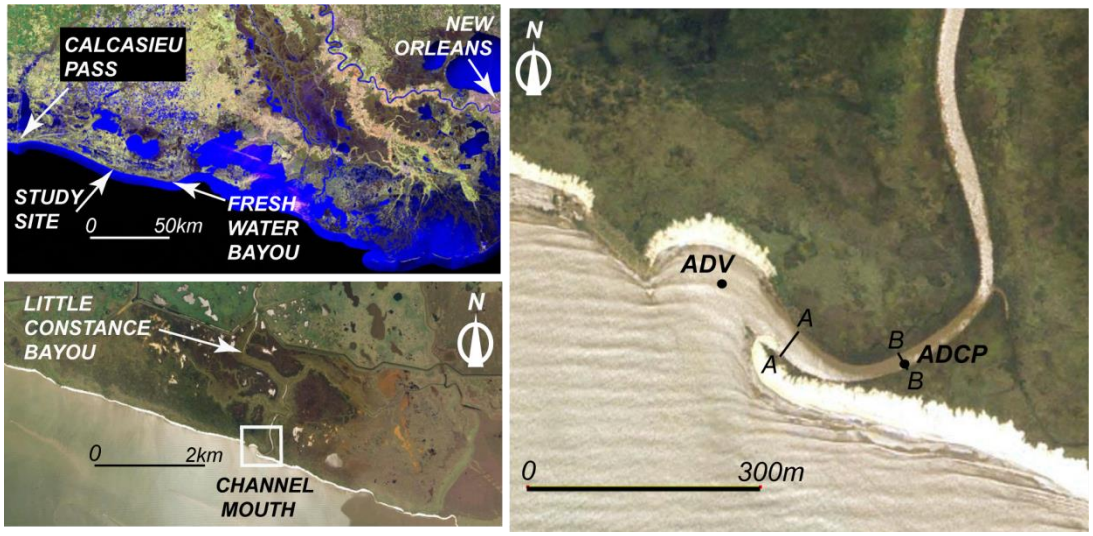

Figure 1.1. Location of the Little Constance Bayou in the Rockefeller National Wildlife Refuge, Louisiana, USA.

A series of artificial levees delimit the watershed of Little Constance Bayou, protecting both oil rigs and coastal settlements from moderate storm surges. The tide is diurnal with a maximum diurnal range of 60 cm at Calcasieu Pass (see Fig. 1.1). The main offshore source of fine sediments is the Atchafalaya subaqueous delta (Draut et al., 2005a), which terminates 10 km east of Fresh Water Bayou (Draut et al., 2005b; see Fig. 1.1). On the contrary, the reduced amount of sediment in our location leads to sediment starving conditions.

The regrading of the shoreline has considerably reduced the length of the critical tidal channel in the last 50 years (Fig. 1.1), so that the bend at the channel mouth in

Figure 1 is in reality a vestige of a channel meander. The channel is deeper and confined at the bend (section B-B, see Fig. 1.2), but widens at the mouth (section A-A in Fig. 1.2).

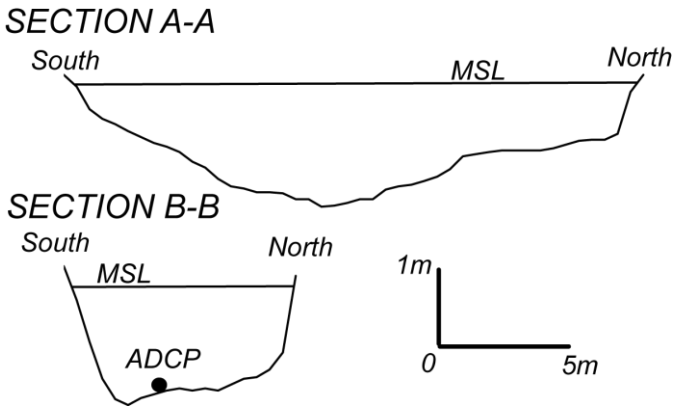

Figure 1.2. Channel cross-sections at the mouth and at the ADCP location (see Fig. 1).

1.3 Methods

We deployed a Sontek Acoustic Doppler Velocimeter (ADV) vertically mounted on a tripod in the bay in front of the channel mouth (see Fig. 1) and measured wave climate every hour from December 17, 2007, at 3 p.m. to January 14, 2008, at 10 a.m. Each wave burst measured 2048 water elevations for 400 seconds at 5 Hz. The pressure data were used to compute wave statistics after removing high frequency components (more than 2 Hz). We extracted the significant wave height H_s (the average of the highest one-third of the waves) and the mean wave period T_{01} (first-order moment) from the wave spectrum.

Within the tidal channel, we deployed a Nortek Acoustic Doppler Current Meter (ADCP) and measured tidal elevation and water velocity (with 10 cm vertical bins) every hour during the same period as the ADV measurements.

Given the shallow depth of the channel, we did not detect variations of velocity along the vertical (barotropic flow). Therefore, we used the sixth interval of the ADCP, which measures the velocity between 0.3 and 0.4 m above the profiler for the determination of channel velocity. The horizontal velocity was rotated thirty degrees to be aligned perpendicularly to the channel axis. In the data shown herein, a positive velocity denotes flood flow (water entering the marsh) whereas a negative velocity denotes ebb (water exiting the marsh).

Similarly, we used the amplitude of the ADCP acoustic signal between 0.3 and 0.4 m as a proxy for sediment concentration, assuming well-mixed conditions. The amplitude was calibrated assuming a linear response of the instrument with sediment concentration (e.g. Voulgaris and Meyers, 2004). Ten water samples of one gallon were collected at the ADCP site under different conditions of sediment concentration. The water was filtered to extract suspended sediments. The filters were dried at 40 ^{o}C for two hours and then weighed to determine the total mass of suspended sediments. The sediment concentration was then correlated to the intensity of the back-scatter signal with a log-log interpolation (Fig. 1.3; see Voulgaris and Meyers, 2004). The tidal data were then compared to tidal and meteorological data at Calcasieu Pass, LA (NOAA station 8768094, see Fig. 1.1).

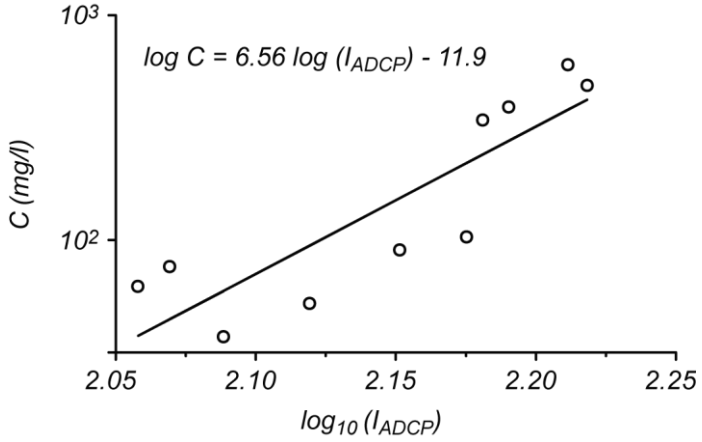

Figure 1.3. Calibration of the Nortek ADCP backscattering intensity with sediment concentration data collected in the field.

1.4 Results

The data collected were organized in an hourly time series. In Figure 4, we report an example of the data resolution from December 18 to December 24, 2007. A moderate storm hit the Louisiana coast from December 20 to December 24, producing two distinct wave events on December 20 and December 22, 2007, with significant wave heights between 0.7 and 1 m. The first event occurred for wind directions from the south while the second was produced by winds blowing from the southwest, perpendicular to the coastline. The wind in Calcasieu Pass was higher for the second event (Fig. 1.4A), even though the lack of offshore data in front of Little Constance Bayou warrants a precise assessment of meteorological conditions at the study site. On December 22, a wind of 9 m/s coming from the northwest produced a moderate storm surge both at Calcasieu Pass (difference between measured and predicted tide in Fig. 1.4C) and our study site (Fig. 1.4F). The storm surge increased water elevations in the

channel (Fig. 1.4F), tidal velocities (Fig. 1.4G), and suspended sediment concentrations (Fig. 1.4H).

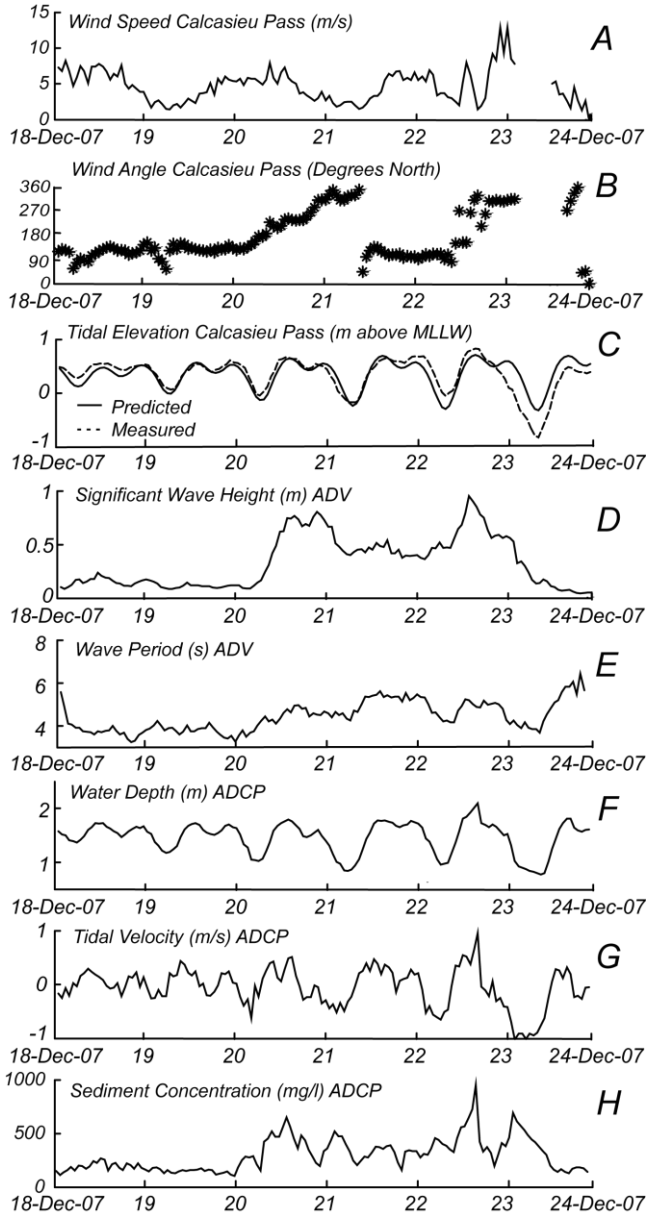

Figure 1.4. Measurement of hydrodynamic and sedimentological parameters at the tidal channel from December 18 to December 24, 2007; (A) wind speed; (B) wind direction; (C) measured and predicted tidal elevations at the NOAA station in Calcasieu Pass, LA; (D) significant wave height; (E) wave period at the channel mouth; (F) water depth; (G) tidal velocity; (H) sediment concentration in the tidal channel.

1.4.1 Correlation between wind, waves and storm surges

The distribution of wind direction and intensity at Calcasieu Pass during the study period is reported in Figure 1.5(A). The most frequent wind direction is southeast followed by north, with only a very intense wind event from the northeast. In Figure 1.5(B) we plot the wave data collected in front of Little Constance Bayou along the wind directions measured at Calcasieu Pass (only significant wave height higher than 0.3 m is reported). As expected, the waves are produced by winds blowing from the ocean (from southeast in our study period), but not from winds blowing from the mainland (i.e. from north and northeast along this stretch of coastline). Wind speed and wave height are positively correlated for winds blowing from the southeast, south and southwest (Fig. 1.5E), indicating that strong winds from these directions produce energetic wave events at the shoreline. These results need to be accepted with caution, however, since the distance between the NOAA station at Calcasieu Pass, where the wind data were collected, and Little Constance Bayou, where we measured the wave height, is large enough to affect the relationship between wind and waves. Of more interest is the connection between wind and storm surges. In Figure 1.5(C) we plot the positive difference between measured and predicted tidal elevations at Calcasieu Pass (water higher than 0.1 m above the predicted astronomic elevation). All storm surges occur for winds blowing from the southeast, the only direction along which the wind was blowing on water during the study period. Lack of wind events during this period from the south-southwest, and west, unfortunately limits our analysis of storm surges. The storm surge

is positively correlated to wind speed for east, southeast and south directions, and also for winds from the northwest, although fewer data points are available along this direction. As a result, strong winds from the south and southeast are responsible for storm surges at the coastline. Finally, we also investigate the relationship between negative storm surges (measured water elevations lower than the astronomical prediction) and wind. Very low tides occur for winds blowing from the north and northwest, with departures from the tidal prediction up to -0.8 m (Fig. 1.5D). A significant correlation exists between extreme low tides and winds blowing from the north and northwest (Fig. 1.5E). Therefore, when wind comes from the mainland the tidal elevation is lower since the water is locally displaced by wind shear stresses towards the ocean.

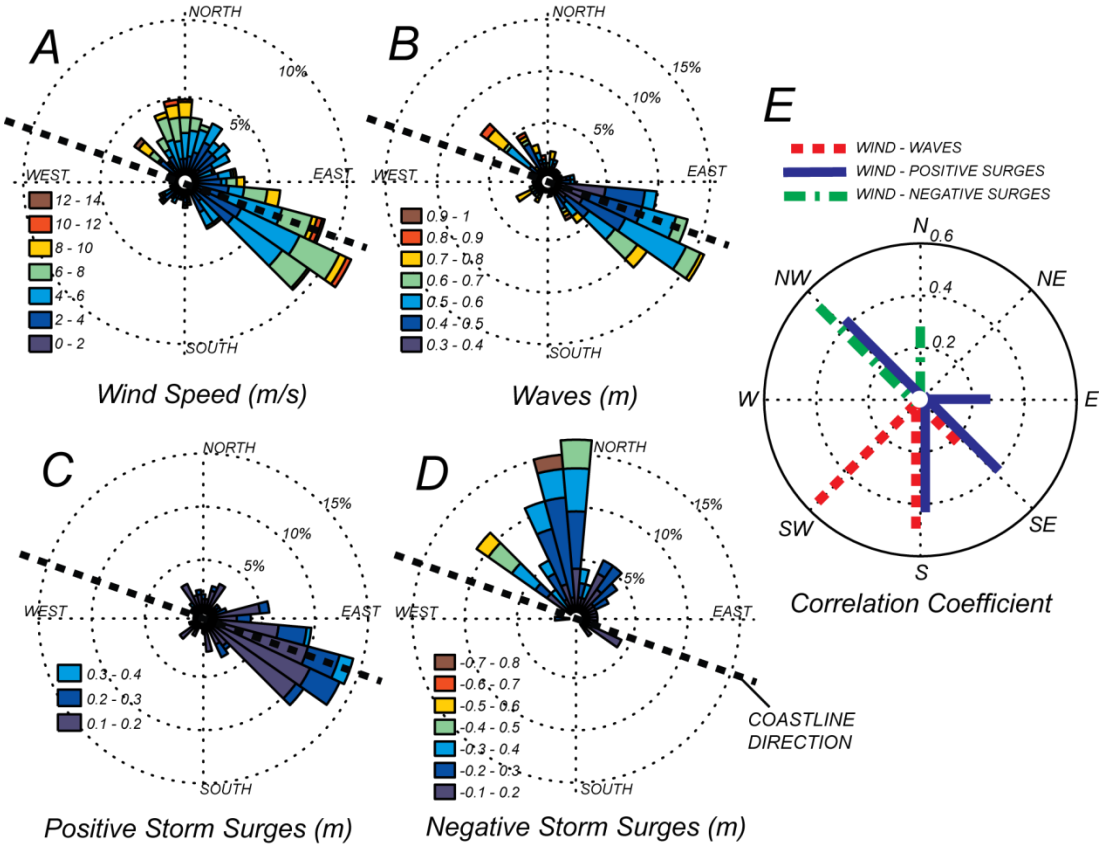

Figure 1.5. Wind, waves, and storm surges distribution from December 17, 2007, to January 14, 2008: (A) distribution of wind intensity and direction at Calcasieu Pass, LA; (B) distribution of wave height in front of Little Constance Bayou as a function of wind direction measured at Calcasieu Pass; (C) distribution of positive storm surges (higher than predicted astronomic tide) at Calcasieu Pass as a function of wind direction; (D) distribution of negative storm surges (lower than predicted astronomical tide) at Calcasieu Pass as a function of wind direction; (E) correlation coefficients between wind speed and wave height, positive storm surges, and negative storm surges. The data are binned in eight wind directions, all correlations are significant with $p < 0.05$.

In general, when the wind blows from the southeast, the result is high waves and storm surges, whereas for winds from the north and northwest there are no waves and very low meteorological tides.

Of interest is also the storm of December 22-23, 2007, during which a wind of 10 m/s blowing from the southwest was followed by winds up to 15 m/s blowing from the northwest, thus producing a wave event superimposed to a storm surge during flood,

followed by a very low meteorological tide during the following ebb (Fig. 1.4). This event created the most favorable conditions for sediment resuspension both during flood and ebb in our study channel.

1.4.2 Controls on sediment concentration in tidal channels

To investigate the relationship between sediment concentration, tidal elevation, wave height, and flow velocity in the channel, we divided the data into six different sets as a function of tidal elevation and flow velocity. The six sets roughly correspond to six different stages in the tidal cycle (Fig. 1.6). For low velocities (less than 0.3 m/s) we have slack conditions and the water is either slowly entering the channel or exiting from it. For high velocities (absolute value higher than 0.3 m/s) we have two distinct events of flood and ebb. We also differentiate between high water (higher than Mean Sea Level, MSL) and low water events (lower than MSL), since the velocity in the channel is never zero (instead of dividing the data into high slack water, low slack water during flood and ebb conditions), which means we also discriminate slowly incoming flow during slack water from slowly exiting flow during slack water. For each stage, we run a correlation between sediment concentration in the channel and wave height, flow velocity, and tidal elevation. We report only correlation coefficients higher than 0.4 and all estimates are significant with $p < 0.05$ (see Fig. 1.6).

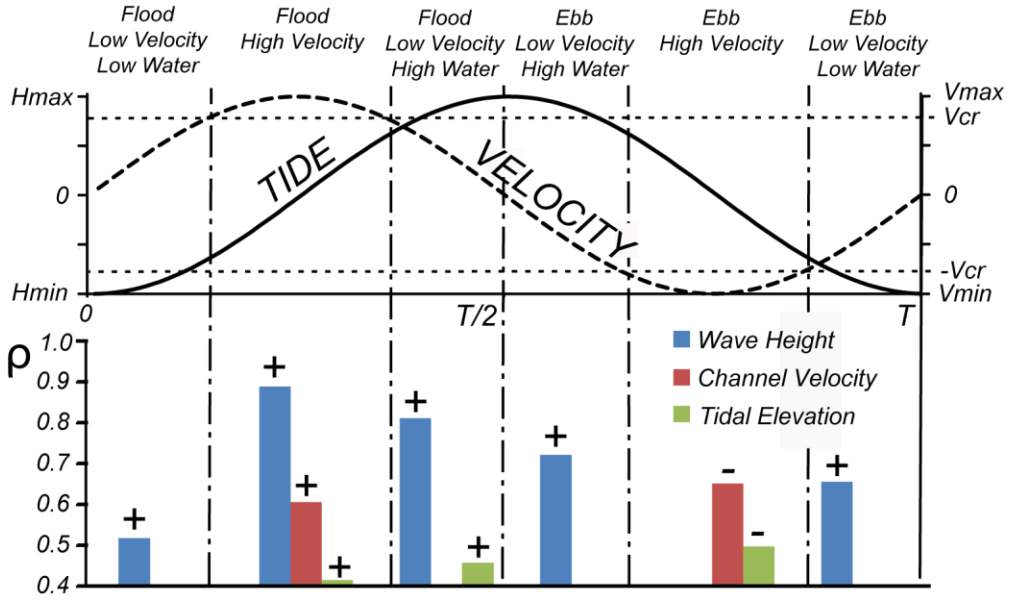

Figure 1.6. Correlations between sediment concentration in the channel, tidal elevation, flow velocity, and wave height in the bay. The data are grouped in six different tidal stages as a function of flow velocity and water elevation.

Sediment concentration in the channel is highly correlated to wave height, particularly during flood events and during high slack water. It is easy to envision that sediment is first resuspended by waves near the channel mouth and then moved in the channel during flood. The transport of sediment continues during high slack water, although with a lower coefficient of correlation, and extends to the first period of the ebb phase, probably because of the combination of low velocities and proximity to energetic conditions in the bay are still influencing the sediment concentration in the channel. During ebb, as expected, the sediment concentration is not influenced by wave climate, since the tidal flow is transporting sediments from the marsh interior to the ocean. During this stage, there seems to be a relationship between sediment concentration and channel velocity, with high (negative) velocities promoting elevated bottom shear

stresses that favor sediment remobilization in the channels and on the marsh surface. Similarly, even during flood there appears to be a positive correlation between flow velocity and sediment concentration, evidence of a combined effect of currents and waves in the resuspension of bottom sediments. We also detect a weak influence of water elevation on sediment concentration during the ebb phase, with high sediment concentration for low tidal elevations. This is probably due to sediment fluxes from the marsh banks during very low tide. In fact, low tidal elevations in the channel create a hydraulic gradient between the marsh surface and the ocean that increases the seepage of sediment-rich water from the channel banks.

A plot of sediment concentration in the channel as a function of significant wave height during flood indicates that the relationship between the two quantities is linear, with higher waves increasing sediment concentration (Fig. 1.7A). Similarly, the relationship between sediment concentration during ebb and tidal channel velocity appears to be linear as well, but with a larger data spread (Fig. 1.7B).

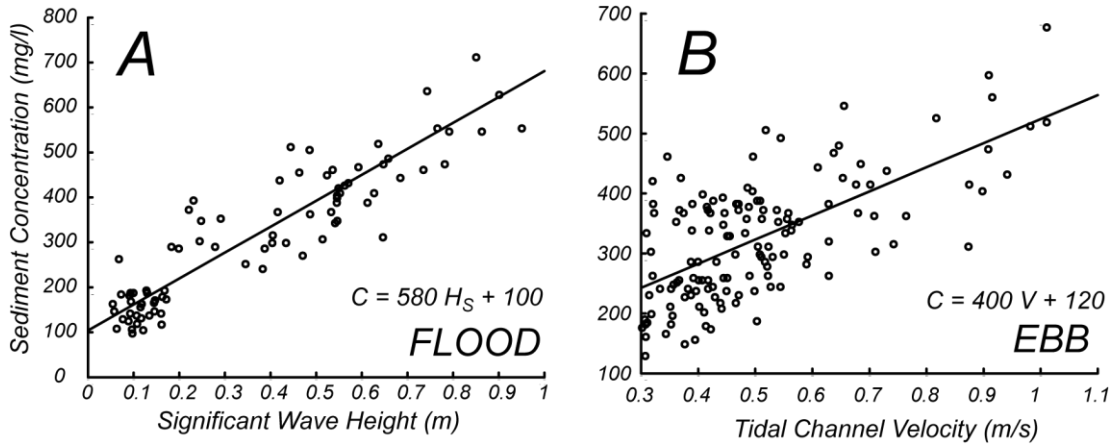

Figure 1.7. Relationship between sediment concentration and (A) significant wave height during flood and (B) tidal channel velocity during ebb.

We also put forward the hypotheses that sediment concentration during ebb is related to (i) the concentration of sediment that entered the channel during the previous flood; (ii) the hydrodynamic conditions during the previous flood. The first hypothesis, which can be defined as the continuity hypothesis, simply states that if water with high sediment concentration enters the marsh during flood, the same suspended sediments will likely exit during the subsequent ebb, since not all sediments will be deposited within the marsh.

The validity of the continuity hypothesis depends on the relative value of the settling velocity, which dictates the residence time of the sediments in the system. In a muddy environment the settling velocity of fine particles is low, so that sediments do not have enough time to deposit on the marsh in a tidal cycle.

A comparison between sediment concentration during ebb and sediment concentration during the previous flood (evaluated at the maximum flood velocity)

shows that the two quantities are correlated (Fig. 1.8). Sediment concentration during ebb is also correlated to the maximum wave height during the previous 24 hours, which is the mechanism initially responsible for sediment resuspension. Furthermore, the correlation increases if we consider only the wave height at the maximum flood velocity, indicating that the synchronous occurring of both high sediment resuspension in the bay and high flood fluxes in the channel determines the amount of sediments entering in the marsh and then exiting during the subsequent ebb. It is also important to stress the limit of this analysis. The fact that the sediment concentrations are correlated to all these quantities might not prove causality, since all these quantities could be cross correlated just because they all depend on the same external driver, with no direct causal relation between them.

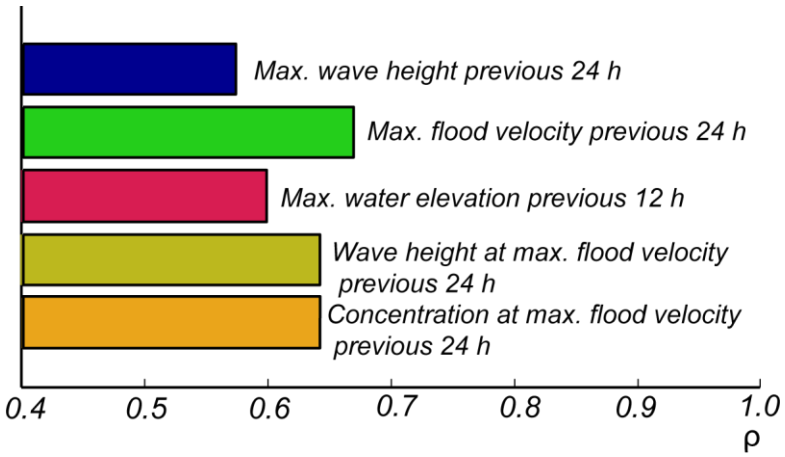

Figure 1.8. Correlation coefficient ρ between sediment concentration during ebb and (i) maximum wave height in the previous 24 hours; (ii) maximum flood velocity in the previous 24 hours; (iii) maximum water elevation in the previous tidal cycle (e.g., previous 12 hours); (iv) wave height at the instant with maximum flood velocity in the previous 24 hours; (v) sediment concentration at the instant with maximum flood velocity in the previous 24 hours.

The second hypothesis, which can be called the energetic hypothesis, states that the sediment concentration in the channel during ebb is also influenced by the velocity of the flow entering and exiting the marsh, since higher velocities give rise to larger shear stresses that remobilize sediment in the channels and, possibly, on the marsh surface. Furthermore, we can explore whether the sediment concentration during ebb is directly linked to the total volume of water that enters the marsh in the previous tidal cycle, or is instead a function of the speed at which the water is moved within the marsh boundaries. In the first case, we should expect a correlation with the peak water elevation during the previous flooding event, whereas in the second case we should find a correlation with the flood velocity during the previous tide. Our data suggest that both mechanism are present (Fig. 1.8), with a higher correlation between sediment concentration during flood and the maximum flood velocity within the previous 24 hours. This suggests that not only is the total tidal prism regulating sediment resuspension during ebb, but also the rate at which water enters (and subsequently exits) the marsh area.

1.4.3 Sediment and water fluxes

An estimate of water discharge can be computed by multiplying the cross-sectional area of the channel at each tidal elevation by velocity. Similarly, the sediment flux is simply obtained by multiplying discharge by sediment concentration. Both estimates assume that the values of velocity and sediment concentration at 30 cm from the bed are representative of average flow conditions. Results show that a high flux of

sediments enters the marsh during the storm surge of December 22 (Fig. 1.9D), much higher than the relative increase in discharge (Fig. 1.9C). Two low tide events exported sediments to the ocean (December 28 and January 1). Spring tides between January 4 and January 12 increased the exchange of water between the ocean and the marsh (Fig. 1.9C), and the corresponding sediment fluxes are enhanced by the presence of waves at the channel mouth (Figs. 1.9A and 1.9D), whereas during the period of fair weather (e.g. December 29—January 4) the sediment fluxes are reduced. It is also important to note that the wave height seems to be modulated by the tide (Figs. 1.9A and 1.9B for the period from January 5 to January 11), with lowers waves during low tide. This is probably due to higher wave dissipation at the bottom when water depth is low (Fagherazzi et al., 2007). To determine the long-term effect on the marsh sediment budget, we computed the cumulative volume of water and mass of sediments that enters the channel (the time integral of discharge and sediment flux, respectively). These results are only qualitative in nature, since residual fluxes are often of the same order of magnitude as the measurement errors associated with larger gross tidal transports (French et al., 2008). In fact, the cumulative water volume stored in the marsh is not the same for a given water level (Fig. 1.9E), thus violating water conservation. The difference can probably be ascribed to the fact that the system is not completely closed (the channel eventually connects to two shallow lakes and back to the ocean) or to approximations in the measurement of velocities. Interestingly, it appears that during wave conditions more water enters the system than expected, and is then stored in the lakes upstream of returned to the ocean through a different pathway (Fig. 1.9E). Of more

significance is the accumulation of sediment in time within the marsh. The storm surge of December 22 transported and estimated 130 tons of sediments in the marsh through the channel, but the same amount was then exported to the ocean in the subsequent ebb phase (Fig. 1.9F). In fact, the cumulative sediment flux in Figure 1.9(F) is identical before and after the storm surge of December 22, indicating that the net accumulation of sediments in the marsh as a result of the surge is negligible. Instead, exceptionally low tides during fair weather and absence of waves produced a net loss of sediments to the ocean that was not recovered in subsequent tidal cycles (16 tons on December 28 and 32 tons on January 1). A series of spring tidal cycles during wave events (January 4—January 10) produced a net accumulation of sediment in the chenier plain that roughly balanced the loss during fair weather conditions. Part of this net accumulation is due to the higher estimated discharges, and should not be accounted for. In fact, Figure 1.9(E) indicates that during the period the cumulative water volume increased in time, so that not all the water entering the marsh is then returned during the following ebb (although this result might be affected by errors in estimating cumulative water and sediment balances). Since the sediment flux is the product of water discharge and sediment concentration, a net water flux also produces a net sediment flux (more water with sediments is stored in the marsh).

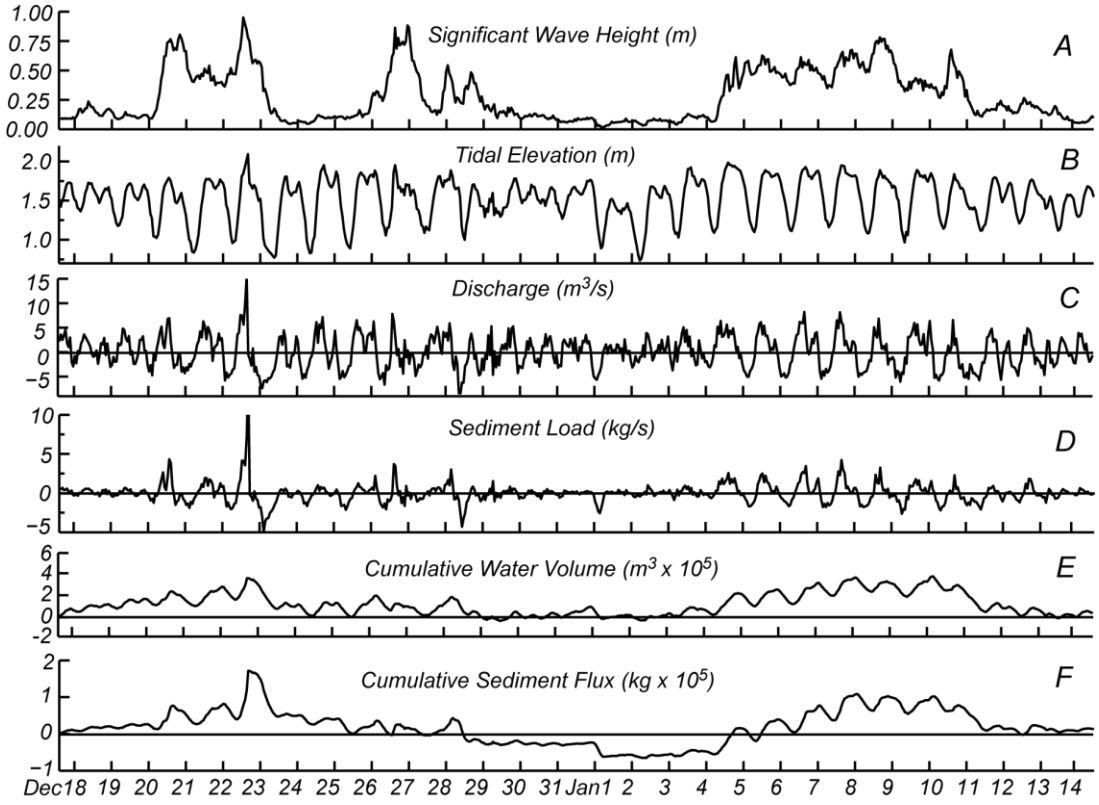

Figure 1.9. Time series of (A) wave height at the channel mouth, (B) tidal elevation in the channel, (C) channel discharge, (D) sediment load in the channel for the entire study period, (E) cumulative water volume and (F) cumulative sediment mass that entered the marsh.

Regardless of this effect, the cumulative sediment mass grew faster than the cumulative water volume. This means that water with high sediment concentration entered during flood and water with relatively low sediment concentration exited during ebb, thus producing, qualitatively, a net accumulation of sediments. Given that the net water accumulation in the marsh at the end of the study period was only 5% of the gross tidal fluxes, this suggests our methodology does conserve water mass in the long term with an estimated error of only 5% of the total volume of water mobilized by the tide. Similarly, the net accumulation of sediments in the marsh during the same period was

only 3% of the total sediment fluxes, suggesting that the system is close to morphological equilibrium (in terms of the balance between marsh surface accretion and erosion), and that the only residual sediment budgets can lead to long-term accretion. It is important to note, however, that the inherent error in the measurement of water velocity and sediment concentration means the root mean square error goes as $\pm\sigma\sqrt{n}$, or the standard deviation of the measurement error times the square root *n* measurements; thus the cumulative uncertainty of those parameters grows large in time and the residual water and sediment budgets should be accepted with caution.

1.4.4 Storm surge of December 22

A detailed analysis of the December 22 storm surge reveals that at our study site, and at Calcasieu Pass, both wind and wave set-up increased the water elevation several centimeters (13 cm at Calcasieu Pass and 23 cm in the study channel; the tidal measurements at Calcasieu Pass were referenced to the average sea level at the study site calculated during the entire deployment period, see Fig. 1.10A). The maximum storm surge at 3 p.m. is delayed three hours with respect to the highest waves measured in the bay (at 1 p.m., Fig. 1.10B). This notwithstanding, the peak in sediment concentration in the channel is reached when flood velocity also peaks (Figs. 10C and 10D). Presumably, higher velocities in the channel favor resuspension and hinder deposition, thus increasing sediment concentration. Moreover, it might take some time to resuspend sediment in the coastal area and then move it into the channel, so that we would expect the highest concentrations to occur at some time after the beginning of a wind event.

During the slack water period after the storm surge, the sediment concentration decreases in the channel due to lower tidal velocities and lower waves in the bay. The following ebb was particularly intense, with an ebb velocity around 1 m/s lasting for five hours. Sediment concentration increased with ebb velocity, reaching a peak when ebb velocity was at a maximum (at 2 a.m. on December 23). The higher tidal velocities probably favored sediment remobilization in the channel, and a large fraction of the sediment transported in the marsh during flood was thus returned to the ocean. After the maximum ebb velocity was attained, the sediment concentration decreased almost linearly, even though the ebb velocity remained constant at around 1 m/s. We interpret this behavior as a slow depletion of available sediment in the channel, so that most of the material is transported out of the system in the first stages of ebb, whereas during the last stages there is not much left to be remobilized despite high tidal velocities. The sediment concentration decreased as soon as the velocity dropped in the channel after 8 a.m. on December 23. Interestingly, the water elevation during ebb in the channel did not drop as much as at Calcasieu Pass, although the water elevations during the storm surge were similar (Fig. 10A). In the last six hours from 2 a.m. to 8 a.m. the velocity in the channel was close to 1 m/s and the water depth just slightly decreased. We put forward the hypothesis that during very low ebbs there is always a higher water level in the channel compared to the ocean, and that this difference is due to the draining water collected from the marsh that refills the channel. Under these conditions the gradient in water elevation dominates the temporal variations in water level, so that the tidal channel resembles a river draining the chenier plain. To test this hypothesis, we utilize a uniform

flow equation to explore whether the channel velocity and the water difference between channel and bay are comparable to the tidal channel hydraulic characteristics. The Manning equation reads:

$$v = \frac{1}{n} R_H^{2/3} S^{1/2} \quad (1)$$

where n is the Manning coefficient, which we assume equal to 0.025 s/m$^{1/3}$ (typical value for earth channels with vegetation), and a hydraulic radius R_H of 0.65 m from channel geometry (Fig. 1.1). We also adopt a channel slope S of 0.0015, assuming that the maximum difference in water level between the channel cross-section and the water level in the bay, equal to 0.47 m (Fig. 1.9), is gradually achieved along a length scale of 300 m, comparable to the distance between the channel cross-section and the bay (see Fig. 1). With these parameters, we compute a channel velocity of 1.16 m/s, which is of the same order of magnitude as the measured velocity in the channel (Fig. 1.9). Therefore, during very low tides the channel discharge is determined by friction and channel geometry, and not by tidal oscillations, thus justifying the departure from the tidal elevation in Figure 1.9(A). The gravity regime continues until the increasing tide produces a backwater effect in the channel; from this moment the water depth in the channel follows the tidal oscillation. Channel geometry and bottom friction limit the channel velocity during the gravity phase. As a result, the ebb velocity never exceeded 1 m/s during the entire period of measurement. It is important to note that Equation 1 is valid only for uniform flow, and cannot account for temporal variations in water surface

and velocity; thus, it can only be applied for slack water conditions, and it cannot model the rise of the tide during flood.

The high sediment concentrations during ebb subsequent to the storm surge indicate that a large fraction of the sediments carried by the storm surge is not deposited within the marsh, but is instead released to the ocean, as already shown in Figure 1.9(F). Our detailed analysis also indicates that the largest sediment export to the ocean is reached as soon as the channel velocity peaks, and then dwindles in the late stages of the ebb phase. Our results clearly show that, during ebb, sediment concentration in the channel is affected by high tidal velocities, which in turn remobilizes material and maintains it in suspension.

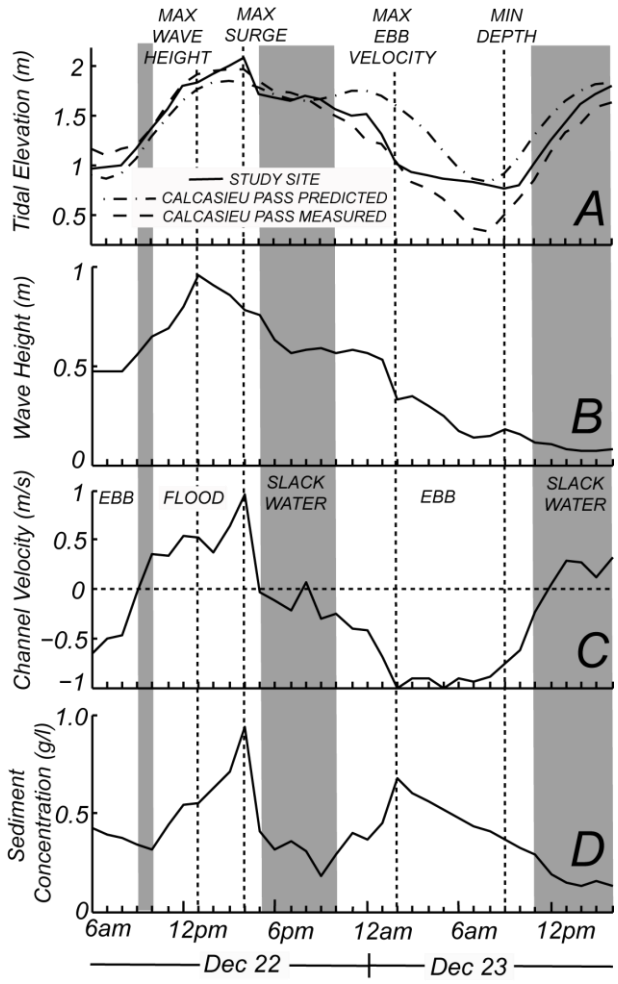

Figure 1.10. Detail of the December 22, 2007, storm surge: (A) tidal elevation in the channel compared to the predicted and measured tidal elevations at Calcasieu Pass; (B) significant wave height in the bay; (C) channel velocity; (D) sediment concentration in the channel. The gray intervals denote slack water (channel velocity less than 0.3 m/s).

1.4.5 Low tides of January 1 and 2

On January 1 at 2 a.m. and January 2 at 5 a.m. two meteorological low tides decreased the channel depth 0.35 m and 0.45 m with respect to the predicted tidal elevation at Calcasieu Pass (Fig. 1.11A). Both low tides were caused by sustained wind conditions (around 10 m/s) blowing from the north, with wave heights less than 0.1 m in

the bay (Fig. 1.8A). The first low tide followed a moderate storm surge so that the marsh had a larger volume of water (i.e. tidal prism) to be delivered to the ocean during ebb. Consequently, the ebb velocity was relatively high (0.67 m/s) peaking two hours before the minimum elevation (Fig. 1.11B). The high velocities in the channel remobilized marsh sediments, increasing the sediment concentration in the channel (Fig. 1.11C). The high velocities combined with resuspension produced a net export of material to the ocean (see Fig. 1.8F). Since wind waves were negligible during the tidal cycle, a limited amount of sediment entered the channel during flood, and the sediment export during ebb was determined by the remobilization of sediments previously stored in the marsh.

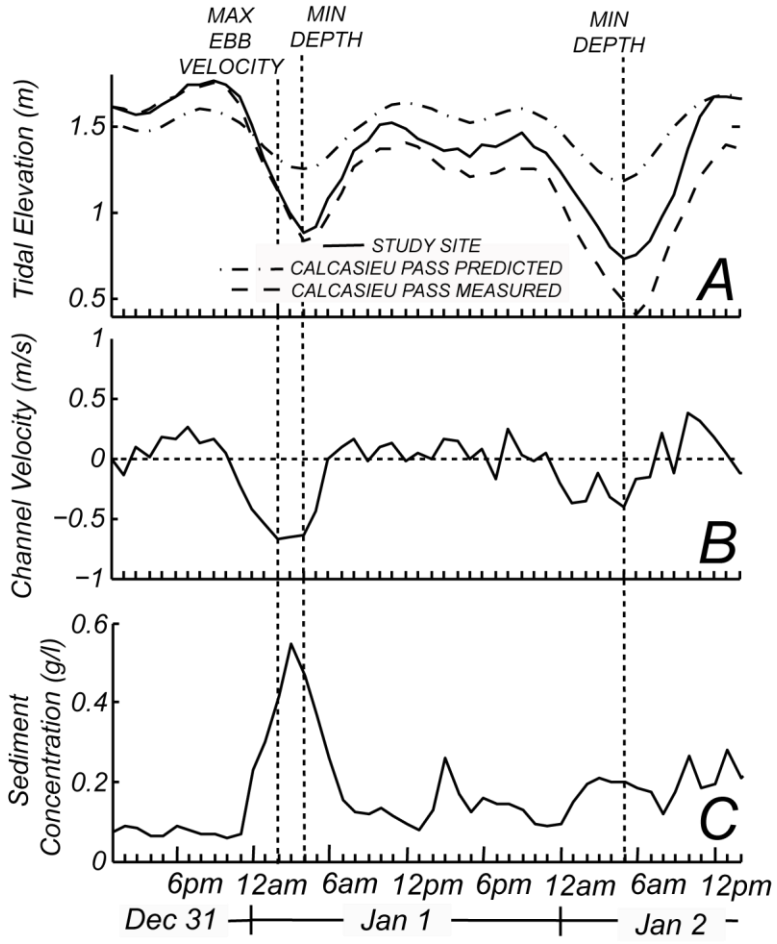

Figure 1.11. Detail of the January 1 and January 2, 2007, meteorological low tides: (A) tidal elevation in the channel compared to the predicted and measured tidal elevations at Calcasieu Pass; (B) channel velocity; (C) sediment concentration in the channel.

The meteorological low tide persisted even during the subsequent tidal cycle, resulting in a second exceptional low water elevation on January 2. However, this time the volume of water accumulated in the marsh during the previous flood was much less (the maximum tidal elevation on January 2 was 25 cm less than January 1); therefore, the reduced tidal prism did not give rise to high velocities in the channel. From a sediment budget viewpoint the second lowest tide, although being much lower than the

first, had a limited effect (Fig. 1.8F). Once again our data highlight the role of ebb velocities in sediment remobilization in a muddy coastline.

An important observation arises from the integration of the meteorological and sediment concentration data. Strong winds blowing from the south and southeast generate high waves and storm surges, and thus a large flux of sediments to the marsh during flood. However, the surge is often followed by an ebb phase with very high flow velocities, when the extra volume of water stored in the marsh is restituted to the ocean. Hence, most of the sediments accumulated during the surge are remobilized during the following ebb, producing a limited net effect. On the contrary, strong winds from the mainland (from the north and northwest) trigger very low tides—but not wave events—at the shoreline. As a consequence, the net export of sediments facilitated by high ebb velocities is not compensated by an import of sediments during the flood phase, since calm conditions at the shoreline do not favor sediment resuspension. Extreme low tide conditions are therefore favorable for net sediment loss through channel fluxes. Finally, moderate winds from the ocean can produce wave events that are decoupled from storm surges, thus avoiding fast ebb flows and sediment export during ebb. These events seem more favorable for sediment retention and marsh accretion.

The three possible meteorological conditions observed during the study are summarized in Figure 1.12. Moderate storms that do not trigger storm surges seem to be the most effective mechanism for sediment transport into the marsh, whereas very low tides without waves lead to sediment export out of the marsh. It is necessary to note that

this discussion is valid for the chenier plain studied herein, in which the marsh platform is very high in the tidal range and flooded only during spring tides.

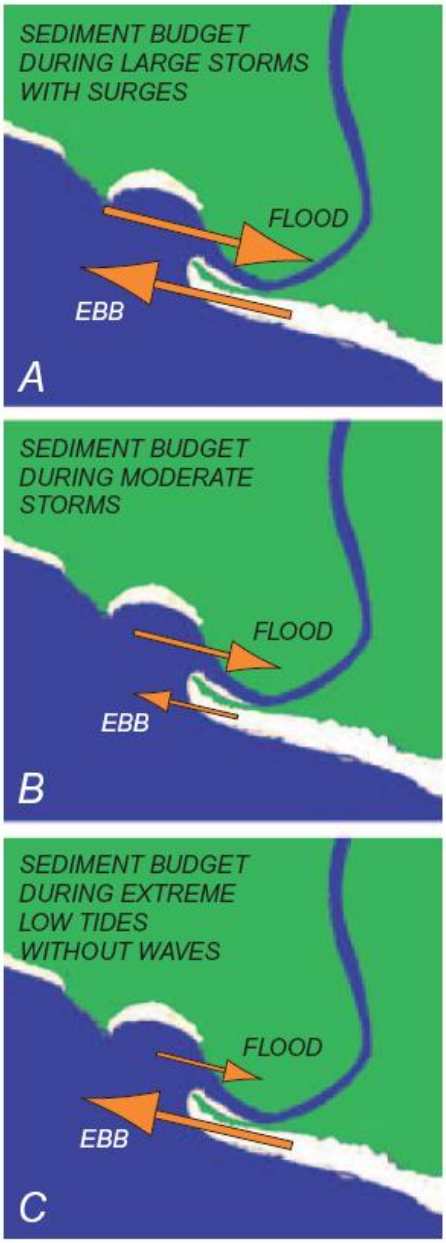

Figure 1.12. Sediment fluxes under different meteorological conditions: (A) during large storms triggering storm surges, large volumes of sediment enter the channel but then exit during ebb tide; (B) moderate storms with waves yield net sediment input to the salt marsh (the volume of sediments entering during flood is much larger than the volume of sediments exiting during ebb); (C) extreme low tides occurring when the wind blows from the mainland, leading to sediment export during ebb that is not compensated by sediment input during the subsequent flood.

1.5 Conclusions

The following conclusions can be derived from our measurements in a muddy coastline:

(1) Sediment fluxes in a tidal channel during flood are determined by wave climate. During storms, waves resuspend sediment in the nearshore area. These sediments are then funneled in marsh channels by the tide. Sediment concentration is linearly proportional to significant wave heights in the ocean.

(2) The rate at which water flows in the channel during flood is an important control on sediment concentration, but not as critical as the presence of waves in the nearshore zone.

(3) During ebb, the total sediment remobilization on the marsh is directly related to the tidal velocity in the channel, so that outgoing sediment fluxes increase for high tidal velocities. We found a linear relationship between sediment concentration in the channel and ebb velocity.

(4) Sediment concentration in the channel during ebb is also related to the amount of sediment entering the marsh during the previous flood, indicating that only a fraction of suspended sediment has time to settle in the marsh in a tidal cycle, whereas the remnant stays in suspension and exits during ebb.

(5) Storm surges carry large volumes of sediment to the marsh, but most of the material is returned to the ocean during the subsequent tidal cycle.

(6) Conversely, long period waves, even of mild intensity and not necessarily linked to storm surges, produce a net accumulation of sediments in a marsh.

(7) Meteorological low tides during fair weather conditions result in large ebb velocities that export sediments to the ocean. This sediment is not replaced in subsequent tidal cycles, giving rise to a net negative budget for the system.

(8) During very low tides the water elevation in the channel is higher than in the water in the bay, since water is still exiting from the marsh. This gradient in water elevation regulates the velocity of the water in the channel, which is then gravity driven rather than tidally driven. Water discharge is thus determined by channel geometry and bottom friction, like in terrestrial systems.

1.6 References

Byrnes MR, McBride RA, Tao Q, Duvic L. 1995. Historical shoreline dynamics along the Chenier Plain of southwestern Louisiana. *Gulf Coast Association of Geological Society Transactions* **45**:113–122.

Carniello L, *et al.* 2005. A combined wind wave-tidal model for the Venice lagoon, Italy. *Journal of Geophysical Research – Earth Surface* **110**(F4): 15.

D'Alpaos A, Lanzoni S, Marani M, *et al.* 2007. Landscape evolution in tidal embayments: modeling the interplay of erosion, sedimentation, and vegetation dynamics. *Journal of Geophysical Research – Earth Surface* **112**(F1): F01008.

D'Alpaos A, *et al.* 2006. Modeling the influence of hydroperiod and vegetation on the cross-sectional formation of tidal channels. *Estuarine Coastal and Shelf Science* **69**(3–4): 311–324.

Defina A, Carniello L, Fagherazzi S, D'Alpaos L. 2007. Self organization of shallow basins in tidal flats and salt marshes. *Journal of Geophysical Research* **112**: F03001. DOI. 10.1029/2006JF000550

Draut AE, *et al.* 2005a. Coastal mudflat accretion under energetic conditions, Louisiana chenier-plain coast, USA. *Marine Geology* **214**(1–3): 27–47.

Draut AE, *et al.* 2005b. Influence of the Atchafalaya River on recent evolution of the chenier-plain inner continental shelf, northern Gulf of Mexico. *Continental Shelf Research* **25**(1): 91–112.

Elgar S, Raubenheimer B. 2008. Wave dissipation by muddy seafloors. *Geophysical Research Letters* **35**(7): L07611.

Fagherazzi S, *et al.* 2003. Tidal flow field in a small basin. *Journal of Geophysical Research – Oceans* **108**(C3); 3071.

Fagherazzi S, *et al.* 2004. The effect of bidirectional flow on tidal channel planforms. *Earth Surface Processes and Landforms* **29**(3): 295–309.

Fagherazzi S, Sun T. 2004. A stochastic model for the formation of channel networks in tidal marshes. *Geophysical Research Letters* **31**(21); L21503.

Fagherazzi S, *et al.* 2005. Climatic oscillations influence the flooding of Venice. *Geophysical Research Letters* **32**(19): 5.

Fagherazzi S, *et al.* 2006. Critical bifurcation of shallow microtidal landforms in tidal flats and salt marshes. *Proceedings of the National Academy of Sciences of the United States of America* **103**(22): 8337–8341.

Fagherazzi S, *et al.* 2007. Wind waves in shallow microtidal basins and the dynamic equilibrium of tidal flats. *Journal of Geophysical Research – Earth Surface* **112**(F2); F02024.

French JR. 1993. Numerical-simulation of vertical marsh growth and adjustment to accelerated sea-level rise, North Norfolk, UK. *Earth Surface Processes and Landforms* **18**: 63–81.

French JR, Burningham H, Benson T. 2008. Tidal and meteorological forcing of suspended sediment flux in a muddy mesotidal estuary. *Estuaries and Coasts* **31**(5): 843–859.

Goni MA, Gardner LR. 2003. Seasonal dynamics in dissolved organic carbon concentrations in a coastal water-table aquifer at the forestmarsh interface. *Aquatic Geochemistry* **9**(3): 209–232.

Green MO, Coco G. 2007. Sediment transport on an estuarine intertidal flat: measurements and conceptual model of waves, rainfall, and exchanges with a tidal creek. *Estuarine, Coastal, and Shelf Science* **72**: 553–569.

Jaramillo S, Sheremet A, Allison MA, Reed AH, Holland KT. 2009. Wave-mud interactions over the muddy Atchafalaya subaqueous clinoform, Louisiana, United States: wave-supported sediment transport. *Journal of Geophysical Research – Oceans* **114**: C04002.

Kineke GC, *et al.* 2006. Fine-sediment transport associated with coldfront passages on the shallow shelf, Gulf of Mexico. *Continental Shelf Research* **26**(17–18): 2073–2091.

Kirwan ML, Murray AB. 2007. A coupled geomorphic and ecological model of tidal marsh evolution. *Proceedings of the National Academy of Sciences of the United States of America* **104**(15): 6118–6122.

Lanzoni S, Seminara G. 1998. On tide propagation in convergent estuaries. *Journal of Geophysical Research – Oceans* **103**(C13): 30793–30812.

Marani M, D'Alpaos A, Lanzoni S, Carniello L, Rinaldo A. 2007. Biologically-controlled multiple equilibria of tidal landforms and the fate of the Venice lagoon. *Geophysical Research Letters* **34**(11): L11402.

Moeller I, *et al.* 1996. Wild wave attenuation over saltmarsh surfaces: preliminary results from Norfolk, England. *Journal of Coastal Research* **12**(4): 1009–1016.

Moller I, *et al.* 1999. Wave transformation over salt marshes: a field and numerical modelling study from north Norfolk, England. *Estuarine Coastal and Shelf Science* **49**(3): 411–426.

Morris JT, Sundareshwar PV, Nietch CT, Kjerfve B, Cahoon DR. 2002. Responses of coastal wetlands to rising sea level. *Ecology* **83**: 2869–2877.

Mwamba MJ, Torres R. 2002. Rainfall effects on marsh sediment redistribution, North Inlet, South Carolina, USA. *Marine Geology* **189**(3–4): 267–287.

Russell RJ, Howe HV. 1935. Cheniers of southwestern Louisiana. *Geographical Review* **25**(3): 449–461.

Sheremet A, Mehta AJ, Liu B, Stone GW. 2005. Wave-sediment interaction on a muddy inner shelf during Hurricane Claudette. *Estuarine Coastal and Shelf Science* **63**(1–2): 225–233.

Tambroni N, Seminara G. 2006. Are inlets responsible for the morphological degradation of Venice Lagoon? *Journal of Geophysical Research – Earth Surface* **111**(F3); F03013.

Temmerman S, Govers G, Wartel S, Meire P. 2003. Spatial and temporal factor controlling short-term sedimentation in a salt and freshwater tidal marsh, Scheldt Estuary, Belgium, SW Netherlands. *Earth Surface Processes and Landforms* **28**: 739–755.

Torres R, *et al.* 2006. Salt marsh geomorphology: physical and ecological effects on landform. *Estuarine Coastal and Shelf Science* **69**(3–4): 309–310.

Traykovski P, Wiberg PL, Geyer WR. 2007. Observations and modeling of wave-supported sediment gravity flows on the Po prodelta and comparison to prior observations from the Eel shelf. *Continental Shelf Research* **27**(3–4): 375–399.

Voulgaris G, Meyers ST. 2004. Temporal variability of hydrodynamics, sediment concentration and sediment settling velocity in a tidal creek. *Continental Shelf Research* **24**(15): 1659–1683.

CHAPTER 2: MORPHOLOGY AND HYDRODYNAMICS OF WAVE-CUT GULLIES

2.1 Introduction

Along with the well-known functions of providing unique habitats to fish and waterfowl, salt marshes are now known to filter natural and human waste products from water, buffer storms, and play a critical role in the cycling of chemical and biological compounds (Mitsch and Gosselink, 2000). Thus, understanding the rates and processes responsible for marsh erosion is key for the preservation and restoration of these environments. The two primary mechanisms responsible for the deterioration of coastal salt marshes are platform submergence and marsh edge retreat. Deterioration by submergence depends on the competing influences between erosion and deposition processes. Deposition of both inorganic and organic sediments is influenced by sediment supply, vegetation productivity (through organic production) and vegetation effects on sediment transport (e.g., sediment trapping and increase in the threshold shear stress for erosion), and the oscillations of relative sea levels (DeLaune et al., 1983, 1994; Baumann et al., 1984; Orson et al., 1985; Finkelstein and Hardaway, 1988; Reed, 1988; Kearney et al., 1988; Day et al., 1994; Cahoon et al. 2006; D'Alpaos et al. 2007; Marani et al. 2007). Drowning kills the halophytic vegetation that stabilizes the marsh platform, so that the substrate can be easily eroded and dispersed in the ocean (Morris et al., 2002; Kirwan and Murray, 2008).

In contrast, salt marsh deterioration via wave attack is arguably the primary reason for lateral retreat of the seaward edge, and is thus a function of the local wave climate (Schwimmer, 2001; van de Koppel et al., 2005). Salt marshes undergoing lateral retreat tend to have a prominent scarp at its seaward edge. This erosive feature, and the mechanism responsible for its migration, were explained by 2-D modeling efforts by van de Koppel et al. (2005) and more recently by Mariotti and Fagherazzi (2010), even though Pye and French (1993) considered that the formation of a scarp was not necessarily indicative of edge retreat if the rate of sedimentation on the mudflat is lower than that of the adjacent marsh. Mariotti and Fagherazzi (2010) showed that, for a given sediment supply, the marsh progrades or erodes as a function of sea-level rise. A high rate of sea-level rise leads to a deeper tidal flat and, therefore, higher waves that erode the marsh boundary. However, their model is only two-dimensional, and thus might neglect important three-dimensional processes affecting marsh erosion. The bathymetry of the adjacent tidal flats is also critical for the erosion of the marsh boundary, since water depth controls wave formation and propagation, and ultimately the energy with which the waves impact the scarp (Fagherazzi and Wiberg 2009). Recent results by Mariotti et al. (2010) indicate that wave energy at the marsh boundaries is sensitive to wind direction, and increases remarkably with higher sea-level elevations and storm surges. The process of marsh erosion by wave impact is complex and modulated by tides. Tonelli et al. (2010) show with a high resolution Boussinesq model that wave thrust on the marsh scarp strongly depends on tidal level, increasing with tidal elevation until the marsh is submerged and then rapidly decreasing. Similarly, wave energy dissipation reaches the

maximum just above the marsh platform elevation when breaking occurs at the marsh edge, beyond which, wave energy is further dissipated through the marsh vegetation canopy (Möller et al., 1999, Möller, 2006).

Edge retreat is increasingly recognized in the literature as a significant cause of marsh erosion, and though the relative contribution of salt marsh loss due to edge retreat or drowning is still unclear, the dominance of one of the two processes likely depends on the geographic setting. For example, investigating Louisiana salt marshes, Turner et al. (2004) speculated that shoreline erosion may not be as significant as that from increased flooding. Kearney et al. (1988) reported interior ponding was the primary mechanism for wetland loss in the upper reaches of the Nanticoke Estuary, Chesapeake Bay. Finally, Ravens et al. (2009) argued that decreased sediment supply from damming operations was the principle cause of marsh loss in West Galveston Bay, Texas. In contrast, Schwimmer (2001) found that salt marshes in Rehoboth Bay, Delaware, are mostly eroded via wave attack, rather than platform drowning, as supported by Pb210 sediment accumulation rates. He correlated the short-term erosion rates of the marsh edge to a function of wave power, which was hindcast from local wind, fetch, and bathymetric data. For marshes in East Galveston Bay, Texas Hall et al. (1986) reported that prolonged exposure to wind-generated waves could be responsible for more erosion than the effects of submergence during hurricanes.

Van der Wal and Pye (2004) indicated that changes in the wind/wave climate near estuaries in the Greater Thames area of the UK corresponded to rapid and recent erosion of the marsh edge, while Chauhan (2009) reported that edge retreat at a study site in

northwest England is one stage of autocyclic erosion and progradation — though the evidence for such cycles (e.g., visibly abandoned clifflets from local sedimentation of the adjacent mudflat) does not appear to be present in microtidal salt marshes in the United States.

Our research involving sediment and tidal fluxes along the Louisiana chenier plain (Fagherazzi and Priestas, 2010) led to the recognition of a unique mechanism for salt marsh boundary erosion by waves in gullies. These peculiar geomorphic features incise the shoreward edge of the marsh, and appear to be created by persistent and direct wave impact. Herein termed wave-cut gullies, they are morphologically similar to features described by previous researchers. For example, Hall et al. (1986) noted "points" and "cuts" along the eroding edge. Likewise, Schwimmer (2001) described a "cleft" and "neck" formation as a series of v-shaped notches cut along the marsh shoreline. Wave-cut gullies were also observed in Plum Island Sound, MA, and Hog Island Bay, Virginia, though they differ somewhat in size, extent, and spacing. Gully formation gives rise to an undulating pattern along the marsh boundary, though this is not to be confused with a "wave-etched shoreline" which is defined an initially straight shoreline made irregular by differential wave erosion of materials of varying resistance (Gary et al., 1974).

The origin of wave gullies is still unknown, but they might form as a self-organized process by which small perturbations of the scarp morphology facilitate wave erosion. These initial indentations then develop into gullies due to compression of wave crests and wave shoaling in a positive feedback by which erosion increases gully length, thus enhancing erosive wave processes within the gully.

In this chapter, a high resolution survey is used to capture the morphologic character, evolution, and erosion rates of wave-cut gullies over a two month period. We seek to relate changes in morphology to geometric factors and shoreline retreat. Furthermore, the first analysis of wave data captured by Acoustic Doppler Velocity Profilers (ADCPs) is presented to show how propagating waves are transformed and concentrated (by changes in velocity and wave height) inside a wave-cut gully as an explanation for non-uniform shoreline erosion. Finally, a simple conceptual model is presented in order to describe their origin and evolution in time.

2.2 Study site

The study site is located in Little Constance Bayou within the Rockefeller Wildlife Refuge, along the central chenier coastal plain of southwest Louisiana, USA (Fig. 2.1). The Louisiana chenier plain is composed of Late Holocene deltaic muds interspersed by a series of widely separated sand and shell ridges termed “cheniers” (Otvos and Price, 1979). During the last 3000 years, net long-term westward currents transported fine sediments from the Mississippi delta to this location forming a 30 km-wide chenier plain (McBride et al., 2007). In recent years, these plains have been affected by rapid erosion. Shoreline retreat in this area is one of the highest in the United States, averaging rates greater than 10 m/year between 1884 and 1994 (Byrnes et al., 1995) probably due to a decrease of sediment inputs from the Mississippi (Draut et al., 2005b), to the high rate of relative sea-level rise of 0.57 m/year (Penland and Ramsey, 1990), and

to an offshore slope of about 1° coupled with wind waves propagating from offshore (Elgar and Raubenheimer, 2008).

An exception to this occurs along the eastern chenier plain, 30 km east of the study site, where sediments from the Atchfalaya river combined with resuspended shelf sediments in energetic conditions promote chenier accretion (Draut et al., 2005). The primary source of offshore sediments to the study site is likely the Atchafalaya subaqueous delta (Draut et al., 2005a) which terminates 10 km east of the study site (Draut et al., 2005a). Fagherazzi and Priestas (2010) found that despite the large volumes of sediment carried into the marsh at the study site, most of the material is returned to the ocean during the subsequent tidal cycle, which implies that the marsh can capture only a small fraction of the available mineral sediment. Many Louisiana marshes accrete via below-ground root production (organogenic sedimentation) (Nyman et al., 2006) and the combination of organic and inorganic sedimentation allows the marsh surface to keep pace with sea-level rise despite high subsidence rates (Reed, 2002).

The regression of the shoreline has considerably reduced the length of the tidal channel indicated in Figure 2.1 in the last 50 years, so that the embayment in front of the channel mouth is in reality a vestige of a channel meander.

While storm waves periodically rework and deposit shell fragments along the beach (white areas in Fig. 2.1C), the entire system is mud-dominated. The region is microtidal with a maximum diurnal tidal range of 60 cm measured at Calcasieu Pass (~70 km west of the study site). The 15-year average significant offshore wave height is approximately 1 m with a dominant wave period of about 6 s, as measured from National

Data Buoy Center station 42035 located about 30 km offshore of Galveston, Texas, and approximately 170 km from the study site (the closest available data). However, significant wave heights as measured 30 m offshore of the embayment (Fig. 1) were only 0.50–0.75 m, and were typically produced by southerly winds of 10–15 m/s (Fagherazzi and Priestas, 2010). Large storm events, however, can produce offshore (30 km) significant wave heights of 4–5 m. The offshore bathymetry is very shallow and gently sloping, reaching 5 m in depth at a distance of 2 km from the shoreline. The muddy seafloor causes considerable wave energy dissipation, reducing the height of the waves impacting the shoreline (Elgar and Raubenheimer, 2008).

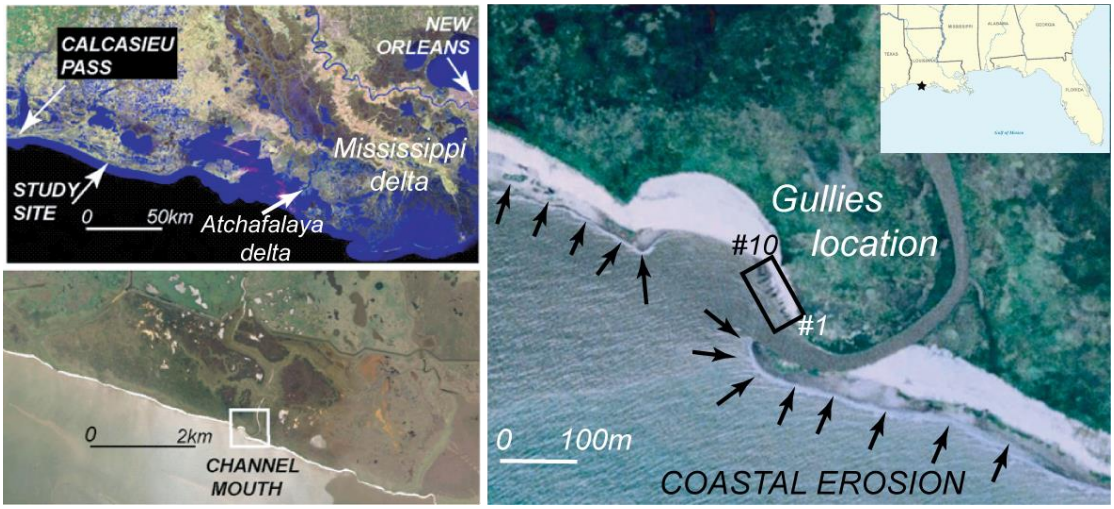

Figure 2.1. Study site at the mouth of the Little Constance Bayou along the Louisiana chenier plain. The shoreline near the channel is under fast erosion. Gullies are numbered from 1 to 10 in the direction as shown next to the box labeled "Gullies' location." Images courtesy of Google Earth.

2.3 Methods

2.3.1 Short-Term Erosion Measurements

Ten gullies were identified at the study site, and their short-term headward and lateral erosion rates were monitored using erosion pins inserted horizontally (and vertically where noted) into the head-, side-walls, and shore-facing ends of each gully (see Fig. 2.2). The gully head represents the landward point, while the gully end is the location within the gully entrance estimated at the approximate shoreline. The sides represent the gully surface and floor at the approximate midpoint of each (see Fig. 2.2). Erosion pins were inserted on 01/15/2008 and recorded erosion measurements on 01/16/2008 (1 day), 01/17/2008 (1 day), 03/12/2008 (2 months), and also on 03/14/2008 (2 days) (see Fig. 2.3). Over the two month period, 15 of the pins were missing and subsequently replaced. Consequently, gully head erosion across that time was derived by subtracting the difference in gully head positions measured from total station surveys.

2.3.2 Topographic surveying

Gully geometry and morphology was measured using a Topcon© surveying total station. Width measurements were taken at the midpoint of each gully while lengths were measured from the headward tip to the approximate shoreward extent. The spacing between gullies was measured between the midpoints of each headward tip. The slope of each gully floor was determined from two measured points which was then converted to degrees. Moreover, the average relative elevations of the surface (top) and floor

(bottom) of each gully were measured with respect to the total station elevation (which we called zero reference elevation) and qualitatively noted the presence or absence of surrounding vegetation.

To capture the gully morphology, the survey measurements were focused to a single gully (#3). The first survey was completed on 1/14/ 2008 while the subsequent survey was completed on 03/14/2008. For each survey, measurements were conducted along the surface edge, the adjacent floor edge directly below the surface, and selected cross-sections across the floor width; each survey consisted of greater than 100 measurement points. To visualize and compare changes in gully morphology, the raw data were transformed to a 0.2 m × 0.2 m gridded data matrix. In order to fill the data using a bi-linear interpolation, data points were inserted into the data matrix to close the boundaries along the marsh surface and the gully floor. The upper gully boundary was closed by inserting the measured elevation of the marsh surface (0.05 m everywhere since the marsh displays a constant local elevation around the gully). Similarly, the boundary of the gully floor was closed based on nearest neighbor values. Additional data points were inserted into the data matrix to ensure a more realistic representation of the topography (also based on nearest neighbor values). Finally, the outlines of the two gully surveys were overlaid to directly compare lateral changes caused by erosion.

2.3.3 Wave data collection and analysis

A Sontek Acoustic Doppler Velocimeter (ADV) vertically mounted on a tripod was deployed in the bay in front of the channel mouth and measured wave climate every

hour from December 17th, 2007, at 3 p.m. to February 20th, 2008, at 3 p.m. The location of the tripod is shown in Figure 1 and has an average water depth of 1.9 m. Given the very soft bottom, the tripod was anchored with three PVC pipes driven in the substrate. Each wave burst measured 2048 water elevations for 400 s at 5 Hz. Each wave burst (2048 points) was divided in three overlapping sub-bursts of 1024 points and filtered with a Hamming window.

The pressure data were used to compute wave statistics after removing high frequency components (more than 2 Hz). The significant wave heights Hs were extracted from the 0th moment (m0) of the wave spectrum.

In addition, two 2 MHz Nortek Aquadopp ADCPs were deployed within gully #3 (ADCP-1, near the gully head at an elevation of 1.2 m below the marsh platform, and ADCP-2, near the gully entrance, at an elevation 0.9 m below the marsh platform) and measured the wave climate and water velocities for a 72-hour period from March 11th, 2008 at 2 p.m. until March 14th, 2008 at 2 p.m. Wave climate was recorded every 30 min with a burst interval of 512 measurements. The ADCPs were mounted directly on the gully floor, on a plastic shingle flush with the bottom. The ADCP, with a right angle head looking upward, was strapped to the shingle with zip ties, while the shingle was solidly grounded to the bottom with metal spikes. The sampling frequency was set at 2 Hz with a 60-second averaging interval and 0.05 m blanking distance (the distance between the instrument transmitter and first measurement bin). Velocity measurements were analyzed from the first bin of the velocity profile, thus the center of the sampling volume (10 cm^3) was located approximately 15 cm above the gully floor. Given the upward-sloping

bathymetry of the gully, ADCP-1 was submerged only when tidal elevations exceeded about 10 cm above mean-sea level. Pressure data were corrected for internal instrument offsets (by comparing data to the known measured water depth at the time of deployment) as well as for atmospheric contributions using meteorological data collected from NOAA tide gage station 8768094, Calcasieu Pass, Louisiana. Wave statistics extracted from the ADCPs were computed using an upward zero-crossing method routine. The significant wave height H_S was calculated as the average wave height of the one-third largest waves. To compare meaningful changes in water velocity between the two ADCPs, the average significant velocity ($\bar{U}s$) was computed; $\bar{U}s$ is defined as the highest one-third along-axis velocity measurements for a given wave burst.

2.4 Results

2.4.1 Short-term gully erosion rates

Ten gullies were identified and photographed along 75 m of the study site, with gully#1 being the most eastward and gully #10 the most westward. The gullies are documented in Figure 2.2 along with the net erosion (indicated by arrows) for the time periods shown; the images were taken January 15th, 2008 (Fig. 2.2A) and March 12th, 2008 (Fig. 2.2B). The first and second sets of erosion values (separated by a slash mark) correspond to the time periods shown at the top of Figure 2.2A and B; no data, due to either missing pins or high water, are annotated as a double dash.

Gully head erosion averaged 10 cm between 1/15/2008 and 1/16/2008, and again averaged 10 cm from 1/16/2008 to 1/17/2008. The narrower gullies incised the marsh even more aggressively. For example, gully #10 incised the marsh 16 cm in one day, while gully #3 incised the marsh a remarkable 19 cm in one day (see Fig. 2.2A). In contrast, erosion at the gully ends averaged only 2 cm over the second 24 hour period

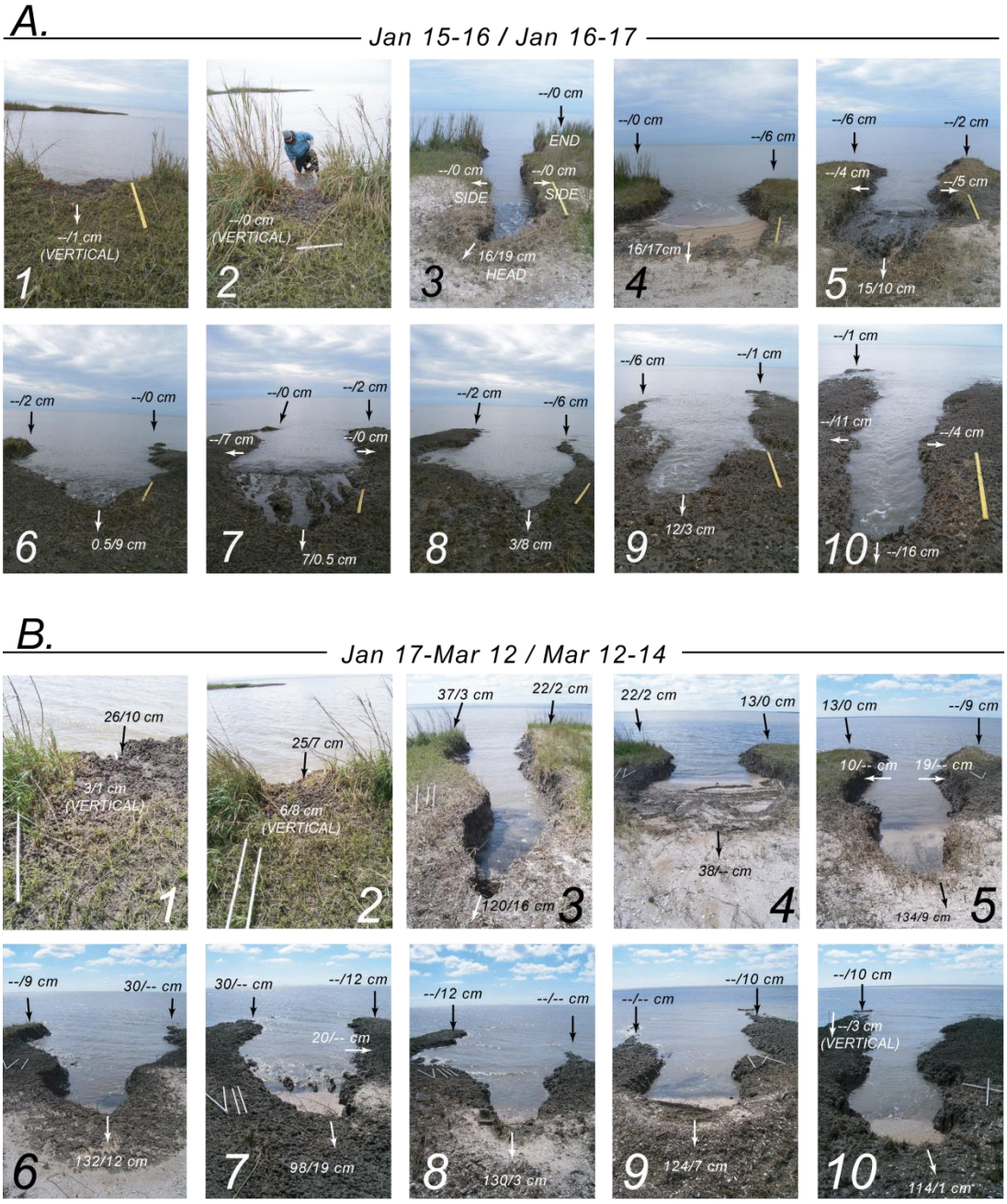

Figure 2.2. Morphology of ten wave gullies and related erosion rates. The gullies are numbered from East to West reflecting an increase in age. The two photo sets were taken on January 15, 2008 (A) and on March 13, 2008 (B). Erosion rates measured with erosion pins are also reported, and refer to four different periods, two per figure: (A) 01/15/08 to 01/16/08 (left number), 01/16/08 to 01/17/08 (right number); (B) 01/17/08 to 03/12/08 (left number), 03/12/08 to 03/14/08 (right number). The double dash indicates when the erosion pin went missing or high water such that data collection was not possible.

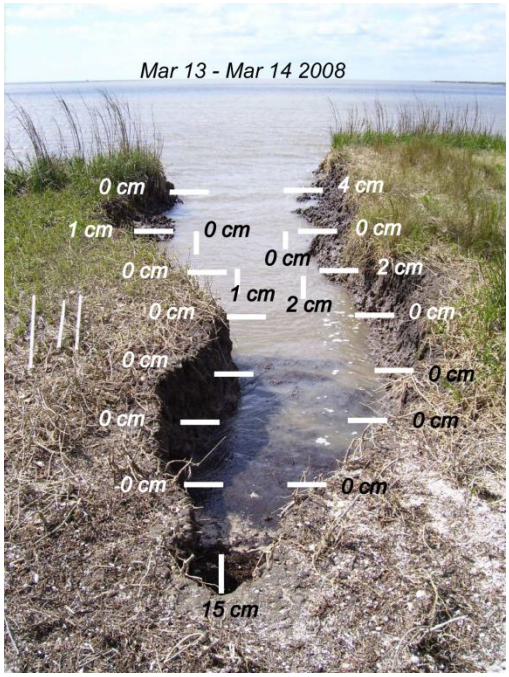

Figure 2.3. Lateral, headward, and vertical erosion in gully 3 measured with erosion pins from 03/12/08 to 03/15/08.

(data for gully ends were not collected over the first 24 h). Thus, the average incision rate at the gully heads was about five times greater than that measured at the gully ends.

A similar erosion pattern emerged over a two month timescale. From 1/17/2008 to 3/12/2008, the average erosion at the gully heads was about 110 cm. In contrast, the gully ends eroded only an average of 26 cm over the same time period, again with considerable variability (see Fig. 2.2B). Thus, similar to before, the erosion rates were four times greater at the gully heads than the gully ends. However, in the two following days, the incision rate was only about 1.5 times the erosion that occurred at the gully ends. We speculate that this was due to the large accumulation of shell hash within the gullies

(especially at the heads), deposited after a small storm event, which acted as a buffer against further wave attack.

Spatially distributed measurements in gully #1 from March 13th to March 14th, 2008, show that the erosion occurred mostly at the gully head (15 cm), with very limited lateral widening and deepening at the gully entrance (between 1 and 4 cm) (Fig. 2.4).

In general, we hypothesize that the convergent geometry of the gullies will always give rise to differential erosion rates between the gully heads and ends. The variability in the erosion rates are probably due to differences in gully slope, gully geometry, presence or absence of a vertical scarp, and presence or absence of scouring agents such as shells, which may either enhance or delay erosion depending on the thickness of the deposits.

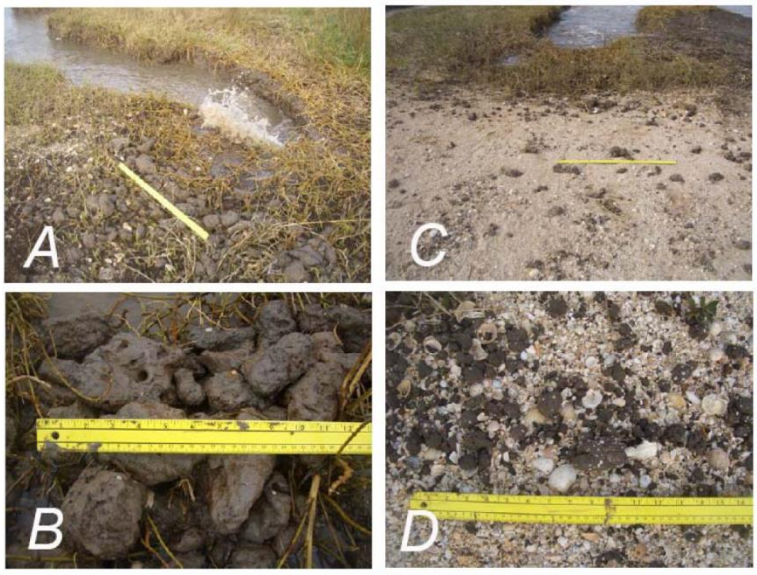

Figure 2.4. Size of mud ball measured near different gully heads: (A) gully 3, (B) gully 4, (C) gully 5, and (D) gully 6. The photographs were taken on January 16, 2008. In (C) and (D) the mud balls are mixed with shell fragments deposited on the platform from waves hitting the gully head. Size variations may reflect variations in intensity of wave impact.

Gully incision into the marsh platform by direct wave impact (versus some other mechanism such as overmarsh drainage) was evident from the accumulation of "mud balls" on the marsh platform adjacent to the gully head. Mud balls are the eroded fragments of cohesive mud detached from the head and side walls of the gully through hydraulic action when water is forced into cracks and fissures as a result of wave impact (Fig. 2.4A–D). The mud fragments are then rolled across the gully floor by subsequent waves, assuming a rounded shape. When the water splashes against the gully head, it can carry, and subsequently deposit on the marsh platform, both reworked pieces of detached mud (mud balls) and shell fragments (Fig. 2.5). The mud balls ranged in size from 10–15 cm near gully #3 to 2–3 cm near gully #6, beyond which they did not exist. The size of the mud balls may give a qualitative indication of the forces acting upon the gully head, which are probably influenced by the gully geometry and bottom slope. In fact only if the wave velocity is high enough will large mud balls be detached and lifted on the platform. For example, the geometries and slopes of gullies #4 and #5, which are broad at the head and have slopes of about 10°, would dissipate wave energy much more than that of gully #3, which is narrow, convergent at the head, and has a slope of about 70°.

2.4.2 Gully morphometric analysis

Measurements of basic geometric aspects for gullies #3–10 are given in Fig. 5, and refer to the date 01/15/08. The widths and lengths of the first two gullies were not reported since their boundaries were not well-defined (see Fig. 2.2). The spacing between each gully was quasi-periodic, particularly after gully #3, and was found to be about 8 m

on average (Fig. 2.5A). Gully width tended to increase from 2 m at gully #3 to 7 m at gully #6, and then remained nearly constant at 5 m with a slight decrease to 4 m at gully #10 (Fig. 2.5B). The gully lengths consistently increased, at first gradually from 11 m at gully #3, to 13 m at gully #6, while the lengths of gullies #7–10 increased much more rapidly from 13 m to 19 m (Fig. 2.5C).

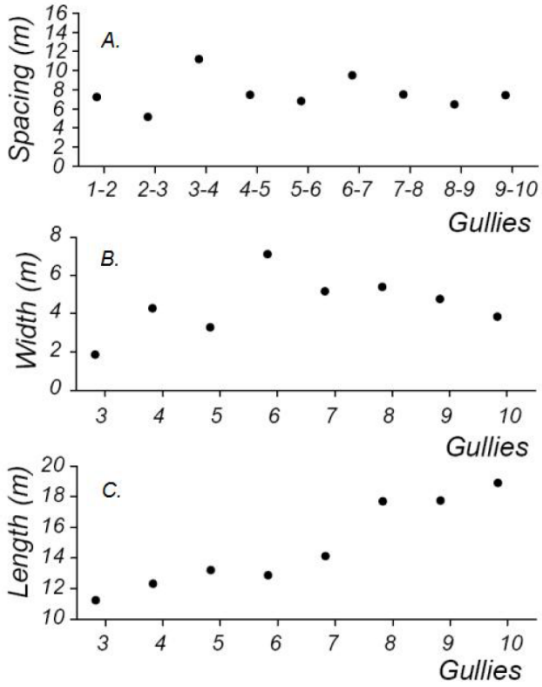

Figure 2.5. Spacing, width and length of the wave gullies indicated in Figure 2. Spacing is defined as the distance between two adjacent gullies. Gullies 1 and 2 were omitted given their small dimensions without a defined geometry.

Furthermore, the marsh surface progressively deflated from gully #3 to gully #10. Figure 2.6 shows elevation measurements taken at the surface and floor (labeled top and bottom in Fig.. 2.6A, respectively) of each gully at the heads, sides, and ends. The bottom elevations measured across the gully heads on 01/14/08 showed a linear decrease

from about −0.4 m to −0.8 m (black dots, Fig. 2.6A) while measurements taken from the gullies' sides also showed no general trend, although there was considerable variability. This is in contrast to bottom elevations measured across the gully entrances (Fig. 2.6D), which are more or less constant around−1.0 m to −1.2 m below the reference surface. Measurements of the upper surface taken near the same locations have distinct differences, which are apparently related to the presence or absence of vegetation. There is a marked decrease in elevation at the transition from vegetation to no vegetation, which occurs at gully #6 (white squares, Fig. 2.6A–F). This drop in elevation was measured to be nearly double at the sides and ends (~40 cm), than what was measured at the heads (~20 cm). Additional measurements collected on 03/13/08 highlight the evolution of gully geometry. Vegetation was stripped between gullies #5 and #6, leading to the erosion of the bare marsh platform (Fig. 2.6D). The gully floor decreased both at the end (Fig. 2.6F) and at the sides of the gullies (Fig. 2.6D), with a higher floor erosion for gullies #8–10. On the contrary, the elevation of the gully floor increased at the gully head in all gullies (Fig. 2.6B), and was accompanied to a slight increase in marsh elevation in front of the marsh head for gullies #8–10. This elevation increase was due to accumulation of shell fragments within the gully head and on the surrounding marsh platform (Fig. 2.2B).

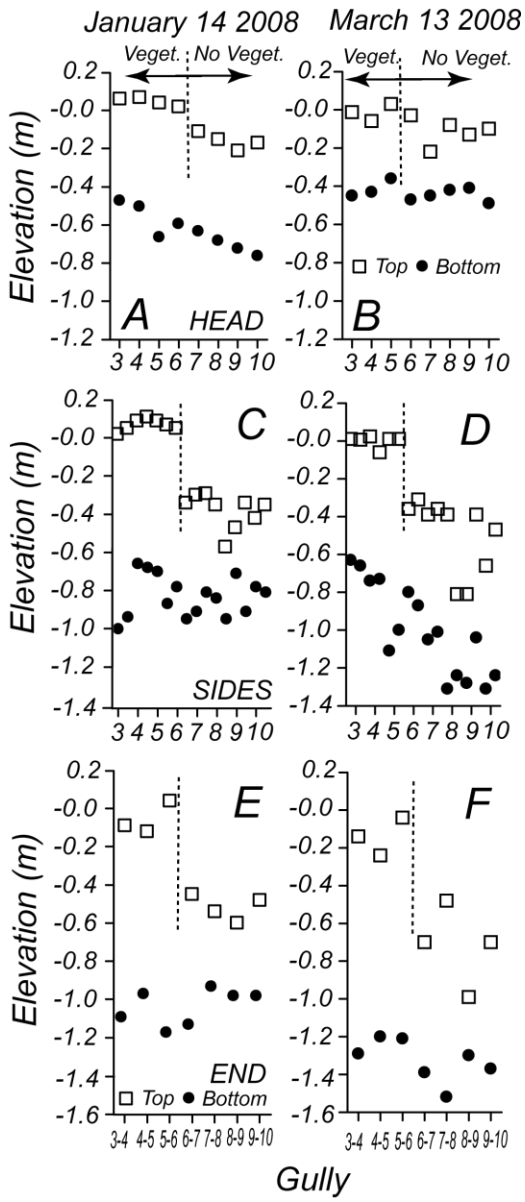

Figure 2.6. Elevation of the marsh platform and gully bottom at the gullies' heads on (A) 01/14/08 and (B) 03/13/08; at the gullies' sides (C) 01/14/08 and (D) 03/13/08; and at the gullies' ends on (E) 01/14/08 and (F) 03/13/08. A dotted vertical line separates the vegetated marsh platform from the unvegetated marsh bare platform. The reference elevation is the average elevation for the vegetated marsh platform.

We also measured the slope of the head scarp from the gully floor to the marsh platform, and the basal slopes of the gully floors along their lengths to determine trends

in slope evolution. Both in January and March the upper slopes display an increasing trend from gully #3 to gully #10, although with large variations (Fig. 2.7A–C). In contrast, the basal slopes generally decreased from gullies #1–10 in January (Fig. 2.7C); however, this trend was reversed in March (Fig. 2.7D) because of the accumulation of shell fragments at the gully head (see Fig. 2.2B).

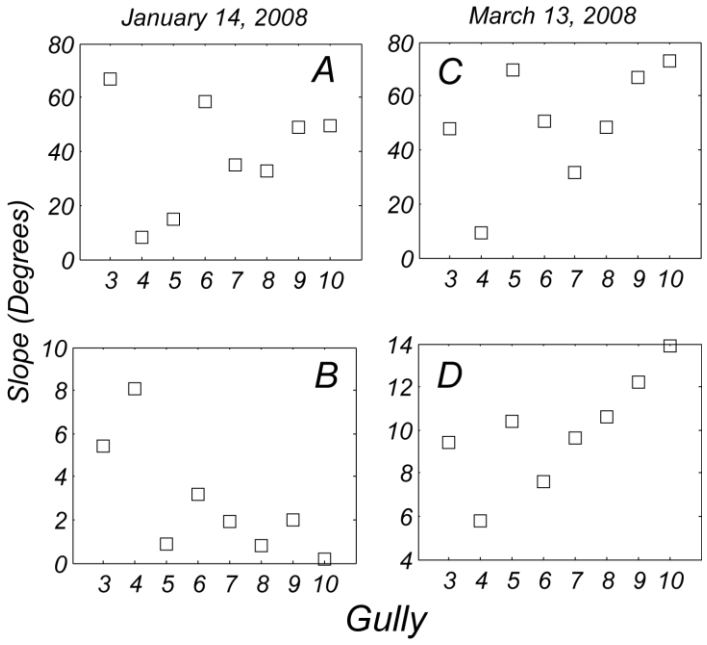

Figure 2.7. Slope of gullies' heads (inclination of the marsh scarp from gully floor to marsh platform) on (A) 01/14/08 and on (C) 03/13/08; basal slopes of the gullies' floors (inclination along the gully length from gully head to gully end) on (B) 01/14/08 and on (D) 03/13/08. The trend inversion of basal slope from 01/14/08 (B) to 03/13/08 (D) is due to shell accumulation near the gullies' heads (see also Figure 2B).

We then explored a possible correlation between erosion rates and the slope of the gully scarp and gully bottom (basal slope). On January 14–15th, when the gullies were flushed and without shell fragments at the bottom, the erosion rate qualitatively correlated to scarp slope (Fig. 2.8A) and to basal slope (Fig.. 2.8B); therefore, a steep

scarp at the gully head may favor erosion. On March 13–14th most of the gully heads were clogged by shell fragments deposited during previous storms (Fig. 2.2B). The shell deposits increased the elevation of the gully bottom, resulting in higher slopes. Under these conditions, the erosion rate is inversely proportional to both the scarp and the basal slopes (Fig. 2.8C, D), since these slopes were related to thick shell deposits that shelter the gully heads, which prevented erosion.

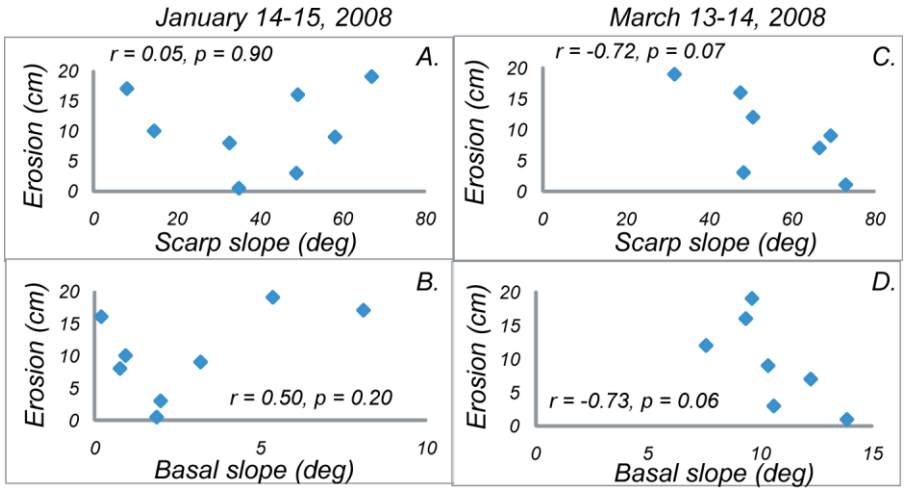

Figure 2.8. Slope of gully head (inclination of the marsh scarp from gully floor to marsh platform) compared to head erosion for the time periods (A) 01/14/08 to 01/15/08, (C) 03/13/08 to 03/14/08. No erosion data for gully 4 during March, thus it was not included in (C) and (D).

2.4.3 Gully morphology changes

To capture changes the gully's morphology, we compared two digital elevation models (DEMs) created from data collected two months apart in gully #3, on 01/14/08 and on 03/13/08 respectively (Fig. 2.9). The gully is a v-shaped, relatively narrow channel that exhibits a curved habit at its apex with a scarped upper slope and gentle basal slope.

Comparing the DEMs in Figures 2.9A–B, it is clear that the gully retained its basic morphology but the dimensions have changed considerably. The total amount of incision into the marsh was approximately 1.5 m, giving an average incision rate of about 2.5 cm/day, while the narrowest reach of the gully widened by nearly 2 m (Fig. 2.7C). Likewise, the extent of terracing had increased as well (shown in green in Fig. 2.7B).

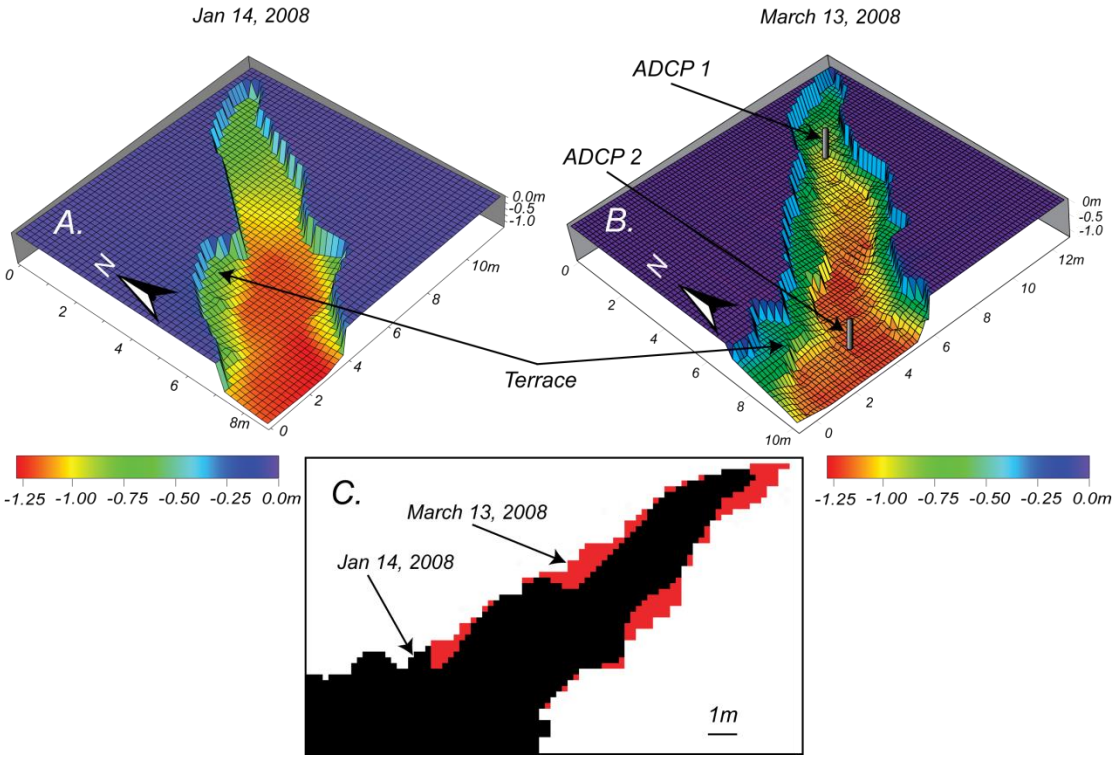

Figure 2.9. Geometry of wave gully 3 on (A) 01/14/08 and on (B) 03/13/08. The lateral erosion of the marsh platform that occurred during this period is reported in red in (C). The location of the two ADCP's located in the gully is reported in (B).

2.4.4 Wave analysis

The offshore wind and wave climate from the ADV data is reported in Figure 2.10. On February 5th, 2008 the ADV frame collapsed and wave recording ceased (Fig. 2.10). The instrument was recovered on February 19th. As a result, wave data in the bay

in front of the channel mouth are available only until February 5th. During the time for which we had successful deployment of the ADV, we noted several events that produced Hs > 0.5 m (Fig. 2.10). These events are generally correlated with sustained wind speeds exceeding 5 m/s and wind directions between 100° and 275° from north (Fagherazzi and Priestas, 2010). Such wind events are in fairly good agreement with the recorded wave data; however, this is not always true (e.g., the period near December 17th and December 30th; see Fig. 2.10). Winds from the northwest to northeast generally do not produce significant wave events.

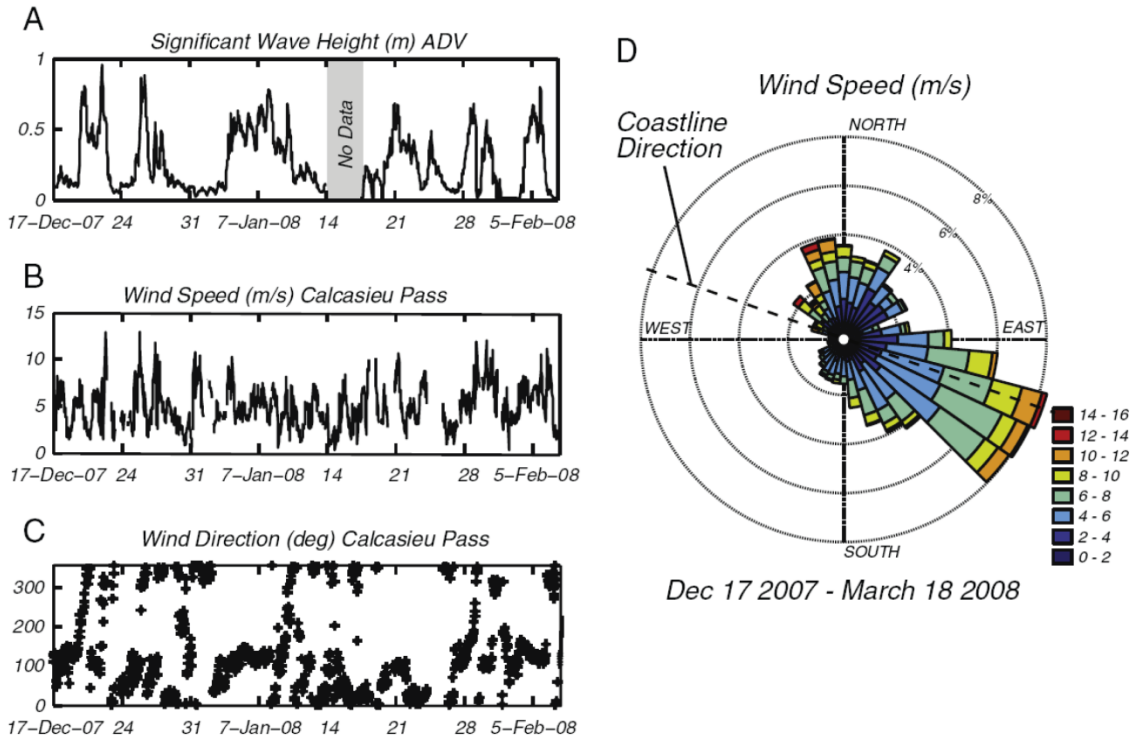

Figure 2.10. (A) Significant wave height measured in the bay in front of the wave gullies from 12/17/07 to 02/19/08; (B) wind speed and (C) wind direction measured at Calcasieu Pass (NOAA station 8768094) during the same period. (D) Distribution of wind intensity and direction at Calcasieu Pass, LA from December 17, 2007 to March 18, 2008.

The recorded wave bursts from ADCP-1 and 2 are shown in Figure 2.11 along with the time positions of selected wave bursts. The ADCP deployment covered three tidal cycles from March 11th to March 14th, 2008. A small storm surge associated with a frontal system moved through the study area during the end of the deployment as indicated by higher water levels and wind conditions for that time period, as can be seen in Figure 2.11.

Waves entering the gully from the embayment are typically small (H_s < 20 cm; see Table 1); however, the significant wave heights and, more importantly, wave velocities were found to increase as they propagated through the increasingly narrow gully from ADCP-2 to ADCP-1 (see Fig. 2.7). Data analyzed from ADCP measurements illustrates the degree to which wave heights and velocities increased for the wave bursts indicated in Figure 2.11 during high tide conditions (Table 1). Exposure of ADCP-1 during low tides resulted in erroneous data. Consequently, data were not included for analysis if water depths recorded at ADCP-2 were less than 35 cm, nor if they met the breaking wave condition (Komar 1976), namely, if the Hs of ADCP-2 was greater than 80% of the depth at ADCP-1. Significant wave heights entering the gully ranged from 6 cm to 22 cm (Table 1), the largest of which occurred during the small storm tide near the end of the deployment period (see Fig. 2.11). The increase in Hs from ADCP-2 to ADCP-1 was minor, typically 2–4 cm (see Table 1).

Table 2.1. Waves and swash characteristics measured at two locations (inner and outer, see Figure 9B) in gully 3. The data refer to selected wave bursts indicated in Figure 11A. $\bar{U}_s$ is the average of the one-third highest velocities in the gully during a wave burst (averaged over water depth), whereas $\bar{U}_{50}$ is the average of the highest half.

	Burst 6		*Burst 33*		*Burst 50*		*Burst 84*		*Burst 100*		*Burst 134*	
	OUTER	*INNER*	*OUTER*	*INNER*	*OUTER*	*INNER*	*OUTER*	*INNER*	*OUTER*	*INNER*	*OUTER*	*INNER*
H_S *(cm)*	7	8	6	8	8	9	10	14	9	13	20	22
H_{mean} *(cm)*	4	6	4	6	6	5	7	10	6	9	14	15
H_{10} *(cm)*	8	10	7	9	10	13	12	17	10	16	23	26
H_{max}*(cm)*	9	11	9	12	12	15	15	20	12	19	28	27
T_{mean} *(s)*	5	7	3	5	3	5	4	5	3	4	5	6
T_S *(s)*	7	9	4	6	3	8	6	7	4	5	6	8
$\bar{U}_S$												
Run-up (cm/s)	25	40	24	33	47	38	29	40	23	32	46	100
Return (cm/s)	-22	-53	-27	-32	-37	-31	-29	-46	-30	-38	-50	-80
$\bar{U}_{50}$												
Run-up (cm/s)	22	31	21	27	41	32	25	35	19	27	40	87
Return (cm/s)	-19	-41	-24	-27	-32	-27	-25	-38	-26	-32	-43	-69

Bottom velocities increased between ADCP-2 and ADCP-1 because of shoaling. Since the velocity in the gully (ADCP-1) was predominantly along the axial direction (average angle of 1.6° with respect to the gully axis oriented toward the gully apex and standard deviation of 36.7°), the significant velocity term ($\bar{U}_s$) is further separated into "run-up" and "return" velocities. The run-up velocity ($\bar{U}_{s+}$), with a direction ±37° with respect to the gully axis, implies a shoreward flow direction, while the return velocity ($\bar{U}_{s-}$) with a direction between 143° and 217° with respect to the gully axis, implies a seaward flow direction. We investigated the percent change in velocity between the two ADCPs as a function of basic wave parameters (Fig. 2.12). Thus, a negative percent change in velocity implies a decrease in velocity from ADCP-2 to ADCP-1, while a positive percent change implies an increase in velocity across the same distance.

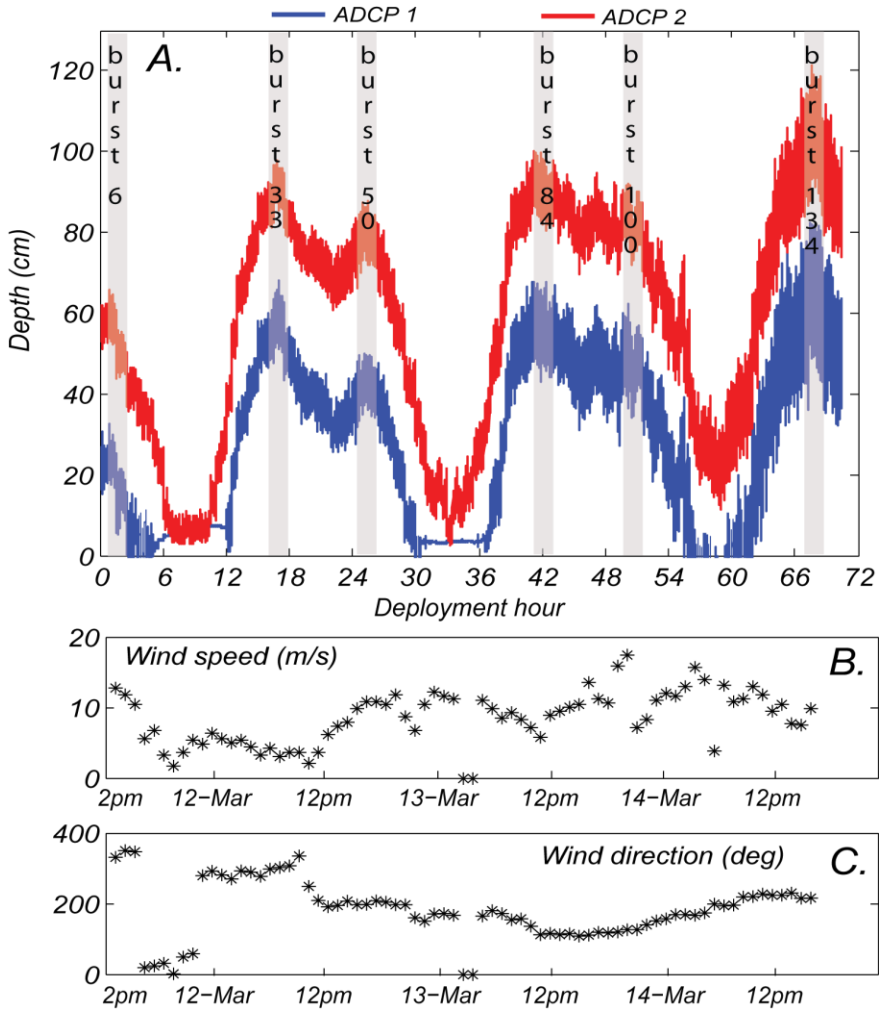

Figure 2.11. (A) Time series of pressure-corrected water elevation at the gully head (ADCP-1 in blue) and the gully entrance (ADCP-2 in red); ADCP-1 is closer to the gully head and therefore in shallower water (see Figure 9). Burst intervals used for the parameters given in Table 1 are also highlighted. (B) Wind speed and (C) wind direction measured at Calcasieu Pass (NOAA station 8768094) during the same period.

Figure 2.12A reports the percent change in velocity as a function of the ratio of significant wave height of ADCP-1 to ADCP-2. The plot illustrates that an increase in run-up velocity and an increase in return flow velocity occurs when H_s(ADCP-1)/H_s (ADCP-2) > 1. In other words, conditions which result in the amplification of wave height between the entrance and head of the gully tend to produce an amplification of

run-up velocity (and subsequent increased return flow velocity measured between ADCP-1 and ADCP-2). The converse is also apparent in Figure 2.12A; there tends to be a decrease in velocity when conditions occur such that H_s (ADCP-1)/H_s (ADCP-2) < 1. In Figure 2.12B, the ratios of the significant wave periods are plotted against the percent change in velocity. Here, a percent increase in run-up velocity between ADCP-2 and ADCP-1 exists if the ratio of the periods is between 1 and 1.6 — in other words, if the period measured at ADCP-1 is at most 60% larger than the period of the incoming waves. This condition occurs if the period of the incoming wave is about 4 s or greater (Fig. 2.12C), thus higher frequency waves results in a net decrease in run-up velocity. Additionally, an increase in run-up velocity mostly occurs if H_s > 8 cm (Fig. 2.12D), though there appears to be no threshold value since the velocity trends depend on the interaction of incoming and reflected waves as a function of water depth, wave height, and wave period. Water depth may play a key role. The highest percent velocity increases corresponded to the greatest water depths, on average. Furthermore, we noted a threshold water depth of 80 cm (measured at ADCP-2) above which the percent change in water velocities were mostly positive, and below were mostly negative.

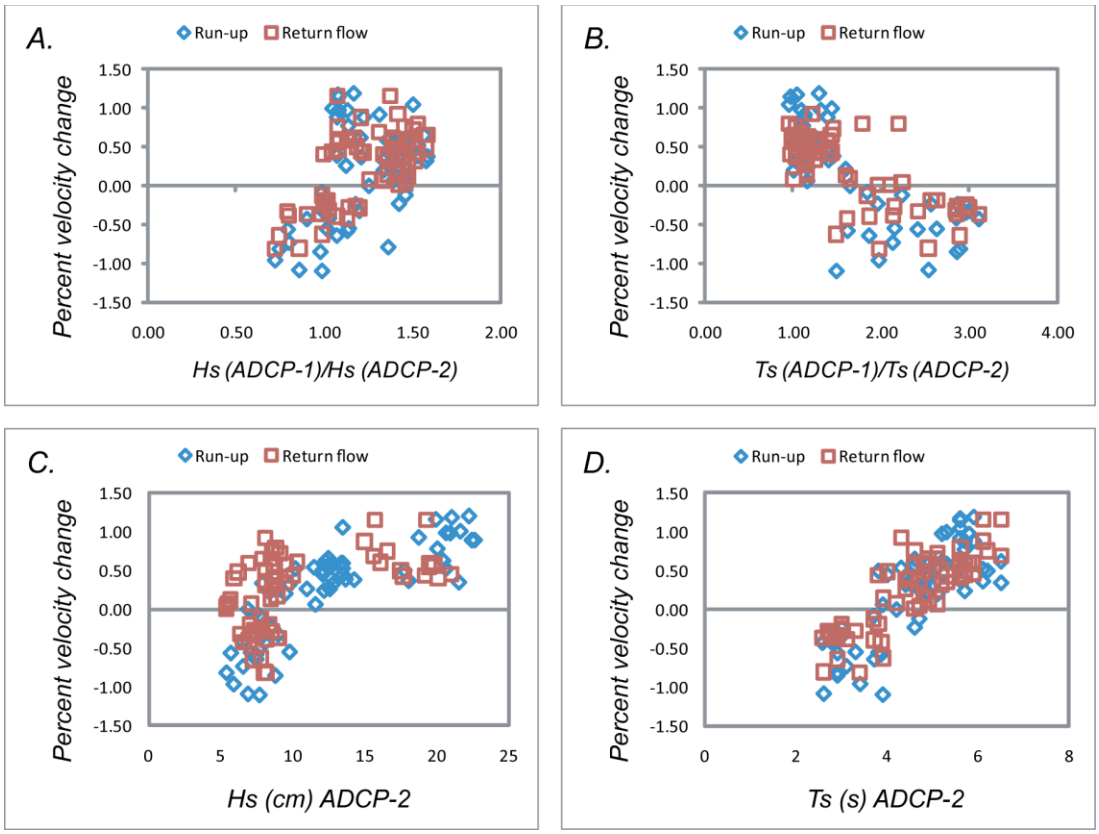

Figure 2.12. (A) Variations in velocity between ADCP-2 and ADCP-1 as a function of relative difference in significant wave height for wave bursts indicated in Figure 11. The data are separated between run-up and return flow velocities; (B) variations in velocity between ADCP-2 and ADCP-1 as a function of relative difference in peak wave period; (C) variations in velocity between ADCP-2 and ADCP-1 as a function of significant wave height of the incoming waves (measured at ADCP-2); (D) variations in velocity between ADCP-2 and ADCP-1 as a function of peak period of incoming waves (measured at ADCP-2).

2.5 Discussion

2.5.1 Wave-gully hydrodynamics

Based on a sequence of photographs during the wave event of March 14th, 2008 we can present a conceptual model of wave gully evolution (Fig. 2.13). An incoming wave propagating from the nearby bay enters the gully (Fig. 2.13A). Given the right

conditions of wave height, period and water depth, the wave is slightly magnified in the gully (Fig. 2.13B). We propose that two separate mechanisms can increase wave height: shoaling due to a reduction in water depth in the gully and compression of wave crest due to the convergent geometry. We further believe that the second process is by far more important than the shoaling effect. An increase in wave height and, more importantly, a decrease in water depth lead to an increase in bottom velocities up to at least 1 m/s (Table 1). Note that ADCP-1 was deployed 2 m from the gully head to avoid the very strong currents produced there by waves (Fig. 2.9B), and therefore we expect the swash velocity to increase even more at the gully head. The fast flow hits the gully head with considerable strength (Fig. 2.13C), detaching bank material and triggering headward erosion (Fig. 2.2). The splashed water spills over from the gully, flooding the surrounding marsh platforms (Fig. 2.13D).

After the reflection of the wave, water is drained into the gully from the marsh platform giving rise to a return flow (Figs. 2.13 E, F and Table 1). Measurements of wave characteristics within the gully indicate that the fast run-up is preferentially triggered by intermediate waves (period 4-6 sec.) rather than by short waves (period 2-4 sec.) (Fig. 2.12 C). Low water conditions in the gully dissipate wave energy thus reducing the speed of the wave run-up; therefore the highest swash velocities occur for intermediate water depths in the gully. Relatively common meteorological conditions during winter storms (wind speed around 10 m/s) are sufficient to trigger waves in ocean that then propagate in the gullies causing fast headward erosion (Fig. 2.10).

Wave energy becomes more concentrated in v-shaped gullies, the magnitude of which may depend on reflective or dissipative conditions within the gully such as a shallow or steep slope, and the presence or absence of a scarp, respectively. This may explain why gully #3 was observed to have the highest incision rates. Based on these observations, we conclude that the dominant phase in the process of gully formation occurs when the fast incoming flow hits the gully, rather than during the return flow which occurs when water is drained from the marsh platform into the gully. Therefore, wave gullies are fundamentally different from tidal creeks (D'Alpaos et al., 2005) and tsunamigenic return channels (Fagherazzi and Du, 2008) which are drainage features. They resemble instead the flood scours that indent levees of existing tidal channels and bays during tsunamis (Fagherazzi and Du, 2008).

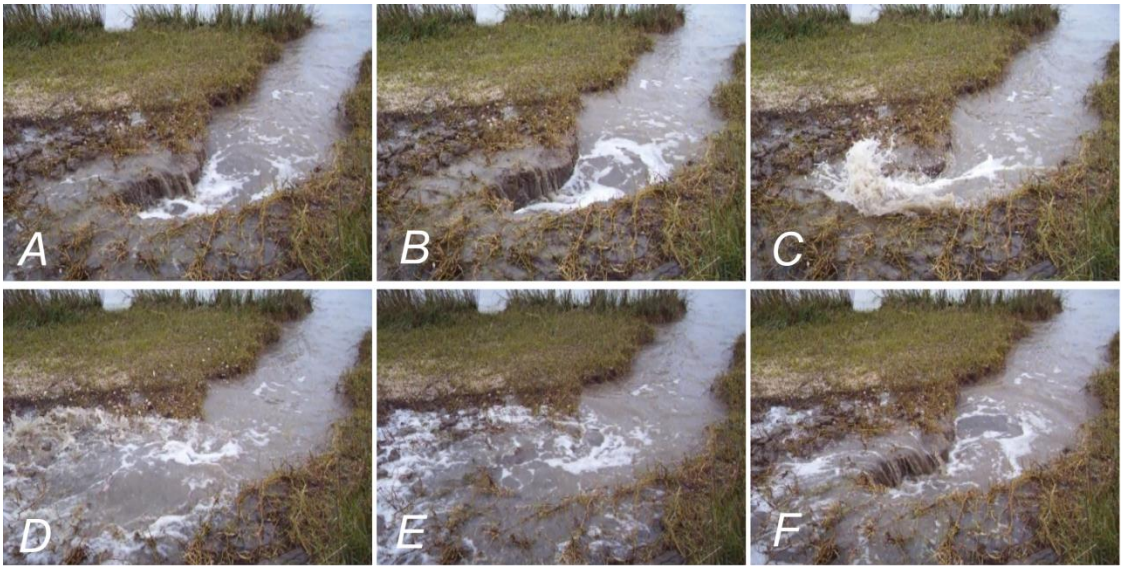

Figure 2.13. Snapshots of a wave propagating in wave gully 3: (A) small wave enters the gully; (B) wave crest in the middle of the gully showing wave setup; (C) wave impact at the gully head and peak force; (D) overmarsh flooding; (E) and (F) return flow into the gully.

2.5.2 Morphodynamic evolution of wave-gullies

We hypothesize that the gullies developed sequentially from west to east (#10 to #1) along the shoreline (Fig. 2.14). As the shoreline retreated nearly 100 m between 1998 and 2004 the channel mouth had widened to the point to allow waves to impinge in the outer bank of the meander (near gully-10 in Fig. 2.14). Continued erosion of the shoreline and the eastward retreat of the spit caused the channel mouth to become an embayment allowing for more exposure of the channel bank to wave attack. The increasing trend of the length and width of the gullies (Fig. 2.5A–B) is related to the total period of wave exposure. As the spit retreats, a new section of marsh is attacked by vigorous waves which form a gully. The gully then increases in length after subsequent wave events. Therefore gully #10 is the oldest and has been subject to wave erosion for the longest period, since it was the first to lose the sheltering effect of the spit. Conversely, the incipient gully #1 is the youngest, since the spit is still protecting this marsh location from wave attack.

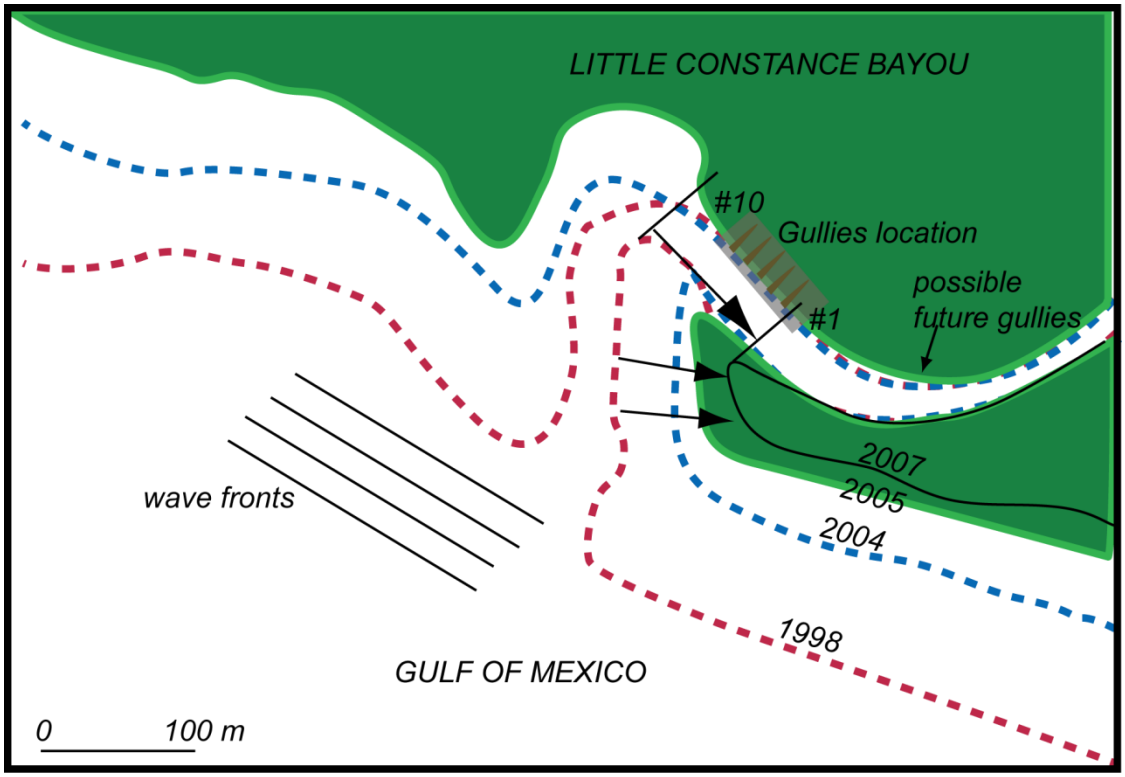

Figure 2.14. Evolution of the chenier plain shoreline at the study site from 1998 to 2007. The location of the present gullies is indicated. Coastline extracted from four aerial photographs, USGS 1999, USDA Farm Service Agency 2004, 2005, and 2007.

There is a substantial increase in gully width from gully #3 to gully #6, while gullies #7–10 are more uniform (Fig. 2.5). This is probably due to loss of vegetation cover on the gully sides, triggering an increase in vertical erosion and a decrease in lateral widening. In fact, lower gully sides might attenuate the wave impact and reduce the funneling effect.

We can then apply the ergodic principle and substitute space with time in order to reconstruct the evolution of the wave-gullies. As a result, the sequence of photographs in

Figure 2.2 can be seen roughly as the evolutive trajectory of a gully in time, likely on the order of months.

The conceptual model is summarized in Figure 2.15. A cohesive, vegetated scarp bordering a salt marsh (Fig. 2.15A) is attacked by waves that remove the vegetation in selected points (Fig. 2.2 photos 1, 2 and Fig. 2.15B). At these locations, waves with sufficient energy (H_s of ~20 cm or more) impose a mechanical loading to which gullies develop, incising the marsh boundary (Fig. 2.15C). The gullies grow in length, and partly in width, under the attack of waves during normal and storm conditions (Fig. 2.5 and Fig. 2.14D). The greatest headward erosion seems mainly connected to the convergent geometry of the gully, but also to the slope of the gully floor (Fig. 2.8B), with young and steep gullies eroding faster (Fig. 2.8B). Although the results in Figure 2.8A are inconsistent, we observed that the impact force of waves upon the gully head seemed considerably higher for gullies with steep head scarp slopes. In time, the gully bottom deepens until reaching the elevation of the bay (compare Fig. 2.6C, D and E, F). It is likely that the combined effect of wave shoaling, wave breaking, and oscillatory motion eroded the gully floor, most of which occurred in the shallow area near the gully head where bottom shear stresses are the greatest, and where wave breaking occurs during lower to mid tidal elevations.

Waves then remove the vegetation from the marsh between the gullies, stripping the entire area probably on the order months after exposure to waves (Fig. 2.2 photos 4–10, Fig. 2.6 and 2.15E). Once the platform is bare, waves corrode the muddy substrate in a short period, since vegetation is not offering protection anymore (Fig. 2.15F). Now two

possible scenarios take place: i) a new scarp develops near the gully heads while the remnant marsh between the gullies is completely destroyed. In this case, the original scarp presented in Figure 2.15A is recovered and the cycle of wave gully erosion can start again (Fig. 2.14E); ii) the entire area dissected by the gullies erodes forming a ramp without a distinctive scarp. In this case, the marsh boundary evolves into a mud beach, common along the Louisiana coastline, with waves breaking and shoaling on it; in the latter case gullies do not form again.

A key factor for the formation of wave gullies is then the presence of a steep scarp composed of cohesive material. Since the driving forces are wind waves, a second critical factor is the presence of relatively deep water in front of the scarp (at least 50–100 cm) so that the waves can propagate to the scarp and erode it. All of these elements are typical of marsh boundaries, where often halophyte vegetation, combined with fine sediments and organic material, give rise to vertical scarps that emerge from subtidal flats.

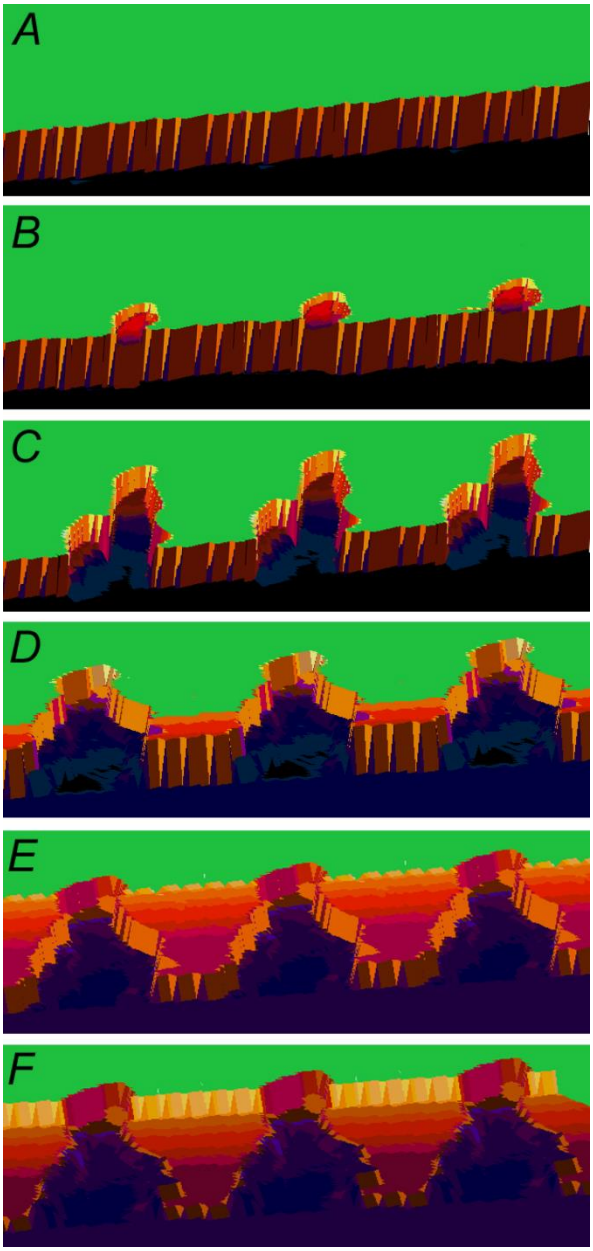

Figure 2.15. Schematic evolution of wave gullies: (A) vegetated scarp at the marsh boundary; (B) waves remove the vegetation in selected locations creating incipient gullies that are more vulnerable to wave attack; (C) wave gullies develop, incising the marsh platform; (D) the gullies lengthen and widen under wave attack ; (E) high water waves and overmarsh flooding remove vegetation from the marsh platform between the gullies; (F) once the platform is bare, waves corrode the muddy substrate in a short period of time resulting in rapid platform deflation.

2.5.3 The role of shell fragments

The simplified model presented in the previous paragraph is complicated by the role of shell fragments. Chenier plains are composed by narrow ridges of sand and shells alternated with fine sediment deposits (Otvos and Price 1979). Typically, shells form a bar on the foreshore that then migrates landwards through swash action. During storms, waves rework the shells creating ridges at the shoreline (Woodroffe et al., 1983). Our survey in March 2008 indicates that all gullies were filled with shell fragments near the head (Fig. 2.2B). Swash movement and splashing against the gully walls deposited some of these fragments on the marsh platform near the gully heads (Fig. 4). Shell deposits changed the elevation of the gully floor at the head (Fig. 2.6B) and the slope of the gully floor (Fig. 2.6D); however, these fragments seem to have an ambivalent role in gully erosion, supported by a lack of correlation between the deposits and headward erosion (Fig. 2.8D, where the basal slope is a proxy for the thickness of shell deposits). In fact, shell fragments could easily become abrasive tools thus enhancing the erosion of the mud (which was the case for the first two data points in Fig. 2.8A), or if deposited near the head they could shelter the marsh boundary from wave action (Fig. 2.8C). The fact that thick layers of shell fragments were found on the marsh platform indicates that this material was remobilized by the swash flow and splashed with energy against the marsh scarp.

More research is needed to fully unravel the feedbacks between shells and mud, although we believe that the relative mobility of the fragments during a storm event

determines whether they enhance or reduce erosion—this may also be the case for sand deposits.

2.5.4 Implication for the erosion of marsh boundaries

The formation of wave-cut gullies underscores the non-uniform erosional nature of muddy coastlines. The variation in the erosion rates in the ten wave gullies may be explained by simply noting that the mud here is very cohesive which promotes this style of erosion; thus, in those places not scoured by shells, relatively large portions of mud could be removed abruptly.

The rate of erosion of the gully head is three to four times higher than the rate of shoreline retreat, i.e. the frontal erosion of the marsh platform between the gullies (Fig. 2.2). As a consequence, wave gullies accelerate marsh deterioration by first dissecting the marsh and weakening the platform so that waves can destroy the marsh platform between them. Marsh boundaries characterized by wave gullies are thus fast eroding, and the process of wave energy concentration that forms them is key for the evolution of the entire intertidal landscape.

The manifestation of wave-cut gullies appears to be quite common along the leading edges of salt marshes, although their spacing and geometric aspects differ among physiographic settings. As noted before, the (possibly episodic) retreat of the spit in this study site could explain the spacing of these gullies. Every time a large storm erodes the spit, a new part of marsh bank is exposed to wave action which triggers the formation of

a new gully. The gully spacing is, therefore, just an expression of the frequency of storms causing the retreat of the spit. However, we have recognized similar spacing patterns based on our ongoing work in Virginia, and evidence from the work of others. For example, gullies were observed as "points and cuts" along the eroding edge in Galveston Bay, Texas (Hall et al., 1986), and as "v-shaped notches that cut into an initially straight shoreline" in Rehoboth Bay, Delaware (Schwimmer, 2001, p. 672). Likewise, they are further observed in abundance along the marsh shorelines of Hog Island Bay, Virginia, and to a lesser extent in Plum Island Sound, Massachusetts (unpublished data). It is important to mention that the quasi-periodic (as opposed to periodic) spacing is probably because of the ability of gullies to merge and destroy themselves resulting in a new geometry.

While we offer a general conceptual framework for the evolution of wave-cut gullies, the forcing mechanism that leads to their initial formation is currently not understood. It seems clear, however, that their formation has two basic requirements: 1) they develop along the scarped edges of cohesive mud substrate, and 2) there must be waves large enough (H_s > ~20–30 cm) to impact the scarp with enough force to remove material. It follows, then, that gullies will not form in those areas with very shallow offshore slopes due to wave energy dissipation despite the presence of relatively large waves (which is the case for the rest of the shoreline adjacent to the gullies location as shown in Fig. 1), or in those locations that are insufficient for wave development (small fetch, low water, etc.). Whatever mechanism is invoked to explain the initiation of wave-cut gullies, it must be able to explain their observed quasi-periodic spacing.

One possible explanation for the initiation of gullies is that of a self-organizing process whereby incident waves impinge upon a scarped edge containing small perturbations and irregularities. Removal of the cohesive substrate enlarges and merges the perturbations until they grow to an extent that waves become concentrated and gully development begins (as perhaps was occurring for gullies 1 and 2; see Fig. 2.2). The size and spacing of gullies could be related to the strength of the eroding material relative to the wave power. Indeed, it may be reasonable to think that notches and coves carved into coastal bluffs are, in fact, wave-cut gullies. Thus, relatively small waves would produce small, closely spaced gullies in geologically soft materials, while much larger waves would produce larger (and more stable) gullies in geologically hard materials with less frequency. However, it appears that most coastal coves have a non-converging geometry at their heads, thereby dissipating energy across widening wave crests, though this configuration could be the natural end product for geologically hard materials; i.e., the development of a diverging head, and a ramped configuration with a protective sand cover.

Another possibility may be that gullies are initiated from the development of edge waves. Edge waves are often cited to explain rhythmic cuspate shoreline features as various spatial scales (Guza and Inman, 1975), though this explanation has been a source of contention with some researchers (Coco et al., 1999; Coco and Murray, 2007). The creation of edge waves, especially in reflective settings, set up alongshore velocity fields whereby maximum velocities occur at their anti-nodes (Bowen and Inman, 1971; Guza and Inman, 1975), which may facilitate a rhythmic formation of gullies whose spacing

may depend on the spacing of these anti-nodes. The points of increased velocity may locally denude the marsh platform of vegetation making the substrate more vulnerable to wave attack causing incipient gullies to form (see gullies 1–2, Fig. 2.2A–B). Over time they would enlarge and deepen enough that wave energy is concentrated producing a feedback between gully geometry and wave energy, which would explain the differential erosion rates observed between the gully head and end. We suspect this feedback is abated as the gully geometry widens (especially when gullies merge) and lengthens, and if the gully head becomes ramped versus scarped by gully infilling or otherwise.

The conceptual framework offered does not address wave resonance that is likely occurring within the gully. This is an important issue that needs future attention in order to fully describe wave gully hydrodynamics.

2.6 Conclusions

The following set of conclusions can be derived from our analysis:

1) Erosion of marsh boundaries by wave attack can be concentrated in selected locations giving rise to wave gullies. Wave gullies are triangular features that cut through the marsh scarp and extend in time both in length and width. They may be equally spaced and develop in cohesive scarps.

2) The convergent geometry of wave gullies concentrates the energy of incoming waves and creates a very strong swash with velocities higher than 1 m/s. The resulting flow hits the gully head with considerable strength producing headwater

erosion of up to 20 cm/day under relatively common storm conditions along the Louisiana coastline.

3) Waves of intermediate period (4-6 sec) are magnified in the gullies yielding very strong bottom currents, whereas short period waves (2-4 sec) do not trigger a strong swash flow.

4) Wave gullies begin as small depressions in the vegetation mat covering the marsh platform and then grow in length through headward erosion. While lengthening, they also widen and deepen, reducing the overall bottom slope.

5) In time, waves are able to strip the vegetation from the marsh platform separating the gullies. Once the vegetation is removed, the marsh is easily corroded by waves, so that the entire marsh dissected by gullies is destroyed in a short period.

6) Erosion rates of gully heads are three to five times higher than the uniform erosion of the marsh scarp. Therefore, the processes of wave-crest compression and shoaling in gullies enhance marsh deterioration and must be accounted for, when present, in order to determine the evolution of the entire intertidal landscape.

2.7 References

Baumann, R.H., Day, J.W., Miller, C.A., 1984. Mississippi deltaic wetland survival: sedimentation versus coastal submergence. Science 224, 1093–1095.

Bowen, A.J., Inman, D.L., 1971. Edge waves and crescentic bars. J. Geophys. Res. 76, 8662–8671.

Byrnes, M.K., McBride, R.A., Tao, Z., Duvic, L., 1995. Historical shoreline dynamics along the chenier plain of southwestern Louisiana. Trans. Gulf Coast Assoc. Geological Soc. 45, 113–122.

Cahoon, D.R., Hensel, P.F., Spencer, T., Reed, D.J., McKee, K.L., Saintilan, N., 2006. Coastal wetland vulnerability to relative sea-level rise: wetland elevation trends and process controls. Wetlands Nat. Resour. Manag. 190, 271–292.

Chauhan, P.P.S., 2009. Autocyclic erosion in tidal marshes. Geomorph. 10, 45–57. doi:10.1016/j.geomorph.2009.03.016.

Coco, G., Murray, A.B., 2007. Patterns in the sand: from forcing templates to self organization. Geomorph. 91, 271–290. doi:10.1016/j.geomorph.2007.04.023.

Coco, G., O'Hare, T.J., Huntley, D.A., 1999. Beach cusps: a comparison of data and theories for their formation. J. Coastal Res. 15, 741–749.

D'Alpaos, A., Lanzoni, S., Marani, M., Rinaldo, A., 2007. Landscape evolution in tidal embayments: modeling the interplay of erosion, sedimentation, and vegetation dynamics. J. Geophys. Res. 112. doi:10.1029/2006JF000537.

D'Alpaos, A., Lanzoni, S., Marani, M., Fagherazzi, S., Rinaldo, A., 2005. Tidal network ontogeny: channel initiation and early development. J. Geophys Res. Earth Surface 110 (F2), F02001. doi:10.1029/2004JF000182.

Day Jr., J.W., Reed, D., Syhayda, J., Kemp, P., Cahoon, D., Boumans, R.M., Latif, N., 1994. Physical processes of marsh deterioration. In: Roberts, H.H. (Ed.), Critical Physical

Processes of Wetland Loss, 1988–1994. Final Report. Louisiana State University, Baton Rouge. Prepared for U.S. Geological Survey, Reston, VA.

DeLaune, R.D., Baumann, R.H., Gosselink, J.G., 1983. Relationships among vertical accretion, coastal submergence, and erosion in a Louisiana gulf coast marsh. J. Sed. Pet. 53, 147–157.

DeLaune, R.D., Nyman, J.A., Patrick, W.H., 1994. Peat collapse, ponding and wetland loss in a rapidly submerging coastal marsh. J. Coast. Res. 10, 1021–1030.

Draut, A.E., Kineke, G.C., Huh, O.K., Grymes, J.M., Westphal, K.A., Moeller, C.C., 2005. Coastal mudflat accretion under energetic conditions, Louisiana chenier-plain coast USA. Mar. Geol. 214, 27–47. doi:10.1016/j.margeo.2004.10.033.

Elgar, S., Raubenheimer, B., 2008. Wave dissipation by muddy seafloors. Geophys. Res. Lett. 35, L0611.

Fagherazzi, S., Du, X., 2008. Tsunamigenic incisions produced by the December 2004 earthquake along the coasts of Thailand, Indonesia, and Sri Lanka. Geomorph. 99, 120–129.

Fagherazzi, S., Priestas, A.M., 2010. Sediments and water fluxes in a muddy coastline: interplay between waves and tidal channel hydrodynamics. Earth Surf Proc. Land. 35, 284–293. doi:10.1002/esp. 1909.

Fagherazzi, S.,Wiberg, P.L., 2009. Importance of wind conditions, fetch, and water levels on wave-generated shear stresses in shallow intertidal basins. J.Geophys. Res. 114, F03022.

Finkelstein, K., Hardaway, C.S., 1988. Late Holocene sedimentation and erosion of estuarine fringing marshes, York River Virginia. J. Coast. Res. 4, 447–456.

Gary, M., McAfee Jr., R., Wolf, C.L. (Eds.), 1974. Glossary of Geology, 3rd ed. American Geological Institute, Washington D.C.

Guza, R.T., Inman, D.L., 1975. Edge waves and beach cusps. J. Geophys. Res. 80, 2997–3012.

Hall, S.L., Wilder, W.R., Fisher, F.M., 1986. An analysis of shoreline erosion along the northern coast of East Galveston Bay Texas. J. Coast. Res. 2, 173–179.

Kearney, M.S., Grace, R.E., Stevenson, J.C., 1988. Marsh loss in Nanticoke Estuary, Chesapeake Bay. Geographical Rev. 78, 205–220.

Kirwan, M.L., Murray, B., 2008. Temporary vegetation disturbance as an explanation for permanent loss of tidal wetlands. Geophys. Res. Lett. 35 (24), L24401.

Komar, P.D., 1976. Beach Processes and Sedimentation. Prentice-Hall, Englewood Cliffs, N.J.. 429 pp.

Marani, M., D'Alpaos, A., Lanzoni, S., Carniello, L., Rinaldo, A., 2007. Biologically controlled multiple equilibria of tidal landforms and the fate of the Venice lagoon. Geophys. Res. Lett. 34, L11402.

Mariotti, G., Fagherazzi, S., 2010. A numerical model for the coupled long-term evolution of salt marshes and tidal flats. J. Geophys. Res. Earth Surface 115, F01004.

Mariotti, G., Fagherazzi, S., Wiberg, P.L., McGlathery, K.J., Carniello, L., Defina, A., 2010. Influence of storm surges and sea level on shallow tidal basin erosive processes. Journal of Geophysical Research 115, C11012. doi:10.1029/2009JC005892.

McBride, R.A., Taylor, M.J., Byrnes, M.R., 2007. Coastal morphodynamics and chenier plain evolution in southwestern Louisiana, USA: a geomorphic model. Geomorph. 88, 367–422. doi:10.1016/j.geomorph.2006.11.013.

Mitsch, W.J., Gosselink, J.G., 2000. Wetlands. Wiley, New Jersey. 582 pp.

Möller, I., 2006. Quantifying saltmarsh vegetation and its effects on wave dissipation: results from a UK east coast saltmarsh. Estuar. Coast. Shelf Sci. 69, 337–351. doi:10.1016/j.ecss.2006.05.003.

Möller, I., Spencer, T., French, J.R., Legget, D.J., Dixon, M., 1999. Wave transformation over salt marshes: a field and numerical modelling study from North Norfolk England. Estuar. Coast. Shelf Sci. 49, 411–426.

Morris, J.T., Sundareshwar, P.V., Nietch, C.T., Kjerfve, B., Cahoon, D.R., 2002. Responses of coastal wetlands to rising sea level. Ecology 83, 2869–2877.

Nyman, J.A., Walters, R.J., Delaune, R.D., Patrick Jr., W.H., 2006. Marsh vertical accretion via vegetative growth. Estuar. Coast. Shelf Sci. 69, 370–380. doi:10.1016/ j.ecss.2006.05.041.

Orson, R., Panageotou, W., Leatherman, S.P., 1985. Response of title salt marshes to rising sea levels along the U.S. Atlantic and Gulf coasts. J. Coast. Res. 1, 29–37.

Otvos Jr., E.G., Price, W.A., 1979. Problems of chenier genesis and terminology — an overview. Mar. Geol. 31, 251–263.

Penland, S., Ramsey, K.E., 1990. Sea-level rise in Louisiana and the Gulf of Mexico. J. Coast. Res. 6, 323–342.

Pye, K., French, P.W., 1993. Erosion and accretion processes on British saltmarshes, introduction: saltmarsh processes and morphology, final report, Ministry of

Agriculture, Fisheries and Food, report no. ES19B(1). Cambridge Environmental Research Consultants, Ltd. 42 pp.

Ravens, T.M., Thomas, R.C., Roberts, K.A., Santschi, P.H., 2009. Causes of salt marsh erosion in Galveston Bay, Texas. J. Coast. Res. 25.

Reed, D., 1988. Sediment dynamics and deposition in a retreating coastal salt marsh. Estur. Coast. Shelf Sci. 26, 67–79.

Reed, D., 2002. Sea-level rise and coastal marsh sustainability: geological and ecological factors in the Mississippi delta plain. Geomorph. 48, 233–243.

Schwimmer, R., 2001. Rates and processes of marsh shoreline erosion in Rehoboth Bay, Delaware, U.S.A. J. Coast. Res. 17, 672–683.

Tonelli, M., Fagherazzi, S., Petti, M., 2010. Modeling wave impact on salt marsh boundaries. J. Geophys. Res. 115, C09028. doi:10.1029/2009JC006026.

Turner, R.E., Swenson, E.M., Milan, C.S., Lee, J.M., Oswald, T.A., 2004. Below-ground biomass in healthy and impaired salt marshes. Ecol. Res. 19, 29–35.

Van de Koppel, J., Van der Wal, D., Bakker, J.P., Herman, P.M.J., 2005. Self organization and vegetation collapse in salt marsh ecosystems. Am. Nat. 165, 1–12.

Van der Wal, D., Pye, K., 2004. Patterns, rates and possible causes of saltmarsh erosion in the Greater Thames area (UK). Geomorph. 61, 373–391.

Woodroffe, C.D., Curtis, R.J., McLean, R.F., 1983. Development of a chenier plain Firth of Thames, New Zealand. Mar. Geology 53, 1–22.

CHAPTER 3: COUPLED WAVE ENERGY AND EROSION DYNAMICS ALONG A SALT MARSH BOUNDARY, HOG ISLAND BAY, VIRGINIA

3.1 Introduction

The transition between a lower tidal flat and a higher salt marsh platform can occur as a seaward-ramping profile, which may indicate steady state or accretion conditions, or as an abrupt scarp (or cliff) profile, typically indicative of erosion. Marsh erosion at the leading edge by direct wave impact has long been recognized as a mechanism for marsh loss (Yapp, 1917; Redfield, 1962; Hall et al., 1986; Philips, 1986; Finkelstein and Hardaway, 1988; Allen, 1989; Allen, 2000; Coops et al., 1996; Van der Wal and Pye, 2004; Wilson and Allison, 2008; and many others), though much of the work involved qualitative descriptions of edge erosion and mechanics, and/or quantifying erosion rates through time. In contrast, relatively few studies have quantified the processes governing erosion rates and dynamics, although similar research has been conducted with respect to cliffed, rocky shorelines (Sunamura, 1982).

When discussing the physical processes responsible for scarp erosion, it helps to distinguish between two competing factors, namely, those forces which act to remove material from the scarp, and the resistance of the material to such forces. In general, frictional forces such as those derived from moving parcels of water or sediment, in addition to gravity, are arguably the principal forces at play in the erosion of scarped boundaries. The major frictional forces are a result of either wave action, or current velocities. The frictional forces are modulated by a number of other factors, however,

and while waves, currents, and gravity are the underlying physical processes assumed to be responsible for scarp erosion, the modulating factors and resisting forces are probably responsible for modifying erosion rates.

The basic mechanisms of scarp erosion by wave attack occur by hydrodynamic forces, hydraulic action, and corrasion. Hydrodynamic forces (in this case) involve impact forces and drag and lift forces generated by various styles of both breaking and plunging waves. The impact force on the scarp created during wave breaking can be a factor of 30 times the static pressure of the initial wave height (Lundgren and Juhl 1995). The water velocities induced onto the scarp by breaking waves can also be much higher than the phase velocity of the initial wave (Denny et al. 2003). The combination of wave impact and drag and lift forces in the case of breaking waves is thus amplified and may enhance erosion.

Hydraulic action is the fluid pressure (of air or water) forced in to cavities, cracks, and fissures as a result of wave impact (either breaking or non-breaking). The dynamic pressure exerted inside on the walls of such openings can wedge material off of the scarp face and my help to induce mass wasting events (such as slumping or toppling).

Corrasion is the erosional process whereby sediments entrained in a flow field act as an abrasive agent to effectively remove material from rock or soil. In this case, the tidal flat adjacent to the scarp can contain coarse sand, shell fragments, or even cobbles and boulders. Waves impinging the scarp face can thus be sediment laden causing scouring and enhanced erosion.

The rate of erosion likely depends on soil type, water elevation, and possibly other factors such as vegetation and macrofauna. For example, a study of marsh erosion in Galveston Bay, Texas, by Hall et al. (1986) noted in their conclusions that sites with clay soils eroded less than those with loamy soils. This is in agreement with wave-tank experiments conducted by Feagin et al. (2009) in which they showed that marsh soils with higher sand content eroded more easily, and found that vegetation had no net effect on erosion except that the substrate was held together by a matrix of roots which was winnowed of sediment.

Hall et al. (1986) reported that the passage of Hurricane Alicia (which made landfall 80 km from their study site) did very little to accelerate erosion despite such predictions made by Fisher et al. (1972), and concluded that the high water level brought by storm surge protected the shoreline from edge erosion. This process was confirmed by Tonelli et al. (2010), which demonstrated using a high resolution Boussinesq model that the wave thrust acting on a marsh scarp was greatest when the water level was equal in elevation to the marsh platform, above which the thrust decreases rapidly. Therefore, boundary erosion primarily occurs in a period of storminess when the mean water elevation is between the elevation of the platform and the bottom of the scarp.

Work by McLoughlin (2010) proposed that while wave impact was the chief cause of marsh edge erosion in Hog Island Bay, VA, soil characteristics and crab burrow density were responsible for erosion rate heterogeneity and erosion mechanics between study sites within the bay.

Dissection of the marsh shoreline by wave-cut gullies may also influence erosion rates (Priestas and Fagherazzi, 2011). Wave-cut gullies are sub-triangular features that incise the marsh shoreline due to wave impact along scarped shorelines made of cohesive soils. These are previously noted in the literature as “points” and “cuts” by Hall et al. (1986) and “clefts” and “necks” by Schwimmer (2001).

Analysis of the hydrodynamics within a 10 m gully along the Louisiana coast revealed that run-up velocities increased at the gully head as a result of wave-crest compression owing to the gully’s convergent geometry, and was found to be greatest for intermediate wave periods (4-6 s). Because of the increased energy by wave concentration, erosion at the gully head can be greater than that at the shoreline (Priestas and Fagherazzi, 2011). Therefore, this multitude of factors can lead to significant variability when measuring erosion rates.

Erosion of the shoreline does not always occur by hydraulic action of waves acting on the scarp. High marsh platforms in macrotidal areas tend to have large scarps which are subject to erosion by mass wasting through cantilever and rotational failure (Allen, 1989, 2000). Waves and currents can initiate and accelerate mass wasting by undercutting the base of the scarp, especially through corrasion if sand is present on the adjacent tidal flat. It is not known with confidence whether scarps of cohesive material are inherently stable features in the absence of waves. Stability may depend greatly on the height of the scarp, soil properties, and water content, and therefore is a function of tidal range and soil type. It may also depend on the time scale in which failure occurs. Answering this question has important implications in the hypothesized evolution of a

marsh boundary. For example, the erosion model of Van de Koppel et al. (2005) treats scarps as inherently unstable features capable of retreat without external hydrodynamic forcing, and cites the observed regrowth of vegetation in front of eroding scarps as evidence of this process. In contrast, Mariotti and Fagherazzi (2010) treated scarps as inherently stable features, such that the evolution from a scarp to tidal flat, or vice versa, depends on the relative roles of sediment supply, sea-level rise, with or without the influence of vegetation. Both models may represent real-world scenarios. However, additional work by Mariotti and Fagherazzi (2013) proposed a critical marsh basin width that, once exceeded, would result in irreversible marsh loss at the edge, even in the absence of sea-level rise.

The multitude of factors as described above can lead to significant variability when measuring edge erosion rates. However, decadal-scale erosion rates of fringing marshes, as reported in the literature, are typically on the order 0.5 – 2.0 m/yr for many locations within the U.S., the U.K., and the Venice lagoon (though rates many times higher are reported in some cases).

Despite the number of processes that can modify marsh boundary erosion and dynamics, we maintain that direct wave attack is the major driver of erosion in open lagoon fringing marshes. Therefore, we focus primarily on quantifying the relationship between shoreline retreat, wave energy and shoreline geometry. Specifically, the goal of this paper is three-fold: 1) to quantify three-year erosion rates at three specific field sites as a function of marsh shoreline geometry, 2) to quantify seven-year erosion rates as a function of wind-induced wave power, water level, and storm surges intersecting the

shoreline, and 3) to provide an overview of erosion processes and dynamics related to changes in water level and wave gully formation.

3.2 Empirical formulations for wave erosion of marsh boundaries

Schwimmer (2001) quantified marsh boundary retreat rates over a five year period along sites within Rehoboth Bay, Delaware. Wind, bathymetric, and fetch data were used to hindcast the wave climate from which the total averaged wave power at each site was computed.

Based on these data, Schwimmer (2001) derived an empirical time-averaged erosion rate, R (m/yr), as function of wave power, P (kW per meter of shoreline) expressed as:

$$R = 0.35P^{1.1} \quad (1)$$

However, that the exponent is very close to one is perhaps more suggestive of a linear relation.

Mariotti et al. (2010) showed that wave energy impacting the marsh shoreline is sensitive to changes in wind direction and sea-level rise since a deeper tidal basin would result in greater wave energy. Additionally, Mariotti and Fagherazzi (2010) modeled the 1-D evolution of a scarped marsh boundary in which the erosion rate, R, was expressed as:

$$R = \beta(P - P_{cr}) \quad (2)$$

Where β is a constant, P is the average wave power, P_{cr} is a critical threshold below which no erosion occurs. In this case, however, the equation was only used to

determine the evolutive morphology of the marsh scarp considering waves, tides, sediments, and vegetation, and was not empirically derived; therefore, it has not been tested against field data and may lack predictive power.

Marani et al. (2011) derived a theoretically-based equation for boundary retreat using Buckingham's theorem of dimensional analysis using five parameters. In this way, they expressed the erosion process with two non-dimensional groups for which they derived the relationship:

$$\frac{Rhc}{P} = f\left(\frac{h}{d}\right) \tag{3}$$

Where R is the erosion rate, h is the scarp height (with respect to the tidal flat), c is a sediment cohesion factor, P is the mean power density of the waves, d is the water depth (with respect to mean sea-level) and f is a function later found to be nearly constant. Therefore, the volumetric erosion rate was expressed as a linear function of mean wave power in contrast to the power law of Schwimmer (2001):

$$V = \alpha P \tag{4}$$

where

$$V = Rc \tag{5}$$

By determining the erosion rates along 150 sites of the Venice Lagoon using historical aerial imagery, Marani et al. (2011) determined the average volumetric erosion rate (expressed in $m^2\ yr^{-1}$) for the Venice Lagoon can be expressed as a linear function of wave power (W/m):

$$V = 0.03P + 0.19 \tag{6}$$

The slope of the relation, and therefore the rate of erosion, likely depends on the soil type, water elevation, and possibly other factors such as vegetation and macrofauna.

Herein we will test which of these formulations better represents wave erosion of marsh boundaries at our study site in the Eastern Shore of Virginia, USA.

3.3 Study area

The study area is part of the Virginia Coast Reserve Long-Term Ecological Research network (VCR-LTER) which comprises a 110 km dynamic system of barrier islands, shallow lagoons, and salt marshes separated by deep tidal inlets. Our research is focused within Hog Island Bay, a coastal barrier lagoon located along the Atlantic side of the southern Delmarva Peninsula (Fig. 3.1).

Figure 3.1 Location map of the study area located in Hog Island Bay, Virginia. Short-term erosion rates were determined for three study sites and are identified by stars; Upshur Neck (UN), Chimney Pole (CP), and Hog Island (HI). Highlighted marsh boundaries illustrate the locations of 50-year erosion rates determined from historical photography.

The lagoon is roughly 100 km^2 of predominately open water and is characterized by intertidal and subtidal basins with mainland fringe-marshes to the west, backbarrier-fringe marshes to the east, and platform marshes to the north and south. Vegetation on the salt marshes is dominated by short-form *Spartina alterniflora* with an average stem height of 30 cm. The majority of the marshes have a prominent scarp at their seaward edges, which are typically 1.0 - 1.5 m above the elevations of the adjacent tidal flats.

The average water depth for most of the lagoon is about 2 m with respect to mean low water (MLW) and rarely exceeds 3 m (Oertel, 2001). The semidiurnal mean tidal range is about 1.2 m (NOAA station 8631044) and relative sea-level rise is on the order of 2 mm/yr. Water exchange occurs primarily through the Great Machipongo Inlet, maintained by a submerged deep channel that spans the lagoon floor to the mainland (Oertel, 2001).

Local weather patterns are dominated by the Bermuda high-pressure system (Davis and Dolan, 1993), giving rise to mostly calm conditions in the lagoon during the summer months, and the passage of cold fronts and Northeasters during winter (Dolan et al., 1988), which are largely responsible for storm conditions in addition to occasional hurricanes. The area is highly influenced by storm disturbances, receiving an average of 30 extratropical storms per year (Hayden et al., 1999). The distribution of wind direction as measured from 1993-1996 revealed that the most frequent directions originate between 180^O- 210^O N and 330^O- 60^O N with wind speeds usually less than 12 m/s (Mariotti et al., 2010).

3.4 Methods

3.4.1 Surveys of Marsh Shoreline Erosion

Three marsh sites (Upshur Neck (UN), Chimney Pole (CP), and Hog Island (HI)) were selected whose locations circumscribe the lagoon in order to encompass differences relating to shoreline position and orientation (stars in Fig. 3.1.). The retreat and morphology of the marsh shorelines were monitored over a span of three years from August 2007 to April 2010. At each site, direct measurements of edge erosion were made using erosion pins and surveys of the marsh boundary in time.

Short-term erosion of the edge was measured using 6-7 erosion pins inserted horizontally into the marsh scarp. Due to the exploratory nature of field observations at the beginning of this research, the start times differ somewhat between sites. The total duration of erosion pin measurements at each site are as follows: UN (824 days, 01/09/08 – 04/13/10), CP (959 days, 08/28/07 – 04/13/10), HI (959 days, 08/28/07 – 04/13/10).

Shoreline positions were measured using a Topcon laser-surveying total station. Five shoreline surveys were conducted over 705 days between May 6, 2008 and April 13, 2010. The durations between surveys at each marsh site are as follows: period 1, 29 days (05/06/08 – 06/06/08); period 2, 77 days (06/06/08 – 08/21/08); period 3, 202 days (08/21/08 – 03/11/09); period 4, 397 days (03/11/09 – 04/13/10).

Shoreline surveys yielded three pieces of information: 1) estimation of erosion rates along the length of the boundary, 2) characterization of shoreline morphology changes, and 3) computation of shoreline sinuosity to be related to boundary retreats.

The action of waves on the marsh boundary produces a series of alongshore undulations previously described as wave-cut gullies (Priestas and Fagherazzi, 2010), and the rate at which the marsh boundary recedes may therefore be a function of sinuosity, since it was previously noted that gullies tend to produce greater erosion rates at the gully head due to wave concentration. To test this hypothesis, shoreline surveys at each location were divided into either 5 or 6 sections roughly 20 m in length, and the erosion for each was estimated between the first and last surveys (May 2008 – April 2010). The cumulative retreat is then correlated with respect to the sinuosity of the initial survey (May 2008).

Erosion estimates from shoreline differences were calculated by integrating the difference in area between shoreline sections, defined as the segment between each erosion pin. The segments were first rotated to orient them as close to horizontal as possible, and end points truncated to match subsequent surveys (Fig. 3.2). Integration of the difference in area was performed using a simple finite difference scheme, the result of which was divided by the straight line segment between the two end points providing an estimation of the total erosion between measurement periods. The sinuosity was then determined by the ratio of the sinuous path length divided by the straight line length between end points. Surveys that were taken close in time would sometimes result in overlapping sections of the boundary producing an anomalous accretion value, as the location of the boundary is sometimes ambiguous. These values were not included in the mean and subsequent analyses, which represented 17% of the data.

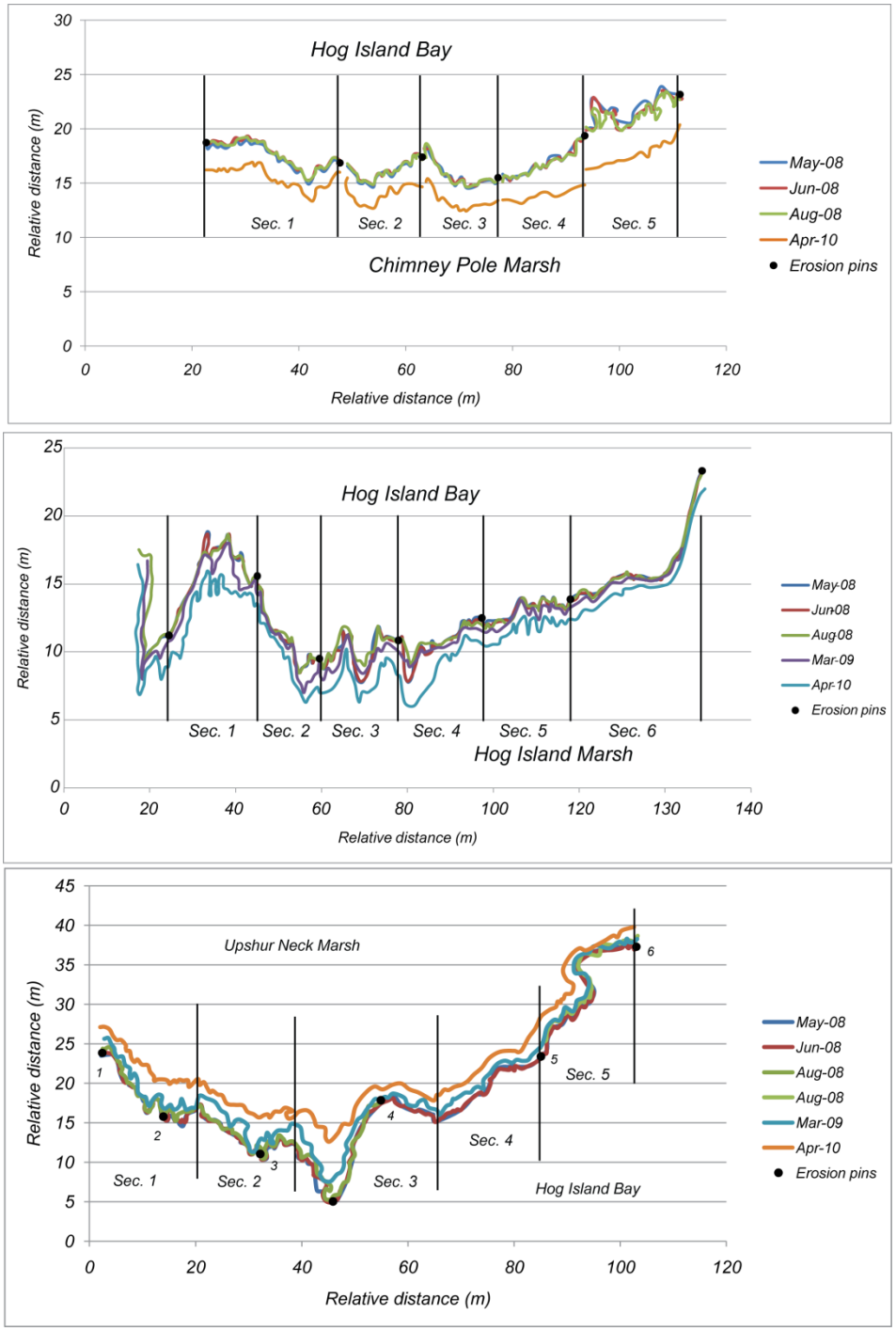

Figure 3.2 Changes in marsh shoreline positions for the three study sites between May 2008 and April 2010 along with erosion pin locations (black dots). Sections indicate partitions used to determine erosion rates by boundary area method and sinuosity index (see text for details). Significant changes in sinuosity indicate the development and destruction of wave-cut gullies between surveys (e.g., see Section 5 of A between May 2008 and Apr 2010).

Limitations in the estimation of boundary retreat with erosion pins and boundary surveys are important to consider. Erosion pins provide very few data points to represent approximately 100 m of shoreline, and therefore may underestimate the average erosion. Regarding the surveys, the edge of the marsh scarp was not always well defined so the determination was made that the vegetation front would demarcate the boundary (since a marsh, by definition, is a vegetated surface). In this situation, erosion rates determined from surveys would overestimate the total volume of sediment removed since the root mat of the vegetation can recede faster than the scarp itself at some locations, a process termed root scalping (see Fig. 3.10C).

3.4.2 Estimating marsh erosion rates from aerial photographs

Shoreline position as measured by standard laser surveying equipment is obviously limited in the spatial extent. We therefore also determined the seven-year average marsh edge erosion rates at numerous locations around the lagoon using two sets of aerial photographs with Geographical Information Systems (GIS).

Average erosion rates for 33 segments of marsh shoreline were determined in ArcGIS using two sets of aerial imagery. Digital orthophotographs from 2002 are part of the Virginia Geographic Information Network (VGIN) and are made available for public download by the GIS Center at Radford University (geoserve.asp.radford.edu/arcims/arcims.htm), and were produced by VARGIS LLC of Herndon, Virginia. The acquisition date over the study area was 01/19/2002, and the

images were developed at a resolution of 2 m (1:400) referenced in Virginia (south) state plane coordinate system. Digital orthophotographs from 2009 are part of the National Agriculture Imagery Program (NAIP) and were made available through the Aerial Photography Field Office (APFO) of the USDA Farm Service Agency (www.apfo.usda.gov). Images of the study area were acquired 06/30/2009 at a resolution of 1 m (1:200) and were rectified within ±6 m to true ground before being published. The images are referenced to UTM zone 18 coordinate system using the North American Datum of 1983 (NAD 83). Image tiles for the region were added directly into ArcMap using APFO's ArcGIS server.

Image tiles from 2002 were georeferenced in ArcMap to the 2009 imagery. Permanent structures such as buildings are limited in most of this area; therefore control points used in the rectification process were mostly confined to tidal creek intersections. The erosion rate for each of the 33 shoreline segments (outlined in Fig. 3.1) was estimated in a similar fashion as that determined from boundary surveys. First, differences in shoreline positions were annotated as digital polygons. The area and perimeter of each polygon was then calculated automatically within ArcMap. Finally, the average erosion rate was then determined by dividing the differenced area by one-half the perimeter length divided by the time duration and multiplied by 365 days. This methodology was similarly used by Schwimmer (2001).

3.5 Modeling wind waves and determination of wave power

3.5.1 Wave hindcasting

Wave regime in the VCR lagoons was hindcasted using the spectral wave SWAN model, which is based on the discrete spectral action balance equation (Booij et al., 1999). A rectangular grid with 200 by 300 cells with a size of 150 m was used to represent the lagoons' bathymetry (Fig. 3.3). For the wind term, the exponential wind input of Yan (1987) and the linear growth of Cavaleri and Malanotte-Rizzoli (1981) were used in the simulations. The process of whitecapping was represented by the van der Westhuysen et al. (2007) formulation. The depth induced breaking was described by the formulation of van der Westhuysen (2010).

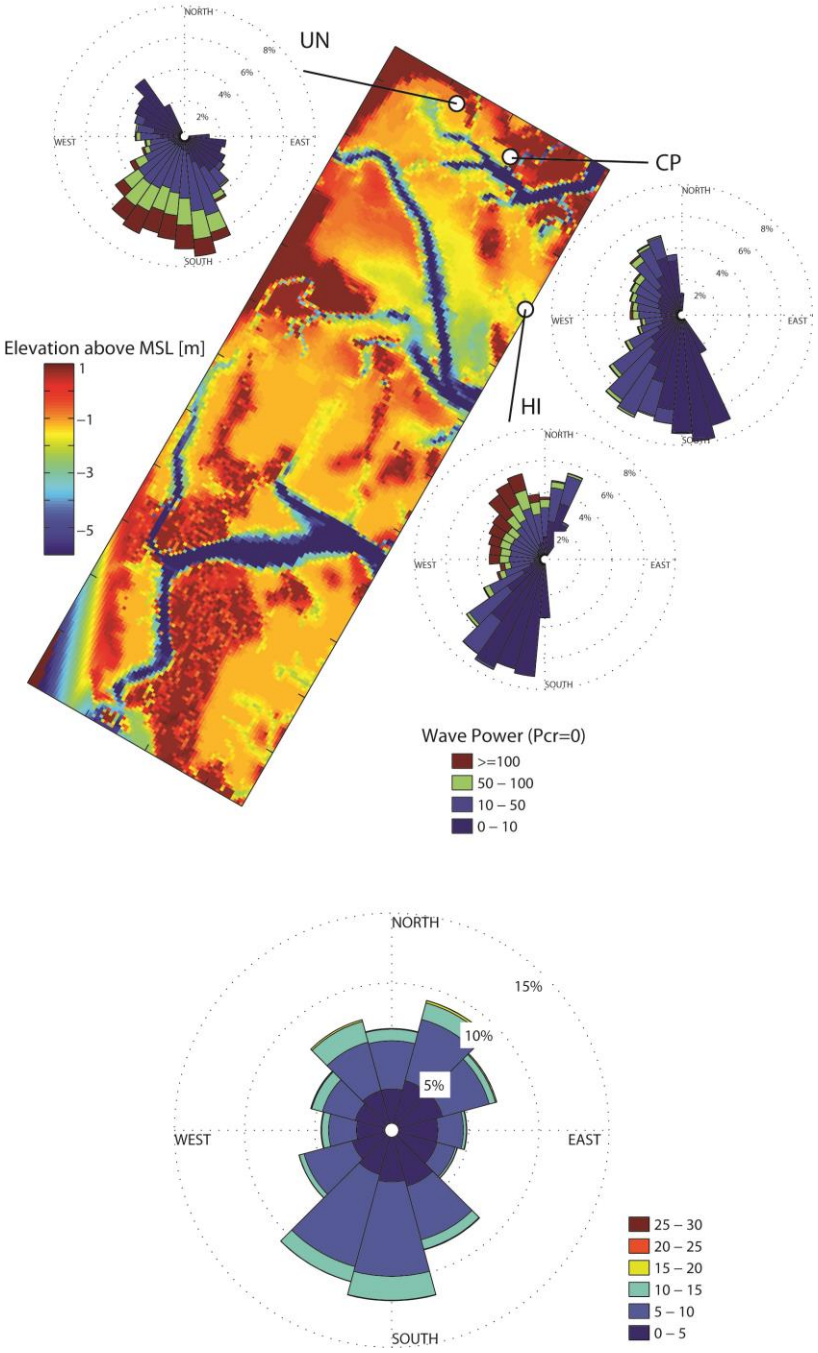

Figure 3.3 Digital elevation model of Hog Island Bay bathymetry (A) used to hindcast wave height and wave period with a SWAN model. The distribution of wave power (W/m) and directions from the model output is shown for each location. The distribution of wind speed (m/s) and directions used to force the model is shown in (B). The model performed a total of 900 simulations combining various water levels, wind speeds and wind directions.

A total of 900 simulations were performed, combining 15 water levels (every 0.2 m, from -0.8 m below M.S.L. to 2 m above M.S.L.), 5 wind speeds (5, 10, 15, 20, 25 m/s) and 12 wind directions (every 30°). In each simulation, water level and wind speed and directions were imposed uniform throughout the domain. Simulations were performed in steady condition, i.e. the wave field was in local equilibrium with the energy sink-source terms.

For each simulation, a single value of the significant wave height, H, and peak wave period, T, were extracted at each marsh boundary position, i. We therefore obtained two discrete functional relationships, relating H and T to the water level, y, wind speed, U, and direction, α, at each marsh boundary position:

$$H_i = f_1(y, U, \alpha, i);\ T_i = f_2(y, U, \alpha, i) \quad (7)$$

The relationship between H_i and T_i were made continuous through a linear interpolation.

3.5.2 Time series and model validation

The next step is to obtain a time series of water level, wind speed and direction, in order to reconstruct the time series of H_i and T_i, using equation 7.

Water level at the Wachapreague NOAA station (ID 8631044) was taken as reference inside the lagoons. We considered both the water level measured and predicted through the harmonic constituents. The difference between the two water levels is caused by storm surges, i.e. variations of the water level not associated to astronomical factors.

For the meteorological data, i.e. wind speed and direction, we considered the NOAA Buoy Station CHLV2-Chesapeake Light, which is placed about 50 km outside the lagoon. This station was chosen for the length of its records, compared to the wind record at the Wachapreague station, which started only in May 2008. In order to take into account the reduction of wind speed from the Buoy to the lagoons, we reduced the wind speed measured at the Buoy by 20%. This reduction was estimated by comparing the wind speed of the Buoy and the wind speed measured at the Wachapreague for the time period when both data were available (approximately 12000 hourly data-points in the years 2009 and 2010).

We obtained a time series of hourly water level, wind speed and direction, from 4/1/2002 to 4/14/2010. The 22% of the time series had missing data on either water level or wind conditions.

For each site, the time series H_i and T_i were reconstructed using equation 7. The results were validated using two wave events: Period 1, from 1/31 to 2/5 2009 and Period 2, from 3/1 to 3/2 2009, using the same data of Mariotti et al. (2010). The performances of SWAN in reproducing wave height and wave period are analogous to the model used in Mariotti et al. (2010): the Root Mean Square Error in the wave height is around 10 cm, while the Model Efficiency for the wave height is between -2.1 and 0.4 (Fig. 3.4).

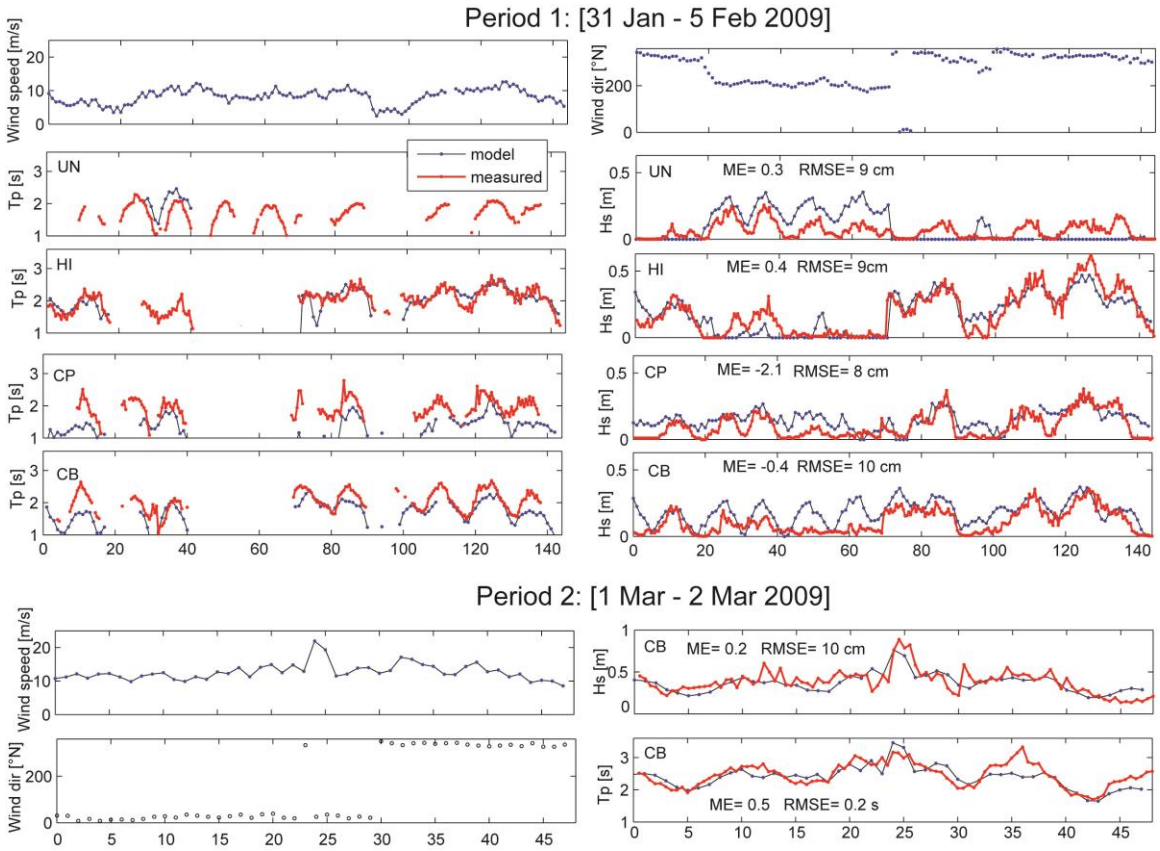

Figure 3.4 Model simulations of significant wave height and wave period validated against measured data for the three study sites. Wind data from NOAA Wachapreague station 8631044.

3.5.3 Proxy for salt marsh boundary erosion

Three proxies for marsh boundary erosion were considered: wave height (m) at the marsh boundary, wave power (W/m) incident to the marsh boundary (Schwimmer 2001) and the wave thrust (kN/m) at the marsh boundary (Tonelli et al. 2010).

In analogy to erosion of a horizontal bed of sediment (Shields), we hypothesize the existence of threshold for wave erosion.

Wave erosion thresholds were designed to address the effects on erosion due to differences in wave energy magnitude versus duration. The goal of this task is to

determine whether erosion is predominately a result of low-energy, frequent events, or high-energy infrequent events. We attempt to address this question by computing the wave power using different erosion thresholds and comparing the correlation between results without the threshold.

The excess incident wave power (W/m) was computed as:

$$P = \begin{cases} c_g E \cos(\vartheta) - P_{cr} & if\ P > P_{cr} \\ 0 & if\ P < P_{cr} \end{cases}, \quad (3)$$

where c_g the group velocity, E the wave energy (J/m^2), and θ the angle between the wave direction and the normal to the marsh boundary. P_{cr} represents a threshold in marsh boundary erosion (Mariotti and Fagherazzi 2010, Mariotti et al. 2010), introduced in analogy with the threshold in bottom sediment erosion.

The wave thrust was computed using the results of Tonelli et al. (2010). The maximum wave thrust (kN/m) for the case of a vertical bank (Fig. 12B in their paper) is approximated as:

$$W_i = \begin{cases} 8.8\,H & if\ h < h_b \\ 8.8\,H - 11(h - hb) & if\ hb < h < h_b + 0.4 \\ 4.4\,H & if\ h > h_b + 0.4 \end{cases} \quad (4)$$

where h is the water depth in front of the marsh boundary and h_b is the height of the marsh platform. The dependence on the period is neglected. Differently to the wave power, the use of the wave thrust takes into account the effect of reduced marsh boundary erosion when the water level is higher than the marsh top.

Using the time series H_i, T_i and y, we reconstructed the times series P_i and W_i, using both the measured and the predicted water levels. A sample from the whole time

series is given in Figure 3.5. This example clearly shows the effect of storm surges: the maximum wave power (Fig. 5, t=110 hours) at the HI site computed considered the measured water level is almost double the maximum wave power computed with the predicted (astronomical) water level.

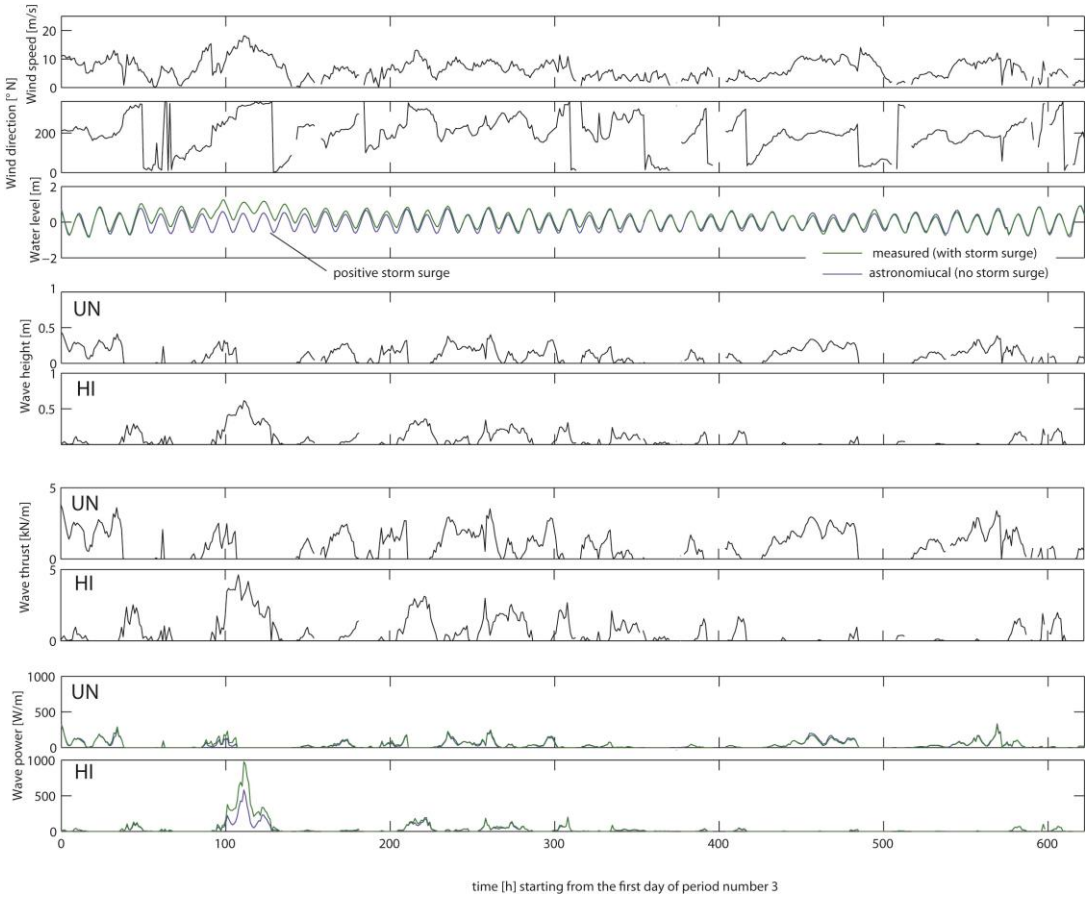

Figure 3.5 Sample time series reconstruction (8/21/2008 to 4/13/2010) of modeled wave height, wave thrust, and wave power using measured (with storm surge) and predicted (no storm surge) water levels for two study sites. The full reconstruction for data analysis spans from 4/1/2002 to 4/19/2010 for all three study sites. Note peak wave power at the HI location (t=110 hrs) due to storm surge, which is double that of the predicted water level.

3.6 Results

3.6.1 Boundary retreat estimates

Since pin measurements may underestimate erosion (due to few data points and missing pins when a slump occurs) while boundary surveys and aerial photos may overestimate erosion (due to difficulty in defining the boundary, and/or root scalping), the average from all three methods is taken as the best estimate for retreat rates at each site (Table 1).

Overall, the shoreline along Upshur Neck eroded the fastest, with an average erosion rate of 1.52 m/yr, followed by Chimney Pole (1.09 m/yr) and Hog Island (0.69 m/yr). The seven year (2002-2009) erosion rates derived from GIS exhibit the same trend as those from erosion pins and surveys (2008-2010)—Upshur Neck had the highest retreat rate at 1.89 m/yr followed by Chimney Pole (1.17 m/yr) and Hog Island (0.85 m/yr), and more closely matched those rates derived from boundary surveys (Table 1). The 33 sites analyzed using aerial photography produced an average erosion rate of 1.47 ± 1.03 m/yr with 75 percent of the values distributed between 1.0 and 2.0 m/yr; only 12 percent of the data exceeded 2.5 m/yr with three values being twice the standard deviation from the mean.

Table 3.1 Erosion rates estimated at the three study sites determined from each method (erosion pins, total station surveys, historical imagery). Average is given as a best estimate since erosion pins may underestimate erosion while survey and imagery methods may overestimate erosion.

	Upshur Neck			*Chimney Pole*			*Hog Island*		
	Cumulative	*Duration*	*Rate*	*Cumulative*	*Duration*	*Rate*	*Cumulative*	*Duration*	*Rate*
Method	*(m)*	*days*	*(m/yr)*	*(m)*	*days*	*(m/yr)*	*(m)*	*days*	*(m/yr)*
Pins	1.68	825	0.74	1.87	958	0.71	0.85	958	0.32
Survey	3.71	705	1.92	2.71	705	1.4	1.77	705	0.91
Photos	13.24	2557	1.89	8.18	2557	1.17	5.98	2557	0.85
Average			**1.52**			**1.09**			**0.69**

3.6.2 Retreat as a function of shoreline sinuosity

There is significant correlation between the shoreline erosion rate and the shoreline sinuosity of relative to the initial May 2008 survey. The rate for each site is plotted as a function of sinuosity in Figure 3.6 and summarized in Table 2.

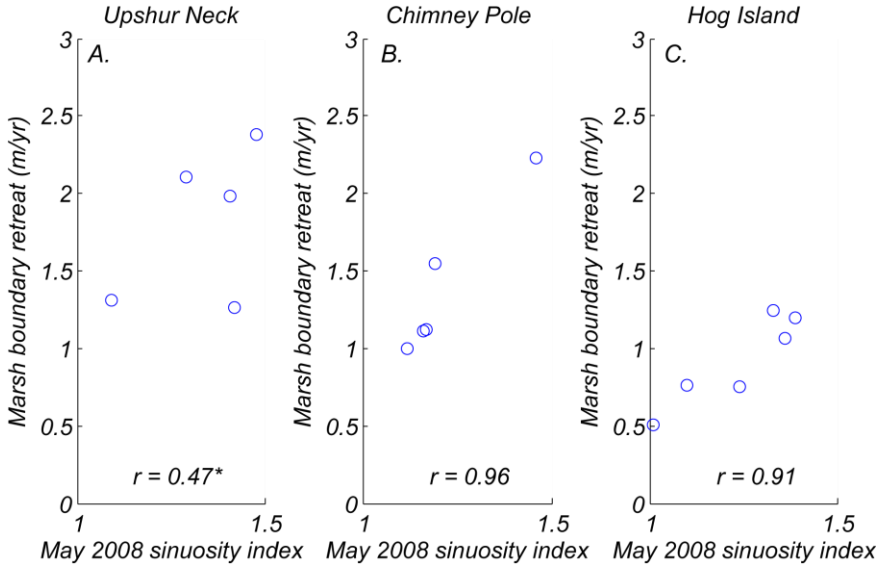

Figure 3.6 Marsh edge erosion as a function of shoreline sinuosity. Each data point represents the average erosion rate and sinuosity within each boundary section (see Fig. 3.2) between May 2008 and April 2010. Sinuosity is used a proxy for the presence of wave-cut gullies, whereby erosion is more vigorous due to concentration of wave energy. These data suggest that the greater the presence of wave gullies resulted in more vigorous erosion.

Table 3.2 Summary values of sinuosity index (SI) and erosion rate (E) for each section at the three study sites (see Fig. 3.2). Greater SI values indicates a more sinuous boundary, which enhances erosion rates due to the presence of wave-cut gullies. Correlation coefficients (r) are also shown and are significant at the 95% confidence level (p=0.05) with the exception of UN.

	UN		*CP*		*HI*	
Section	*SI*	*E(m/yr)*	*SI*	*E(m/yr)*	*SI*	*E(m/yr)*
1	1.41	1.98	1.12	1.00	1.39	1.20
2	1.29	2.11	1.16	1.11	1.24	0.75
3	1.48	2.38	1.17	1.12	1.36	1.06
4	1.09	1.37	1.19	1.55	1.33	1.24
5	1.42	1.26	1.46	2.23	1.10	0.76
6	n/a	n/a	n/a	n/a	1.01	0.51
r	***0.47***		***0.96***		***0.91***	

In general, the greater the sinuosity the more vigorously the marsh boundary retreated. The strength of the relationship is reported as r-values in Table 2, and with the exception of Upshur Neck is statistically significant at the 95% confidence level (one-tailed p=0.05). It is important to note that the rate of retreat reported in Table 2 are localized values and are not necessarily reflective of the average rate across the length of the boundary. For example, the high erosion values reported for CP are due to the retreat of the vegetation boundary (which we define as the marsh boundary), which receded very rapidly between sections 4 and 5, yet the erosion rate overall for CP (1.09 m/yr) is not as great as UN (1.52 m/yr). The degree of erosion underestimation using erosion pins is fairly consistent. In fact, the ratio between erosion measured via erosion pins to that of boundary surveys is similar for all sites, with values 0.39 for UN, 0.51 for CP, and 0.35 for HI, the interpretation being that the retreat rates may be underestimated by roughly 50-65% when using erosion pins.

3.6.3 Retreat as a function of wave power

The investigation of the relationship of wave energy to marsh erosion was analyzed as a function of average wave power and total work done (power*time) in each measurement sub-period. First, we examined the site-specific cumulative boundary erosion (obtained by erosion pins) as a function of the total work done (MJ/m) on the boundary within each of the measurement sub-periods (Fig. 3.8). Predictably, the greater the amount of cumulative wave energy at each site resulted in a greater cumulative retreat of the boundary. However, while larger values of wave energy resulted in greater cumulative erosion, the total amount of erosion for a given cumulative wave energy was site specific. For example, HI experienced much less erosion than CP despite being subjected to the greatest total wave energy (Fig. 3.7).

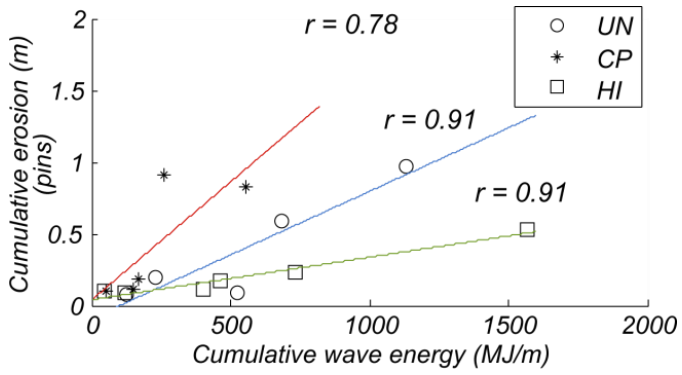

Figure 3.7 Cumulative erosion (measured by erosion pins) plotted as a function of cumulative wave energy. Greater cumulative wave energy results in greater shoreline retreat; however, the response is site-specific due to inter-site variations in soil properties and marsh elevation.

In addition, we examined cumulative erosion calculated from total station measurements within each sub-period from all three sites also as a function of cumulative wave energy. As Figure 3.8 suggests, on average the marsh shoreline should retreat by roughly one meter for every 800 MJ of cumulative wave energy that strikes it, although there is considerable variability related to factors other than wave energy (as illustrated in Fig. 3.6). Furthermore, relating cumulative wave energy to cumulative erosion may not properly address the response of marsh retreat to short-duration, higher magnitude waves vs. long-duration, lower magnitude waves.

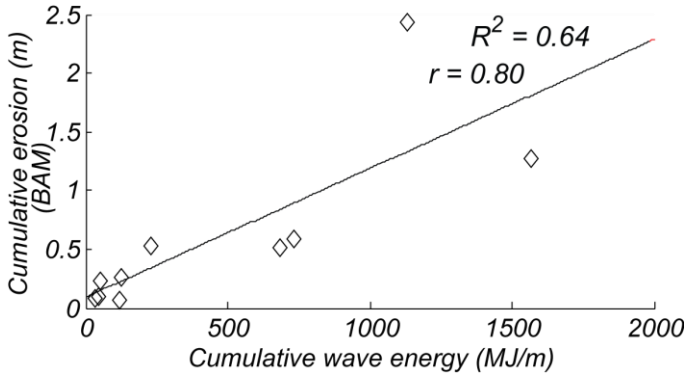

Figure 3.8 Cumulative erosion (determined from shoreline surveys) plotted as a function of cumulative wave energy. Each data point represents the average erosion among boundary sections (see Fig. 3.2) between four consecutive measurement periods from 5/8/2008 to 4/13/2010.

Using our calibrated model results, we propose that the rate of marsh boundary retreat is primarily a linear function of average wave power. The erosion rate estimates obtained from GIS analysis at all 33 sites along the bay produce a generalized relationship between erosion rate and average wave power (Fig. 7A). Despite the large variability in erosion rates, there is a strong relationship ($r = 0.50$, $p=0.05$) between wave

power and erosion rate The linear regression equation in Figure 3.9(A) predicts that an average wave power of 16 W (or 500 MJ/yr) per meter shoreline would give rise to an erosion rate of 1.69 m/yr, similar to the average long-term erosion rates measured at our sites (Table 1), though somewhat of an overestimate. However, if the 6 largest outliers are removed from the data, the linear regression model as shown in Figure 3.9(B) predicts an erosion rate of 1.1 m/yr for the same average wave power of 16 W/m, which is the same as the averaged erosion rate between all three sites (Table 1). Additionally, the regression equation in Figure 3.9(B) is very similar to that obtained by Marani et al. (2011) for the Venice Lagoon (eqn. 1).

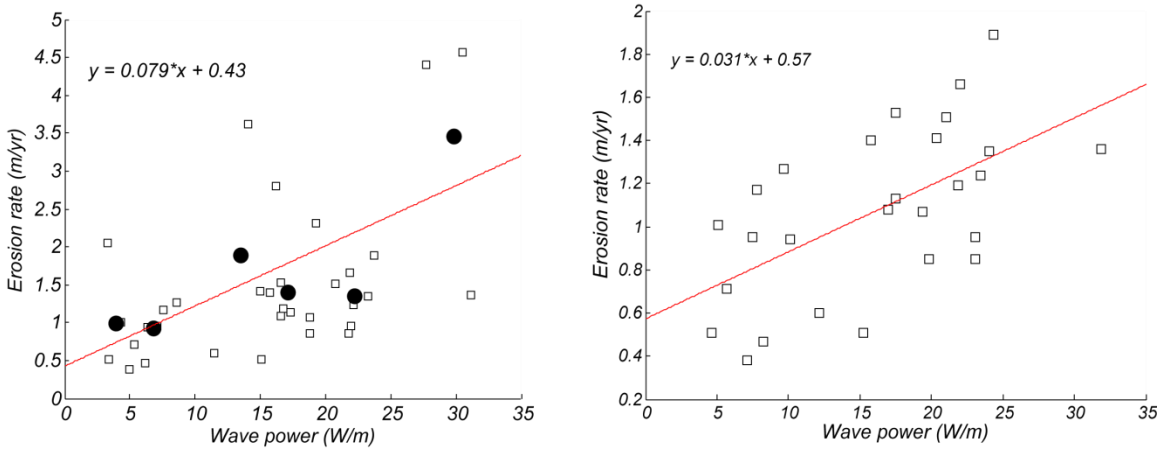

Figure 3.9 Marsh boundary erosion rate derived from GIS shoreline analysis (1/19/2002 – 6/30/2009) as a function of average wave power computed from the SWAN model with all 33 sites used (A) and the six largest outliers removed (B).

3.6.4 Retreat as a function of wave erosion thresholds, wave height, and water level

To explore the possible presence of a threshold in wave power below which the erosion rate is negligible, we performed several experiments using a prescribed wave erosion threshold on the model data. The total wave power includes only the difference between the computed wave power and a prescribed threshold. Therefore, if the wave power at a specific event was below the threshold, the event was discarded altogether. Similarly, we also explored thresholds on wave thrust and wave height, positing that only events with a wave height or wave thrust above a specified value are causing marsh erosion. For each new dataset, we computed the correlation coefficient between the modified wave variable and the erosion rate using different threshold values for wave power (P_{cr}), wave height (H_{cr}), and wave thrust (T_{cr}). The goal is to determine which wave variable and threshold value yields the highest correlation coefficient.

The results are provided in Table 3. Changes in correlation are subtle, though each correlation was tested for significance at the 95% confidence interval. The strongest correlations are related to wave power, of which the highest correlation (0.50) is reached with P_{cr} = 0 W/m.

In a second analysis, we removed the effect of storm surges by utilizing in the calculation of wave power, wave height, and wave thrust, the astronomic tidal elevation computed by the harmonic constants of the NOAA station 8631044. In this way we can single out the effect of storm surges on marsh erosion. The resulting correlation coefficients are similar to the values computed including storm surges, which suggests that large storms do not have much control on erosion rates.

Table 3.3. Summary of correlation coefficients to show the strength between GIS-derived erosion rates and thresholds in the wave variable (meaning values below the threshold are discarded from the computation; see eqns. 3 and 4) with and without the effects of storm surge.

	Wave Power			*Wave Height*			*Wave Thrust*		
	Pcr (W/m)			*Hcr (m)*			*Wcr (kN/m)*		
No Storm Surge	**0**	**10**	**50**	**0**	**0.1**	**0.2**	**0**	**0.1**	**0.2**
Correlation (N=33)	0.50	0.48	0.49	0.32*	0.36	0.39	0.33*	0.38	0.38
With Storm Surge	**0**	**10**	**50**	**0**	**0.1**	**0.2**	**0**	**0.1**	**0.2**
Correlation (N=33)	0.49	0.50	0.53	0.33*	0.35	0.34*	0.32	0.36	0.33*

**Indicates values that are not statistically significant*

3.7 Discussion

3.7.1 Erosion rate variability

Present retreat rates of marsh edge are commonly on the order of 1 m/yr. The high degree of erosion rate variability is most likely due to a combination of factors such as sediment composition, marsh elevation, and the extent of burrowing crabs at each site. For example, research by McLoughlin (2010) determined that crab burrow densities at the marsh edge were about 300% higher at UN (200/m^2), relative to CP and HI (~50/m^2). More notably, however, was that the burrow volumes at CP and UN (~11,000 cm^3/m^2, and 8,000 cm^3/m^2, respectively) were more than ten times greater than at HI (~500 cm^3/m^2). Greater burrow densities and volumes may act to enhance erosion under wave impact due to hydraulic action within the pore spaces, especially given the reduced material strength resulting from the "swiss cheese" nature of the marsh boundary.

Breaking waves at various tidal elevations affects the morphology of the marsh boundary profile. For the study areas in this project, waves tend to break offshore at low tides while also being small due to decreased water depth, which can result in a local lowering of the intertidal basin by removing previously eroded material (Fig. 3.10A). At intermediate tide elevations, waves can develop higher and break or surge at the toe of the scarp. Such wave action is often combined with corrasion and is thus very effective at undercutting the scarp (Fig. 3.10B). Higher tidal elevations produce larger wave heights since there is less wave decay, yet, these waves may break against the wall without entrained sediments, reducing the role of corrasion. When waves occur at water elevations near that of the marsh platform, they may strike against the weak boundary separating the active (live) vegetation root layer from the peat layer, which occurs at about 20 cm depth. The upward force of the impinging waves was observed in the field to torque the root mat upward, which results in uprooting and removal of the active root layer, a process termed "root-scalping" (Fig. 3.10C). Toppling and cantilever failure appear to be common as well (Fig. 3.10D), as also reported by Allen (2000).

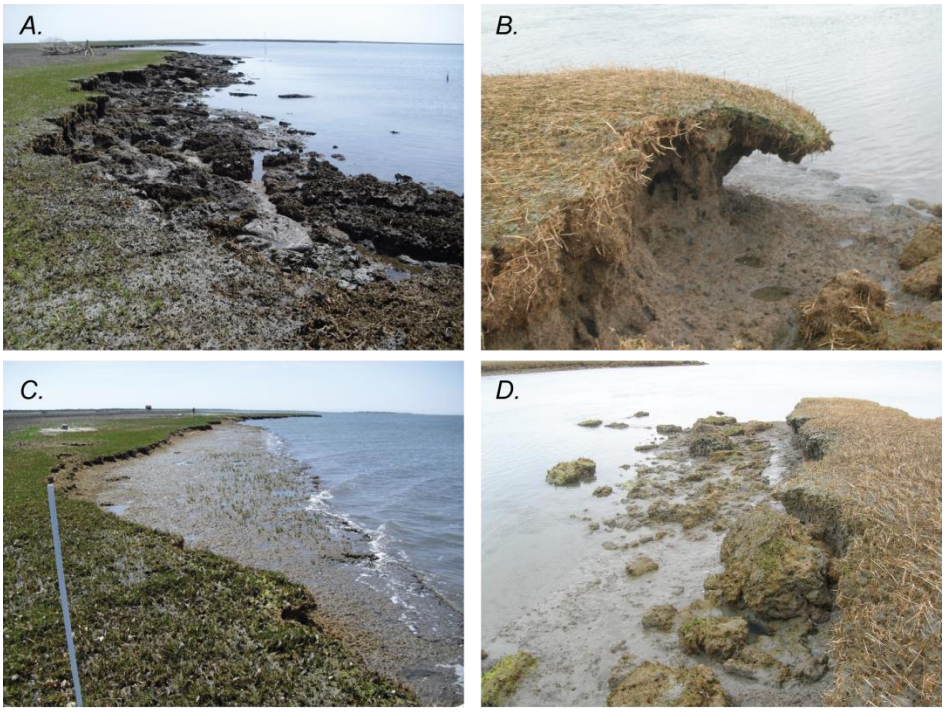

Figure 3.10 Degradation of marsh scarps in Hog Island Bay, Virginia (A-D) and Plum Island, Massachusetts (E-F). The action of waves at lower water levels can remove previously eroded material (A) and cause undercutting (B). The process of root scalping occurs when waves attack the marsh at water levels approaching the marsh platform elevation (C); toppling is also common (D).

The erosion rates measured with pins represents the amount of material that is slowly removed on the marsh scarp surface by waves and currents (corrasion), that is, the action of hydraulic pressure on the scarp with or without sediment entrainment. Here, the material is detached in small quantities from each wave impact but can amount to considerable sums over the span of a few months. Erosion pins, however, are unable to capture the detaching of large blocks, scarp slumping, undercutting, or other mass wasting processes (Fig. 10.3D). Comparing the erosion rate from pins against the total erosion rate from the boundary surveys may help elucidate the relative role of corrasion versus mass wasting with respect to the total scarp retreat. If this simple analysis reflects

reality, then the effect of corrasion is similar at UN and HI (39% and 35% respectively), and even higher at CP (51%). These results suggest that mass wasting processes are important, perhaps accounting for 50-70% of the total marsh boundary retreat at our sites.

Marsh erosion is highly correlated to wave power, as also indicated by Schwimmer (2001) and Marani et al. (2011), and less related to wave height or wave thrust (Table 3). The introduction of a threshold value for wave power, below which erosion is thought to be negligible, (see Eq. 2) slightly increases the correlation coefficient indicating that the threshold is not a critical component of a model for marsh erosion by wind waves. Similarly, neglecting storm surges does not increase the correlation between erosion and wave power. We can therefore conclude that, at the level of approximation of our study, the utilization in the numerical model of astronomic tidal elevations rather than measured water levels does not affect much our estimate of marsh erosion.

Sediment composition may affect erosion rates by altering the cohesive strength of the marsh sediments. Feagin (2010) determined experimentally that marsh soils with a high sand fraction resulted in the greatest erosion. McLoughlin (2010) reported that HI had the coarsest sediments (d_{50} = 140 μm), while CP and UN were mostly clay and silt (d_{50} = 46 μm and 14 μm, respectively); however, HI experienced the least amount of erosion despite having the coarsest sediments.

Marsh elevation may also have significant control on erosion rates since it controls for how long a marsh cliff may be exposed to waves and tides, and therefore,

the total amount of wave power acting on the cliff. Modeling efforts by Tonelli et al. (2010) showed that maximum wave thrust (kN/m) occurs when the water elevation equals the elevation of the marsh platform. Tidal elevations higher than the marsh platform resulted in a rapid decrease of wave thrust, suggesting that marsh boundaries are protected from waves when drowned. This may explain why HI has the lowest erosion rates since its elevation above mean sea level is 10 cm below that of UN and 20 cm below CP (McLoughlin, 2010). However, it must also be noted that Hog Island's shoreline orientation is somewhat protected from the strongest dominant winds, which are from the N-NE in winter and SSE-SSW in the summer. Conversely, summer winds may strongly affect sites in the northern sectors of the lagoon. To illustrate, marshes that undergo aggressive erosion at their boundary may have extensive litter (blocks of marsh peat) strewn upon the platform and on the tidal flat, most of which are between 0.5 and 1 m^2 (Fig. 3.11) The blocks tend to disintegrate over the span of a year and act as a local source of sediment to the marsh platform (Fig. 3.12).

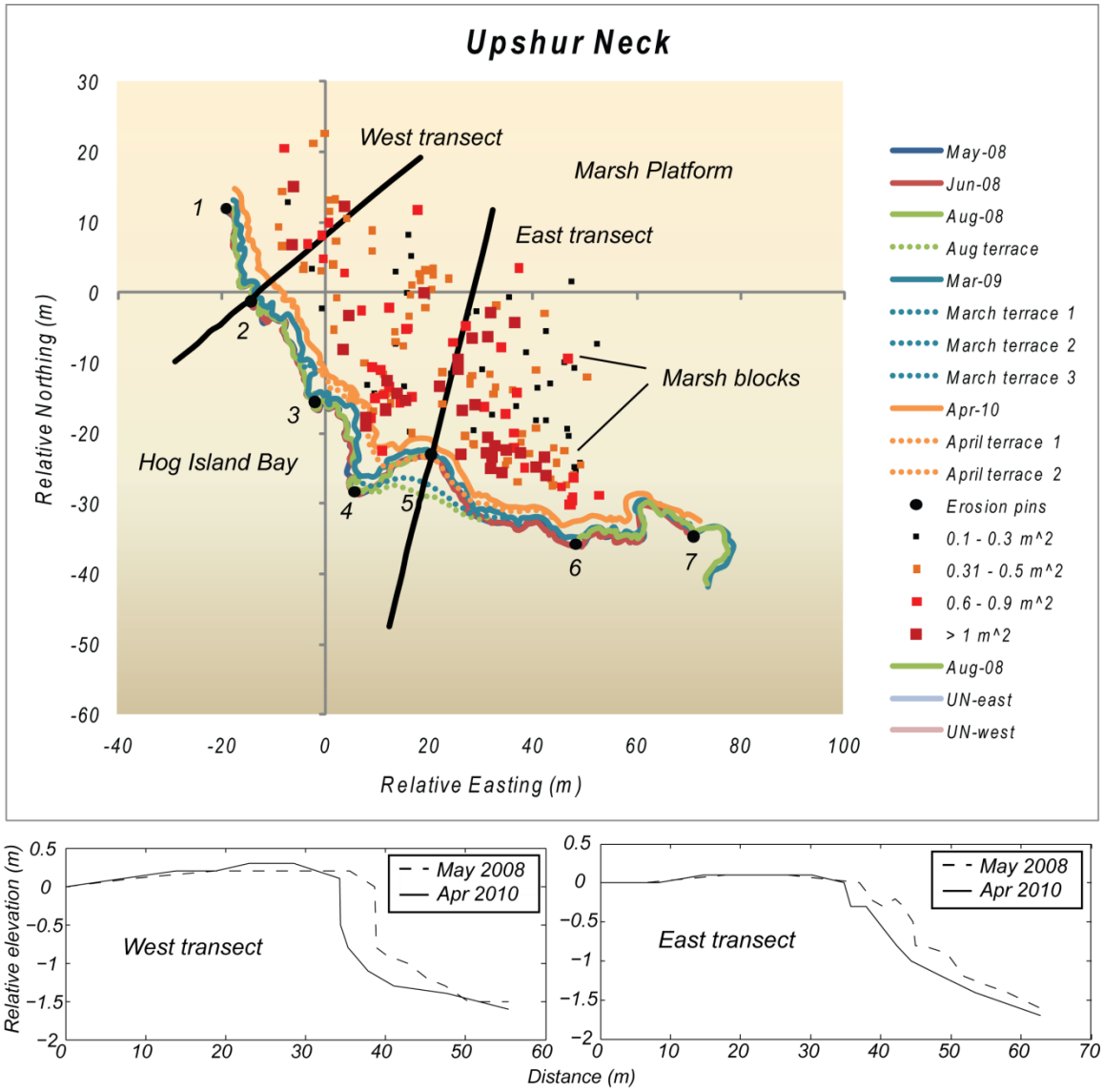

Figure 3.11 Upshur Neck marsh shoreline boundary mapped through time with two representative transects. Aggressive erosion at this site resulted in a blocks of eroded material being strew upon the marsh platform, many of which are greater than 1 m^2. The blocks tend to disintegrate over the span of one year.

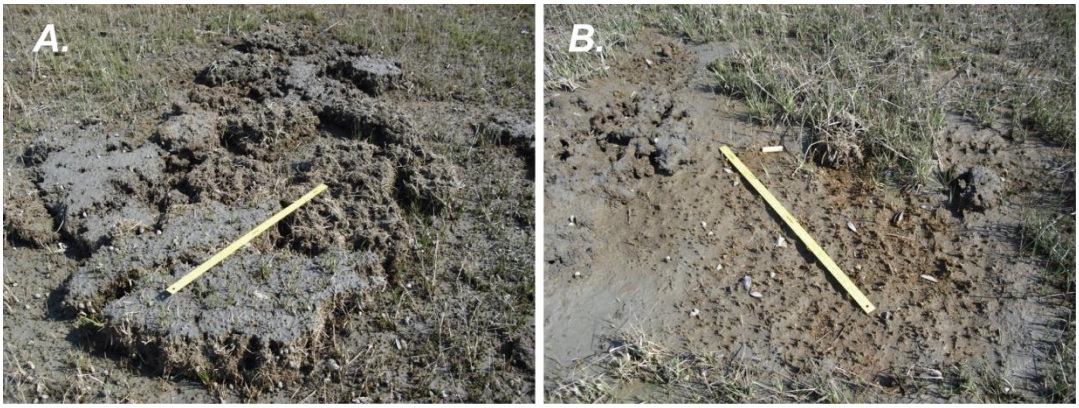

Figure 3.12 Example of a marsh block before (A) and after (B) disintegration. The scale in the photos is 1 m.

3.7.2 Future marsh survival and sediment fate

Knowlton (1971) reported a net 16% marsh loss within Hog Island Bay, VA over a 116 year period (1852 – 1968). Erosion rates at the marsh boundary over the past 50 years are similar to modern rates (McLoughlin, 2010) and their average is on the order of 1.3 m/yr. This implies that the marsh boundary will retreat another 65 meters over the next half century, and may therefore completely vanish over the next half millennia.

Considering the predominately eroding perimeter of the marshes to be approximately 28,000 m with average thickness of 1.3 m, then the volume of sediment released to Hog Island Bay is estimated to be on the order of 50,000 m^3/yr when considering an average erosion rate of 1.3 m/yr. Given the average bulk density of marsh sediments in this area to be 0.78 g/cm3 (McLoughlin, 2010), this translates to approximately 39,000 tons/yr of eroded material. In comparison, the average sediment load of the Atchafalaya River is on the order of 300,000 tons/day.

The fate of eroded sediments from the marsh edge is varied and may depend on sediment size. Some sediments eroded from the edge are reworked and deposited on the marsh platform some 10-20 meters adjacent to the boundary, increasing the platform elevation about 20 cm relative to the interior. Similarly, sediments are typically deposited within a relatively short distance adjacent to marsh creeks, which explains the lower elevations and higher organic content of the marsh interiors compared to the higher elevations along creek banks and marsh boundaries, where sediments typically have less organic content (Kastler and Wiberg, 1996; Mcloughlin 2010). A numerical model of Hog Island Bay's hydrodynamics, conducted by Lawson (2004), showed only slight differences between flood- and ebb-tide velocities (6-8 cm/s) and durations (2 min), therefore the bay does not appear to be strongly flood or ebb dominated. Nonetheless, the slightly higher ebb velocities were modeled near the inlet. Based on a series of grab samples, Lawson (2004) also showed that finest sediments were concentrated near the interior of the bay, where the difference in tidal velocities was minimal. Long-term sedimentation rates in the bay were reported by Oretel et al. (1989) to be 2.3-3.5 mm/yr based on Pb-210 dating of two cores (though these rates do not necessarily reflect a constant upward filling), while sedimentation rates on the marsh platforms were estimated between 1.2-1.8 mm/yr (Kastler and Wiberg, 1996), suggesting that the sediments eroded from the marsh edge are the primary source of sediments to the bay, similar to that of Chincoteague, VA, where an estimated 46% of sediment delivery to its bay was sourced from edge erosion (Bartberger, 1976).

Likewise, cannibalization of the marsh edge is likely the primary source of sediments to the marsh platform.

3.7.3 Sea-level rise and implications for marsh stability

Marsh stability is typically addressed in terms of the balance between marsh platform accretion and sea-level rise. Since the rates of sea-level rise and sediment deposition are likely to vary through time, the notion of repeated cycles of erosion and progradation were realized (Yapp 1917). A shift in research priority to study to ability of marshes to keep pace with RSLR in their vertical extent all but abandoned the notion of the autocyclic growth concept, to which Chauhan (2009) stated was a normal pattern of salt marsh evolution in certain areas. However, given the sediment starved conditions within Hog Island Bay, VA (Boon and Byrne, 1981; Nichols and Boon, 1994), autocyclic growth has likely not occurred here. Despite low minerogenic sedimentation, many salt marshes are able to keep pace with sea-level rise by below-ground organic (organogenic) production (Turner et al., 2001). If sedimentation rates keep pace with sea-level rise, then the marsh elevation will be maintained. On the other hand, if sea-level rise greatly outpaces sedimentation rate, then the marsh may begin to drown or plants become intolerant of the increase in hydroperiod (duration of overmarsh tides) resulting in plant die-back (Reed and Cahoon, 1992). If sedimentation rates are low as well, then perhaps erosion near the marsh-mudflat interface is developed into a scarp (Mariotti and Fagherazzi, 2010); currently, relative sea-level rise in Hog Island Bay (3.5 mm/yr) is currently outpacing marsh sedimentation rates (1.2-1.8 mm/yr).

The lagoon marshes of Hog Island Bay, VA have nearly been converted to open water since their initial development. Most of what is now the subtidal basin was likely once all marsh, as noted by drowned tidal channels that connect to channels on the marsh platform. In fact, recent modeling work by Mariotti and Fagherazzi (2013) suggests that the enlargement of interior ponds leads to a critical width of tidal flats that, once exceeded, results in irreversible marsh erosion by wind waves even in the absence of sea-level rise.

Salt marsh stability must be addressed in the horizontal movement as well as the vertical, and may not actually exist at all. In other words, even if a marsh platform keeps pace with sea-level rise, but the marsh's edge is retreating at 1-2 m/yr, can this arrangement be considered stable? Without sediment supply, the marsh will be lost regardless. Hence, for a given geographic setting, we theorize that salt marshes are either in an environment conducive to growth, or conducive to attrition, the dynamics of which are principally being governed by sediment supply. With this consideration, Hog Island Bay salt marshes, along with numerous others along the U.S. Atlantic coast and elsewhere, are currently unstable features which are not likely to recover or even remain stable unless wave energy can be attenuated at the boundary.

3.8 Conclusions

1) Salt marsh boundary erosion is a primarily a linear function of wave power, the rate of which averages about 1.3 m/yr within Hog Island Bay, VA. The erosion rate was

better predicted by wave power as opposed to wave thrust or wave height. Marsh retreat of 1 meter requires between 200 and 500 MJ of wave energy per meter shoreline length.

2) The primary mechanisms of marsh retreat are corrasion, block detachment, root-scalping, and wave-gullying, which depend greatly on the tidal elevation during wave generation.

3) Erosion rates are modified by a number of factors, including crab burrows, soil composition, marsh platform elevation, and shoreline orientation. The presence of crab burrows and sand increases erosion rates, along with the presence of wave-cut gullies due to wave-crest compression.

4) Increase in shoreline sinuosity (i.e., wave-cut gullies) is significantly correlated to increases in marsh boundary erosion rates.

5) The effect of storm surges on erosion rates is negligible; therefore erosion proceeds primarily through normal meteorological conditions.

6) Due to sediment starving conditions, Hog Island Bay will likely be converted completely to open water within the next half millennia, with the exception of the mainland fringing marshes.

7) Salt marshes are either in conditions conducive to growth or conducive to attrition; therefore the notion of stability must be called into question, and an equilibrium state may not exist at all.

3.9 References

Allen, J.R.L., (1989). Evolution of salt-marsh cliffs in muddy and sandy systems: a qualitative comparison of British west-coast estuaries, Earth Surface Processes and Landforms, 14, 85–92.

Allen, J.R.L., (2000). Morphodynamics of Holocene salt marshes: a review sketch from the Atlantic and southern North Sea coasts of Europe, Quaternary Science Reviews, 19, 1155–1231.

Bartberger, C. E., (1976). Sediment sources and sedimentation rates, Chincoteague Bay, Maryland and Virginia. Journal of Sedimentary Research,46(2), 326-336.

Booij, N., R. C. Ris, and Holthuijsen, L.H., (1999). A third-generation wave model for coastal regions: 1. Model description and validation, Journal of Geophysical Research., 104(C4), 7649–7666, doi:10.1029/98JC02622.

BOON, J.D. and BYRNE, R.J., (1981). On basin hypsometry and morphodynamic response of coastal inlet systems. Marine Geology, 40, 27-48,

Coops, H., Geilen, N., Verheij, H., Boeters, R., and van der Velde, G., (1996). Interactions between waves, bank erosion, and emergent vegetation: An experimental study in a wave tank, Aquatic Botany, 53, 187-198.

D'Alpaos, A., Lanzoni, S., Marani, M., & Rinaldo, A., (2007). Landscape evolution in tidal embayments: Modeling the interplay of erosion, sedimentation, and vegetation dynamics. Journal of Geophysical Research, 112(F1), F01008.

Davis, R. E., & Dolan, R. (1993). Nor'easters. American Scientist, 81(5), 428-439.

Day, J.W., Jr., Reed, D., Syhayda, J., Kemp, P., Cahoon, D., Boumans, R.M., and Latif, N., (1994). Physical processes of marsh deterioration. In H.H. Roberts, ed. Critical Physical Processes of Wetland Loss, 1988-1994. Final Report. Louisiana State University, Baton Rouge. Prepared for U.S. Geological Survey, Reston, VA.

Denny, M.W., Miller, L.P., Stokes, M.D., Hunt, L.J.H., and Helmuth, B.S.T., (2003). Extreme water velocities: Topographical amplication of wave-induced flow in the surf zone of rocky shores. Limnology and Oceanography, 48(1), 1-8.

Dolan, R.; Lins, H., and Hayden, B., (1988). Mid-Atlantic coastal storms. Journal of Coastal Research, 4(3), 417-433.

Draut, A.E., Kineke, G.C., Huh, O.K., Grymes III, J.M., Westphal, K.A., and Moeller, C.C., (2005). Coastal mudflat accretion under energetic conditions, Louisiana chenier-plain coast, USA. Marine Geology, 214, 27-47.

Fagherazzi, S., & Wiberg, P. L. (2009). Importance of wind conditions, fetch, and water levels on wave-generated shear stresses in shallow intertidal basins. Journal of Geophysical Research: Earth Surface, 114(F3).

Fagherazzi, S., & Priestas, A. M., (2010). Sediments and water fluxes in a muddy coastline: interplay between waves and tidal channel hydrodynamics. Earth Surface Processes and Landforms, 35(3), 284-293.

Feagin, R.A., Lozada-Bernard, S.M., Ravens, T.M., Möller, I., Yeager, K.M., and Baird, A.H., (2009). Does vegetation prevent wave erosion of salt marsh edges? Proceedings of the National Academy of Sciences, 106, 10109-10113.

Finkelstein, K., and Hardaway, S.C., (1988). Sedimentation and erosion of estuarine fringing marshes, York River, Virginia. Journal of Coastal Research, 4, 447-456.

Fisher, W.L., McGowan, J.H., Brown, L.F., and Groat, C.G., (1972). Environmental Geologic Atlas of the Texas Coastal Zone: Galveston-Houston Area. Austin, TX: Bureau of Economic Geology, 91p.

Hall, S.L., Wilder, W.R., and Fisher, F.M., (1986). An Analysis of Shoreline Erosion along the Northern Coast of East Galveston Bay, Texas, Journal of Coastal Research , 2(2), 173-179.

Hayden, B.P., (1999). Climate change and extratropical storminess in the United States: an assessment. Journal of American Water Resources Association 35:1387–1397

Kastler, J.A., and Wiberg, P. L. (1996). Sedimentation and boundary changes of Virginia salt marshes. Estuarine, Coastal and Shelf Science, 42(6), 683-700.

Kearney, M.S., Grace, R.E., and Stevenson, J.C., (1988). Marsh loss in Nanticoke Estuary, Chesapeake Bay, Geographical Review, 8, 205-220.

Knowlton, S.M., (1971). Geomorphological History of Tidal Marshes, Eastern Shore, Virginia, from 1852 to 1966. University of Virginia, M.S. Thesis, 186 pp.

Lawson, S.E., (2004). *Sediment suspension as a control on light availability in a coastal lagoon* (Doctoral dissertation, University of Virginia).

Lundgren, H. and Juhl, J., (1995). Optimisation of caisson breakwater design. In 'Wave Forces on Inclined and Vertical Wall Structures', American Society of Civil Engineers, 181-204.

Marani, M., D'Alpaos, A., Lanzoni, S. and Santalucia, M., (2011). Understanding and predicting wave erosion of marsh edges, Geophysical Research Letters, 38, L21401, doi:10.1029/2011GL048995.

Mariotti, G., and Fagherazzi, S., (2010). A numerical model for the coupled long-term evolution of salt marshes and tidal flats, Journal of Geophysical Research, 115, F01004, doi:10.1029/2009JF001326.

Mariotti, G., Fagherazzi, S., Wiberg, P. L., McGlathery, K. J., Carniello, L., & Defina, A., (2010). Influence of storm surges and sea level on shallow tidal basin erosive processes. Journal of Geophysical Research: Oceans, 115(C11).

Mariotti, G. and Fagherazzi, S. (2013). Critical width of tidal flats triggers marsh collapse in the absence of sea-level rise. Proceedings of the National Academy of Sciences, 110 (14) 5353-5356; doi:10.1073/pnas.1219600110.

McLoughlin, S.M., (2010). Erosional processes along salt marsh edges on the eastern shore of Virginia (Masters thesis, University of Virginia).

Morris J.T., Sundareshwar P.V., Nietch C.T.,Kjerve B., Cahoon D.R., (2002). Responses of coastal wetlands to rising sea level. Ecology, 10, 2869-2877.

Nichols, M. M., & Boon, J. D. (1994). Sediment transport processes in coastal lagoons. Coastal lagoon processes, 60, 157-209.

Oertel, G. F., Kearney, M. S., Leatherman, S. P., & Woo, H., (1989). Anatomy of a barrier platform: outer barrier lagoon, southern Delmarva Peninsula, Virginia. Marine Geology, 88(3), 303-318.

Oertel, G. F., Wong, G. T. F., & Conway, J. D., (1989). Sediment accumulation at a fringe marsh during transgression, Oyster, Virginia. Estuaries, 12(1), 18-26.

Oertel, G. F., (2001). Hypsographic, hydro-hypsographic and hydrological analysis of coastal bay environments, Great Machipongo Bay, Virginia. Journal of Coastal Research, 775-783.

Philips, J.D., (1986). Coastal submergence and marsh fringe erosion. Journal of Coastal Research, 2, 427-436.

Priestas, A. M., & Fagherazzi, S. (2011). Morphology and hydrodynamics of wave-cut gullies. Geomorphology, 131(1), 1-13.

Pye, K. and French, P.W., (1993). Erosion and accretion processes on British saltmarshes, Introduction: Saltmarsh processes and morphology, Final Report, Ministry of Agriculture, Fisheries and Food, report no. ES19B(1), Cambridge Environmental Research Consultants, Ltd., 42 p.

Reed, D.J., (1988). Sediment dynamics and deposition in a retreating coastal salt marsh. Estuarine, Coastal, and Shelf Science, 26, 67-79.

Reed, D. J., & Cahoon, D. R., (1992). The relationship between marsh surface topography, hydroperiod, and growth of Spartina alterniflora in a deteriorating Louisiana salt marsh. Journal of Coastal Research, 8(1), 77-87.

Redfield, A. C., and Rubin, M., (1962). The age of salt marsh peat and its relation to recent changes in sea level at Barnstable, Massachusetts. Proceedings of the National Academy of Sciences. 48:1728-1735.

Schwimmer, R.A., (2001). Rate and processes of marsh shoreline erosion in Rehoboth Bay, Delaware, U.S.A. Journal of Coastal Research, 17, 672-683.

Sunamura, T., (1982). A predictive model for wave-induced cliff erosion, with application to Pacific coasts of Japan. The Journal of Geology, 167-178.

Tonelli, M., Fagherazzi, S., Petti, M., (2010). Modeling wave impact on salt marsh boundaries. J. Geophys. Res. 115, C09028. doi:10.1029/2009JC006026.

Turner, R.E., Swenson, E.M., Milan, C.S., (2001). Organic and inorganic contributions to vertical accretion in salt marsh sediments. In: *Concepts and Controversies in Tidal Marsh Ecology* (eds M. Weinstein & K. Kreeger), 583-595. Kluwer Academic Publishing, Dordrecht.

van der Westhuysen, A. J., Zijlema, M., and Battjes, J. A., (2007). Nonlinear saturation-based whitecapping dissipation in SWAN for deep and shallow water. Coastal Engineering, 54(2), 151-170.

van der Westhuysen, A. J., (2010). Modeling of depth-induced wave breaking under finite depth wave growth conditions. Journal of Geophysical Research: Oceans (1978–2012), 115(C1).

Wilson, C. A., and Allison, M. A., (2008). An equilibrium profile model for retreating marsh shorelines in southeast Louisiana. Estuarine, Coastal and Shelf Science, 80(4), 483-494. ISSN 0272-7714, http://dx.doi.org/10.1016/j.ecss.2008.09.004.

Yan, L., (1987). *An improved wind input source term for third generation ocean wave modelling*. Koninklijk Nederlands Meteorologisch Instituut.

Yapp, R. H., and Johns, D., (1917). The salt marshes of the Dovey Estuary. Part II. The salt marshes. J. Ecol. 5:65-103.

Bibliography

Agriculture, Fisheries and Food, report no. ES19B(1). Cambridge Environmental Research Consultants, Ltd. 42 pp.

Allen, J.R.L., (1989). Evolution of salt-marsh cliffs in muddy and sandy systems: a qualitative comparison of British west-coast estuaries, Earth Surface Processes and Landforms, 14, 85–92.

Allen, J.R.L., (2000). Morphodynamics of Holocene salt marshes: a review sketch from the Atlantic and southern North Sea coasts of Europe, Quaternary Science Reviews, 19, 1155–1231.

Bartberger, C. E., (1976). Sediment sources and sedimentation rates, Chincoteague Bay, Maryland and Virginia. Journal of Sedimentary Research, 46(2), 326-336.

Baumann, R.H., Day, J.W., Miller, C.A., (1984). Mississippi deltaic wetland survival: sedimentation versus coastal submergence. Science, 224, 1093–1095.

Booij, N., R. C. Ris, and Holthuijsen, L.H., (1999). A third-generation wave model for coastal regions: 1. Model description and validation, Journal of Geophysical Research, 104(C4), 7649–7666, doi:10.1029/98JC02622.

Boon, J.D. and Byrne, R.J., (1981). On basin hypsometry and morphodynamic response of coastal inlet systems. Marine Geology, 40, 27-48,

Bowen, A.J., Inman, D.L., (1971). Edge waves and crescentic bars. Journal of Geophysical Research Letters, 76, 8662–8671.

Byrnes, M.K., McBride, R.A., Tao, Z., Duvic, L., (1995). Historical shoreline dynamics along the chenier plain of southwestern Louisiana. Transactions: Gulf Coast Association of Geological Societies, 45, 113–122.

Cahoon, D.R., Hensel, P.F., Spencer, T., Reed, D.J., McKee, K.L., Saintilan, N., (2006). Coastal wetland vulnerability to relative sea-level rise: wetland elevation trends

and process controls. Wetlands and Natural Resource Management, 190, 271–292.

Carniello L, *et al.* 2005. A combined wind wave-tidal model for the Venice lagoon, Italy. Journal of Geophysical Research – Earth Surface, **110**(F4): 15.

Chauhan, P.P.S., 2009. Autocyclic erosion in tidal marshes. Geomorphology. 10, 45–57. doi:10.1016/j.geomorph.2009.03.016.

Coco, G., Murray, A.B., (2007). Patterns in the sand: from forcing templates to self organization. Geomorphology, 91,271–290. doi:10.1016/j.geomorph.2007.04.023.

Coco, G., O'Hare, T.J., Huntley, D.A., (1999). Beach cusps: a comparison of data and theories for their formation. Journal of Coastal Research, 15, 741–749.

Coops, H., Geilen, N., Verheij, H., Boeters, R., and van der Velde, G., (1996). Interactions between waves, bank erosion, and emergent vegetation: An experimental study in a wave tank, Aquatic Botany, 53, 187-198.

D'Alpaos, A., Lanzoni, S., Marani, M., Fagherazzi, S., Rinaldo, A., (2005). Tidal network ontogeny: channel initiation and early development. Journal of Geophysical Research, Earth Surface 110 (F2), F02001. doi:10.1029/2004JF000182.

D'Alpaos A, Lanzoni, S., Mudd, S.M., and Fagherazzi, S., (2006). Modeling the influence of hydroperiod and vegetation on the cross-sectional formation of tidal channels. Estuarine Coastal and Shelf Science 69(3–4): 311–324.

D'Alpaos, A., Lanzoni, S., Marani, M., & Rinaldo, A., (2007). Landscape evolution in tidal embayments: Modeling the interplay of erosion, sedimentation, and vegetation dynamics. Journal of Geophysical Research, Earth Surface, 112(F1), F01008.

Davis, R. E., & Dolan, R. (1993). Nor'easters. American Scientist, 81(5), 428-439.

Day Jr., J.W., Reed, D., Syhayda, J., Kemp, P., Cahoon, D., Boumans, R.M., Latif, N., (1994). Physical processes of marsh deterioration. In: Roberts, H.H. (Ed.), Critical Physical

Day, J.W., Jr., Reed, D., Syhayda, J., Kemp, P., Cahoon, D., Boumans, R.M., and Latif, N., (1994). Physical processes of marsh deterioration. In H.H. Roberts, ed.

Critical Physical Processes of Wetland Loss, 1988-1994. Final Report. Louisiana State University, Baton Rouge. Prepared for U.S. Geological Survey, Reston, VA.

Defina A, Carniello L, Fagherazzi S, D'Alpaos L. (2007). Self organization of shallow basins in tidal flats and salt marshes. Journal of Geophysical Research 112: F03001. DOI. 10.1029/2006JF000550

DeLaune, R.D., Baumann, R.H., Gosselink, J.G., (1983). Relationships among vertical accretion, coastal submergence, and erosion in a Louisiana gulf coast marsh. Journal of Sedimentary Petrology, 53, 147–157.

DeLaune, R.D., Nyman, J.A., Patrick, W.H., (1994). Peat collapse, ponding and wetland loss in a rapidly submerging coastal marsh. J. Coast. Res. 10, 1021–1030.

Denny, M.W., Miller, L.P., Stokes, M.D., Hunt, L.J.H., and Helmuth, B.S.T., (2003). Extreme water velocities: Topographical amplication of wave-induced flow in the surf zone of rocky shores. Limnology and Oceanography, 48(1), 1-8.

Dolan, R.; Lins, H., and Hayden, B., (1988). Mid-Atlantic coastal storms. Journal of Coastal Research, 4(3), 417-433.

Draut, A.E., Kineke, G.C., Huh, O.K., Grymes, J.M., Westphal, K.A., Moeller, C.C., (2005). Coastal mudflat accretion under energetic conditions, Louisiana chenier-plain coast USA. Mar. Geol. 214, 27–47. doi:10.1016/j.margeo.2004.10.033.

Draut AE, Kineke, G.C., Velasco, D.W., Allison, M.A., Prime, R.J., (2005). Influence of the Atchafalaya River on recent evolution of the chenier-plain inner continental shelf, northern Gulf of Mexico. Continental Shelf Research 25(1): 91–112. doi: 10.1016/j.csr.2004.09.002

Elgar S, Raubenheimer B., (2008). Wave dissipation by muddy seafloors. Geophysical Research Letters 35(7): L07611. doi: 10.1029/2008GL033245

Fagherazzi S, Wiberg, P.L., Howard, A.D., (2003). Tidal flow field in a small basin. Journal of Geophysical Research – Oceans 108(C3); 3071. doi:10.1029/2002JC001340.

Fagherazzi S, Gabet, E.J., Furbish, D.J., (2004). The effect of bidirectional flow on tidal channel planforms. Earth Surface Processes and Landforms, 29(3): 295–309, doi:10.1002/1016.

Fagherazzi S, Sun T., (2004). A stochastic model for the formation of channel networks in tidal marshes. Geophysical Research Letters**,** 31(21); L21503, doi: 10.1029/2004GL020965.

Fagherazzi S, Fosser, G., D'Alpaos, L., D'Adorico, P., (2005). Climatic oscillations influence the flooding of Venice. Geophysical Research Letters, 32(19): 5, doi:10.1029/2005GL023758.

Fagherazzi S, Carniello, L., D'Alpaos, L., Defina, A., (2006). Critical bifurcation of shallow microtidal landforms in tidal flats and salt marshes. Proceedings of the National Academy of Sciences of the United States of America, 103(22): 8337–8341, doi:10.1073/pnas.0508379103

Fagherazzi S, Palermo, C., Rulli, M.C., Carniello, L., Defina, A., (2007). Wind waves in shallow microtidal basins and the dynamic equilibrium of tidal flats. Journal of Geophysical Research – Earth Surface, 112(F2); F02024, doi: 10.1029/2006JF000572.

Fagherazzi, S., Du, X., (2008). Tsunamigenic incisions produced by the December 2004 earthquake along the coasts of Thailand, Indonesia, and Sri Lanka. Geomorphology, 99, 120–129. 10.1016/j.geomorph.2007.10.015.

Fagherazzi, S., and Wiberg, P. L. (2009). Importance of wind conditions, fetch, and water levels on wave-generated shear stresses in shallow intertidal basins. Journal of Geophysical Research: Earth Surface, 114(F3), doi: 10.1029/2008JF001139.

Fagherazzi, S., & Priestas, A.M., (2010). Sediments and water fluxes in a muddy coastline: interplay between waves and tidal channel hydrodynamics. Earth Surface Processes and Landforms, 35(3), 284-293, doi: 10.1002/esp.1909.

Feagin, R.A., Lozada-Bernard, S.M., Ravens, T.M., Möller, I., Yeager, K.M., and Baird, A.H., (2009). Does vegetation prevent wave erosion of salt marsh edges?

Proceedings of the National Academy of Sciences, 106, 10109-10113. doi: 10.1073/pnas.0901297106.

Finkelstein, K., and Hardaway, S.C., (1988). Late Holocene sedimentation and erosion of estuarine fringing marshes, York River, Virginia. Journal of Coastal Research, 4, 447-456.

Fisher, W.L., McGowan, J.H., Brown, L.F., and Groat, C.G., (1972). Environmental Geologic Atlas of the Texas Coastal Zone: Galveston-Houston Area. Austin, TX: Bureau of Economic Geology, 91p.

French JR. (1993). Numerical-simulation of vertical marsh growth and adjustment to accelerated sea-level rise, North Norfolk, UK. Earth Surface Processes and Landforms, 18: 63–81.

French JR, Burningham H, Benson T. (2008). Tidal and meteorological forcing of suspended sediment flux in a muddy mesotidal estuary. Estuaries and Coasts, 31(5): 843–859, doi: 10.1007/s12237-008-9072-5.

Gary, M., McAfee Jr., R., Wolf, C.L. (Eds.), 1974. Glossary of Geology, 3rd ed. American Geological Institute, Washington D.C.

Goni MA, Gardner LR, (2003). Seasonal dynamics in dissolved organic carbon concentrations in a coastal water-table aquifer at the forestmarsh interface. Aquatic Geochemistry**,** 9(3): 209–232.

Green MO, Coco G. (2007). Sediment transport on an estuarine intertidal flat: measurements and conceptual model of waves, rainfall, and exchanges with a tidal creek. Estuarine, Coastal, and Shelf Science, 72: 553–569, doi:10.1016/j.ecss.2006.11.006.

Guza, R.T., Inman, D.L., (1975). Edge waves and beach cusps. J. Geophys. Res. 80, 2997–3012.

Hall, S.L., Wilder, W.R., and Fisher, F.M., (1986). An Analysis of Shoreline Erosion along the Northern Coast of East Galveston Bay, Texas, Journal of Coastal Research , 2(2), 173-179.

Hayden, B.P., (1999). Climate change and extratropical storminess in the United States: an assessment. Journal of American Water Resources Association 35:1387–1397

Jaramillo S, Sheremet A, Allison MA, Reed AH, Holland KT, (2009). Wave-mud interactions over the muddy Atchafalaya subaqueous clinoform, Louisiana, United States: wave-supported sediment transport. Journal of Geophysical Research – Oceans, 114: C04002, doi: 10.1029/2008JC004821.

Kastler, J.A., and Wiberg, P. L. (1996). Sedimentation and boundary changes of Virginia salt marshes. Estuarine, Coastal and Shelf Science, 42(6), 683-700.

Kearney, M.S., Grace, R.E., and Stevenson, J.C., (1988). Marsh loss in Nanticoke Estuary, Chesapeake Bay, Geographical Review, 8, 205-220.

Kineke GC, Higgins, E.E., Hart, K., Velasco, D., (2006). Fine-sediment transport associated with coldfront passages on the shallow shelf, Gulf of Mexico. Continental Shelf Research, 26(17–18): 2073–2091, doi:10.1016/j.csr.2006.07.023.

Kirwan ML, Murray AB. (2007). A coupled geomorphic and ecological model of tidal marsh evolution. Proceedings of the National Academy of Sciences of the United States of America, 104(15): 6118–6122, doi:10.1073/pnas.0700958104.

Kirwan, M.L., Murray, B., (2008). Temporary vegetation disturbance as an explanation for permanent loss of tidal wetlands. Geophysical Research Letters, 35 (24), L24401.

Knowlton, S.M., (1971). Geomorphological History of Tidal Marshes, Eastern Shore, Virginia, from 1852 to 1966. University of Virginia, M.S. Thesis, 186 pp.

Komar, P.D., (1976). Beach Processes and Sedimentation. Prentice-Hall, Englewood Cliffs, N.J.. 429 pp.

Lanzoni S, Seminara G. 1998. On tide propagation in convergent estuaries. Journal of Geophysical Research – Oceans, 103(C13): 30793–30812.

Lawson, S.E., (2004). *Sediment suspension as a control on light availability in a coastal lagoon* (Doctoral dissertation, University of Virginia).

Lundgren, H. and Juhl, J., (1995). Optimisation of caisson breakwater design. In 'Wave Forces on Inclined and Vertical Wall Structures', American Society of Civil Engineers, 181-204.

Marani M, D'Alpaos A, Lanzoni S, Carniello L, Rinaldo A. 2007. Biologically-controlled multiple equilibria of tidal landforms and the fate of the Venice lagoon. Geophysical Research Letters, 34(11): L11402.

Marani, M., D'Alpaos, A., Lanzoni, S. and Santalucia, M., (2011). Understanding and predicting wave erosion of marsh edges, Geophysical Research Letters, 38, L21401, doi:10.1029/2011GL048995.

Mariotti, G., and Fagherazzi, S., (2010). A numerical model for the coupled long-term evolution of salt marshes and tidal flats, Journal of Geophysical Research, 115, F01004, doi:10.1029/2009JF001326.

Mariotti, G., Fagherazzi, S., Wiberg, P.L., McGlathery, K.J., Carniello, L., Defina, A., (2010). Influence of storm surges and sea level on shallow tidal basin erosive processes. Journal of Geophysical Research 115, C11012. doi:10.1029/2009JC005892.

Mariotti, G. and Fagherazzi, S. (2013). Critical width of tidal flats triggers marsh collapse in the absence of sea-level rise. Proceedings of the National Academy of Sciences, 110 (14) 5353-5356; doi:10.1073/pnas.1219600110.

McBride, R.A., Taylor, M.J., Byrnes, M.R., 2007. Coastal morphodynamics and chenier plain evolution in southwestern Louisiana, USA: a geomorphic model. Geomorph. 88, 367–422. doi:10.1016/j.geomorph.2006.11.013.

McLoughlin, S.M., (2010). Erosional processes along salt marsh edges on the eastern shore of Virginia (Masters thesis, University of Virginia).

Mitsch, W.J., Gosselink, J.G., 2000. Wetlands. Wiley, New Jersey. 582 pp.

Moeller I, *et al.* 1996. Wild wave attenuation over saltmarsh surfaces: preliminary results from Norfolk, England. Journal of Coastal Research, 12(4): 1009–1016.

Moller I, *et al.* 1999. Wave transformation over salt marshes: a field and numerical modelling study from north Norfolk, England. Estuarine Coastal and Shelf Science, 49(3): 411–426.

Möller, I., 2006. Quantifying saltmarsh vegetation and its effects on wave dissipation: results from a UK east coast saltmarsh. Estuar. Coast. Shelf Sci. 69, 337–351. doi:10.1016/j.ecss.2006.05.003.

Morris J.T., Sundareshwar P.V., Nietch C.T.,Kjerve B., Cahoon D.R., (2002). Responses of coastal wetlands to rising sea level. Ecology, 10, 2869-2877.

Mwamba MJ, Torres R. 2002. Rainfall effects on marsh sediment redistribution, North Inlet, South Carolina, USA. Marine Geology, 189(3–4): 267–287.

Nichols, M. M., & Boon, J. D. (1994). Sediment transport processes in coastal lagoons. Coastal lagoon processes, 60, 157-209.

Nyman, J.A., Walters, R.J., Delaune, R.D., Patrick Jr., W.H., (2006). Marsh vertical accretion via vegetative growth. Estuar. Coast. Shelf Sci. 69, 370–380. doi:10.1016/ j.ecss.2006.05.041.

Oertel, G. F., Kearney, M. S., Leatherman, S. P., & Woo, H., (1989). Anatomy of a barrier platform: outer barrier lagoon, southern Delmarva Peninsula, Virginia. Marine Geology, 88(3), 303-318.

Oertel, G. F., Wong, G. T. F., & Conway, J. D., (1989). Sediment accumulation at a fringe marsh during transgression, Oyster, Virginia. Estuaries, 12(1), 18-26.

Oertel, G. F., (2001). Hypsographic, hydro-hypsographic and hydrological analysis of coastal bay environments, Great Machipongo Bay, Virginia. Journal of Coastal Research, 775-783.

Orson, R., Panageotou, W., Leatherman, S.P., (1985). Response of title salt marshes to rising sea levels along the U.S. Atlantic and Gulf coasts. J. Coast. Res. 1, 29–37.

Otvos Jr., E.G., Price, W.A., 1979. Problems of chenier genesis and terminology — an overview. Mar. Geol. 31, 251–263.

Penland, S., Ramsey, K.E., 1990. Sea-level rise in Louisiana and the Gulf of Mexico. J. Coast. Res. 6, 323–342.

Penland, S., Roberts, H.H., Bailey, A., Kuechere, G.J., Suhyada, J.N., Connor, P.C., Ramsey, K.E., (1994). Geologic framework, processes, and rates of subsidence in the Mississippi River delta plain, pp. 7.1.1 – 7.1.51 in Critical physical processes of wetland loss of Wetland Loss, 1988–1994. Final Report. Louisiana State University, Baton Rouge. Prepared for U.S. Geological Survey, Reston, VA.

Philips, J.D., (1986). Coastal submergence and marsh fringe erosion. Journal of Coastal Research, 2, 427-436.

Priestas, A. M., & Fagherazzi, S. (2011). Morphology and hydrodynamics of wave-cut gullies. Geomorphology, 131(1), 1-13.

Pye, K. and French, P.W., (1993). Erosion and accretion processes on British saltmarshes, Introduction: Saltmarsh processes and morphology, Final Report, Ministry of Agriculture, Fisheries and Food, report no. ES19B(1), Cambridge Environmental Research Consultants, Ltd., 42 p.

Ravens, T.M., Thomas, R.C., Roberts, K.A., Santschi, P.H., 2009. Causes of salt marsh erosion in Galveston Bay, Texas. J. Coast. Res. 25.

Redfield, A. C., and Rubin, M., (1962). The age of salt marsh peat and its relation to recent changes in sea level at Barnstable, Massachusetts. Proceedings of the National Academy of Sciences. 48:1728-1735.

Reed, D.J., (1988). Sediment dynamics and deposition in a retreating coastal salt marsh. Estuarine, Coastal, and Shelf Science, 26, 67-79.

Reed, D. J., & Cahoon, D. R., (1992). The relationship between marsh surface topography, hydroperiod, and growth of Spartina alterniflora in a deteriorating Louisiana salt marsh. Journal of Coastal Research, 8(1), 77-87.

Reed, D., 2002. Sea-level rise and coastal marsh sustainability: geological and ecological factors in the Mississippi delta plain. Geomorph. 48, 233–243.

Russell RJ, Howe HV. 1935. Cheniers of southwestern Louisiana. Geographical Review 25(3): 449–461.

Schwimmer, R.A., (2001). Rate and processes of marsh shoreline erosion in Rehoboth Bay, Delaware, U.S.A. Journal of Coastal Research, 17, 672-683.

Sheremet A, Mehta AJ, Liu B, Stone GW. 2005. Wave-sediment interaction on a muddy inner shelf during Hurricane Claudette. Estuarine Coastal and Shelf Science, 63(1–2): 225–233.

Sunamura, T., (1982). A predictive model for wave-induced cliff erosion, with application to Pacific coasts of Japan. The Journal of Geology, 167-178.

Tambroni N, Seminara G. 2006. Are inlets responsible for the morphological degradation of Venice Lagoon? Journal of Geophysical Research – Earth Surface**,** 111(F3); F03013.

Temmerman S, Govers G, Wartel S, Meire P. 2003. Spatial and temporal factor controlling short-term sedimentation in a salt and freshwater tidal marsh, Scheldt Estuary, Belgium, SW Netherlands. Earth Surface Processes and Landforms 28: 739–755.

Tonelli, M., Fagherazzi, S., Petti, M., (2010). Modeling wave impact on salt marsh boundaries. J. Geophys. Res. 115, C09028. doi:10.1029/2009JC006026.

Torres R, *et al.* 2006. Salt marsh geomorphology: physical and ecological effects on landform. Estuarine Coastal and Shelf Science, 69(3–4): 309–310.

Traykovski P, Wiberg PL, Geyer WR. 2007. Observations and modeling of wave-supported sediment gravity flows on the Po prodelta and comparison to prior observations from the Eel shelf. Continental Shelf Research, 27(3–4): 375–399.

Turner, R.E., Swenson, E.M., Milan, C.S., (2001). Organic and inorganic contributions to vertical accretion in salt marsh sediments. In: *Concepts and Controversies in Tidal Marsh Ecology* (eds M. Weinstein & K. Kreeger), 583-595. Kluwer Academic Publishing, Dordrecht.

Turner, R.E., Swenson, E.M., Milan, C.S., Lee, J.M., Oswald, T.A., 2004. Below-ground biomass in healthy and impaired salt marshes. Ecol. Res. 19, 29–35.

van de Koppel, J., Van der Wal, D., Bakker, J.P., Herman, P.M.J., 2005. Self organization and vegetation collapse in salt marsh ecosystems. Am. Nat. 165, 1–12.

van der Wal, D., Pye, K., 2004. Patterns, rates and possible causes of saltmarsh erosion in the Greater Thames area (UK). Geomorphology. 61, 373–391.

van der Westhuysen, A. J., Zijlema, M., and Battjes, J. A., (2007). Nonlinear saturation-based whitecapping dissipation in SWAN for deep and shallow water. Coastal Engineering, 54(2), 151-170.

van der Westhuysen, A. J., (2010). Modeling of depth-induced wave breaking under finite depth wave growth conditions. Journal of Geophysical Research: Oceans (1978–2012), 115(C1).

Voulgaris G, Meyers ST. (2004). Temporal variability of hydrodynamics, sediment concentration and sediment settling velocity in a tidal creek. Continental Shelf Research 24(15): 1659–1683.

Wilson, C. A., and Allison, M. A., (2008). An equilibrium profile model for retreating marsh shorelines in southeast Louisiana. Estuarine, Coastal and Shelf Science, 80(4), 483-494. ISSN 0272-7714, http://dx.doi.org/10.1016/j.ecss.2008.09.004.

Woodroffe, C.D., Curtis, R.J., McLean, R.F., 1983. Development of a chenier plain Firth of Thames, New Zealand. Marine Geology, 53, 1–22.

Yan, L., (1987). An improved wind input source term for third generation ocean wave modelling. Koninklijk Nederlands Meteorologisch Instituut.

Yapp, R. H., and Johns, D., (1917). The salt marshes of the Dovey Estuary. Part II. The salt marshes. Journal of Ecology, 5:65-103.

Curriculum Vitae

Anthony Michael Priestas

675 Commonwealth Avenue
Boston University
Department of Earth and Environment
Boston, Massachusetts 02215
priestas@bu.edu

PERSONAL INFORMATION

Born: Sandusky, Ohio, 1975
Marital Status: Married

EDUCATION

Boston University, Coastal Geomorphology, Ph.D. candidate, (2008-present)
Dissertation: *Salt marsh shoreline erosion and sediment exchange in an open coast and coastal lagoon setting*.

Florida State University, Geology, M.S., (2008)
Thesis: *Morphological barrier island changes and recovery of dunes after Hurricane Dennis, St. George Island, Florida.*

Florida State University, Geology, B.S., (2005), cum laude, with honors
Honors Thesis: *Distribution and origin of authigenic smectite clays in Cape Roberts Project Core 3, Victoria Land Basin, Antarctica*.

Florida State University, Interdisciplinary Geophysics, B.S., (2005), cum laude

St. Petersburg College, A.A., (2002), with honors

HONORS AND AWARDS

Florida State University Honors All-Star selection (2005)

St. Petersburg College Apollo award recipient "Most outstanding sophomore" (2002)

Phi Theta Kappa Leaders of Promise scholarship (2002)

All-Florida Academic Team selection (2002)

MILITARY SERVICE

Florida Army National Guard, 1993 - 2002
Honorably discharged at the rank of Specialist (E-4)
Company C (medical), 53rd Support Battalion, St. Petersburg, FL
Detachment I, 325th Maintenance Co., Crystal River, FL
MOS: Generator and light-wheeled vehicle mechanic
State active duty, Hurricane Opal, 1995

RESEARCH AND EXPERIENCE

Salt marsh boundary erosion rates and dynamics: Louisiana, Virginia, Massachusetts

Post-storm morphologic change analysis, St. George Island, Florida

Distribution and origin of authigenic smectitie clay coats in Antarctic seafloor drillcores

SSV Corwith Cramer, C-226; Sea Education Association, Woods Hole, Massachusetts

New Tools in Processed-based Analysis of Lidar Topographic Data, Short Course, Boulder Colorado, (June 2010)

Teaching Fellow, Boston University, Boston, MA , (2008- 2010)

Instructor, Boston University, Boston, MA, Summer 2008

Teaching Assistant, Florida State University, Tallahassee, FL, (2005 – 2007)

Undergraduate Research Assistant, Florida State University, Tallahassee, FL, (2003)

Research Assistant, Florida Geological Survey, Tallahassee, FL, (2002 – 2003)

Math and Science Tutor, St. Petersburg College, Tarpon Springs, FL, (2001 – 2002)

PUBLICATIONS

Priestas, A.M., and Fagherazzi, S., Coupled wave energy and erosion dynamics along a salt marsh boundary, Hog Island Bay, Virginia (*In preparation*).

Priestas, A.M., Fagherazzi, S., Wilson, C.A., and Fitzgerald, D.M., (2012). Rapid wetland expansion during European settlement and its implication for marsh survival under modern sediment delivery rates: COMMENT, Geology, 40(12), e284-e285, doi: 10.1130/G32597C.1.

Priestas, A.M. and Fagherazzi, S., (2011). Morphology and hydrodynamics of wave-cut gullies, Geomorphology, 131, 1-13, doi:10.1016/j.geomorph.2011.04.004.

Fagherazzi, S. and Priestas, A.M., (2011) Backbarrier flooding by storm surges and overland flow, Earth Surface Processes and Landforms, 37(4), 400-410, doi: 10.1002/esp.2247.

Priestas, A.M. and Fagherazzi, S., (2010). Morphological barrier island changes and recovery of dunes after Hurricane Dennis, St. George Island, Florida, Geomorphology, 11 (4), 614-626, doi: doi:10.1016/j.geomorph.2009.09.022

Fagherazzi, S., and Priestas, A.M., (2010). Sediments and water fluxes in a muddy coastline: Interplay between waves and tidal channels, Earth Surface Processes and Landforms, 35 (3), 284-293, doi: 10.1002/esp.1909

Priestas, A.M., and S. Wise, (2006). Distribution and origin of authigenic smectite clays in Cape Roberts Project Core 3, Victoria Land Basin, Antarctica, in Antarctica: A Keystone in a Changing World – Online Proceedings of the 10th ISAES, edited by A.K. Cooper and C.R. Raymond et al., USGS Open-File Report 2007-1047, Short Research Paper 057, 5 p.; doi:10.3133/of2007-1047.srp057.

PRESENTATIONS AND ABSTRACTS

Priestas, A.M. and Fagherazzi, S., Rates and mechanisms of salt marsh boundary erosion. U.S. Army Corps of Engineers, Engineering Research and Development Center, Coastal and Hydraulics Laboratory, Vicksburg, Mississippi, 2013.

Priestas, A.M., Fagherazzi, S., Morphology and hydrodynamics of wave-cut gullies, AGU annual meeting, San Francisco, December 13-17, 2010.

Fagherazzi S., Priestas A.M., Mariotti G.*, Wiberg PL, McGlathery K., Ecogeomorphic models for the Virginia Coastal Reserve, VCR-LTER All Scientists Meeting, Oyster VA, January 7-8, 2009.

Fagherazzi S., Priestas A.M., Tonelli M., Mariotti G., Modeling Marsh Boundary Evolution, USGS Marsh Modeling Workshop, San Francisco, December 11-12, 2008.

Priestas A.M. and S. Fagherazzi, Non-uniform Salt Marsh Boundary Erosion by Wave Impact in Costal Louisiana and Virginia: Implications for Salt Marsh Stability, AGU Chapman Conference on Physics of Wave-Mud Interaction, Amelia Island, Florida, November 17-20, 2008.

Fagherazzi S., Priestas A.M., Sediments and water fluxes in a muddy coastline: interplay between waves and tidal channels. AGU Chapman Conference on Physics of Wave-Mud Interaction, Amelia Island, Florida, November 17-20, 2008.

Priestas, A.M., Wise, S.W., Authigenic smectite clay coats and other authigenic minerals in Cape Roberts Drill core 3, Victoria Land Basin, Antarctica, 10th International Symposium on Antarctic Earth Sciences, Santa Barbara, August 26-31, 2007.

Priestas A.M., Fagherazzi S., Morphological recovery of Dune Fields in Barrier Islands after Hurricanes, St. George Island Florida AWRA Florida section Meeting, Tallahassee March 17, 2006.

Priestas, A.M., Wise, S.W., Authigenic smectite clay coats and other authigenic minerals in Cape Roberts Drill core 3, Victoria Land Basin, Antarctica, GSA annual meeting, Denver, November 7-10, 2004.